Benha University
Faculty of Engineering - Shoubra
Surveying Engineering Department

Using Single Receiver to Determine Precise Point Positioning (PPP)

A Thesis Submitted in Partial Fulfillment of the Requirements
For the M.Sc. Degree in Surveying Engineering

Submitted By
Eng. Mohammed Nasr Ali Elbeah
B.Sc. in Surveying Engineering (2010)

Supervised By

Dr. Saad Zaki Bolbol
Prof. of Surveying and Geodesy
Faculty of Engineering at Shoubra
Benha University

Dr. Amr H. Ali
Prof. of Surveying and Geodesy
Faculty of Engineering at Shoubra
Benha University

Dr. Mona Saad El Sayed
Assoc. Prof. of Surveying and Geodesy
Faculty of Engineering at Shoubra
Benha University

Cairo – Egypt
2018

Benha University
Faculty of Engineering at Shoubra
Surveying Engineering Department

APPROVAL SHEET

Using Single Receiver to Determine Precise Point Positioning (PPP)

A Thesis Submitted in Partial Fulfillment of the Requirements for the M.Sc. Degree in Surveying and Geodesy

Submitted by
Eng. Mohammed Nasr Ali Elbeah
B.Sc. in Surveying Engineering (2010)

Examiners Committee

Prof. Dr. Mahmoud El Nokrashy Ali Signature: .....

Professor of Surveying and Geodesy,
Faculty of Engineering,
Al Azhar University, Egypt.

Prof. Dr. Saad Zaki Bolbol Signature: .....

Professor of Surveying and Geodesy,
Faculty of Engineering at Shoubra,
Benha University, Egypt.

Prof. Dr. Abd-Alla Ahmed Saad Signature: .....

Professor of Surveying and Geodesy,
Faculty of Engineering at Shoubra,
Benha University, Egypt.

Prof. Dr. Amr H. Ali Signature: .....

Professor of Surveying and Geodesy,
Faculty of Engineering at Shoubra,
Benha University, Egypt.

Acknowledgement

First, I wish to express my sincere thanks and ultimate appreciation to my supervisor Prof. Dr. **Saad Bolbol**, Surveying Department, Faculty of Engineering at Shoubra, for his encouragement and active support given to me during the preparing this thesis.

Also, my special thanks and respect are extended to my supervisor Prof. Dr. **Amr ALi,** Surveying Department, Faculty of Engineering at Shoubra, for his guidance, help and encouragement during the preparing this thesis.

Special thanks and very appreciation go to Assoc. Prof. **Mona Saad Elsayed,** Surveying Department, Faculty of Engineering at Shoubra, for her ultimate help and very valuable suggestions. Her interest, discussions and advices were constructive and helpful.

Many deep thanks go to **GNSS Community** and the **International Research Community.**

I would like to express my deepest gratitude and appreciation to my wife **Gehad**, for her continous help and understanding.

Finally, I would like to didicate this thesis to lovely children, **Reem** and **Raghad** for their patience and sacrifice.

Abstract

Global Navigation Satellite Systems (GNSS) are growing dramatically which allowed the opportunity for further improvements in satellite positioning techniques. Most of GPS applications depends mainly on Differential GPS (DGPS) which allows more accurate positioning than standalone GPS. Differential GPS (DGPS) is a relatively technique involves the use of two receivers. One receiver is located at a reference station with fixed position that is accurately surveyed, while the other is set at unknown point that we need to determine its position. Also, simultaneous observations at reference and unknown stations are required for DGPS and rely largely on the distance between these stations.

Nowadays, a new technique is introduced to combine between the higher needed accuracy and the simplicity of the operational process, which is named Precise Point Positioning (PPP). It is a processing method with the objective of providing high positioning accuracy without the need for a nearby base station or dense network of reference stations operated by the user. This approach uses a stand-alone GNSS receiver for processing un-differenced carrier phase and pseudo-range measurements to compute positions which reaches decimeter or centimeter accuracy. The PPP technique has become very popular in the scientific and research communities for applications that required high accuracy for both post processing and real-time processing such as offshore positioning, aircraft navigation, high-precision farming and meteorology. The main problem at the moment for real-time applications is the relatively long convergence time of the algorithm to the desired accuracy.

The main objective of this research is to study, investigate and evaluate the novel Precise Point Positioning (PPP) technique in static and kinematic modes using undifferenced single and dual frequency observations. In addition to using single and dual code and carrier phase observations, different types of precise orbits and clock products such as final, rapid and ultrarapid ephemeris are also used in processing. The evaluation procedure of the PPP performance in static mode was in terms of positioning accuracy from a reference solution and convergence time, which means how long it takes a position filter to reach a stable condition. As to kinematic PPP, the assessment was relying on the positioning accuracy of PPP results from a differential solution.

Acronyms

AC	Analysis Centers
APC	Antenna Phase Center
ARP	Antenna Reference Point
ANTEX	ANTenna EXchange format
BNC	BKG Ntrip Client
CDDIS	Crustal Dynamics Data Information System
CLK	Clock file
CORS	Continuously Operating Reference Stations
CSRS-PPP	Candian Spatial Reference Service – Precise Point Positioning
DAT	Data Analysis Tool
DCB	Differential Code Biases
DGPS	Differential Global Positioning System
DOP	Dilution Of Precision
DOY	Day Of Year
DPC	Data Processing Core
ECEF	Earth Center Earth Fixed
ESA	European Space Agency
EU	European Union
gAGE	group of Astronomy and GEomatics
GDOP	Geometric Dillution Of Precission
GIM	Global Ionosphere Models
gLAB	gnss LAB tool
GLONASS	GLObal NAvigation Satellite System
GNSS	Global Navigation Satellite System
GPS	Global Positioning System
GUI	Graphical User Interface
IAC	Information Analytical Center
IGR	IGS Rapid products
IGS	International GNSS Service
IONEX	IONosphere EXchange format
JPL	Jet Propulsion Laboratory
NRCan	Natural Resources, Canada
PCV	Phase Center Variation
PPP	Precise Point Positioning
PRN	Pseudo Random Number
RINEX	Receiver INdependent EXchange format
RMS	Root Mean Square error
RTK	Real Time Kinematic
RT-PPP	Real Time Precise Point Positioning
RTS	Real Time Service
SA	Selective Availability
SBAS	Satellite Based Augmentation System

SINEX	Solution INdependent EXchange format
S/N	Signal to Noise ratio
SPP	Standard Point Positioning
SV	Satellite Vehicle
TBC	Trimble Business Center software
TEC	Total Electron Content
TECU	Total Electron Content Unit
TEQC	Translating, Editing and Quality Check
UPC	Universitat Politecnica de Catalunya
US	United States
WAAS	Wide Area Augmentation System
WLS	Weighted Least Squares

Table of Contents

List of Tables

List of Figures

CHAPTER ONE

INTRODUCTION

1.1 Background

Nowadays, Multiple Global Navigation Satellite System (GNSS) constellations are being developed whether it operates fully or partially. The United States GPS system was designed in the seventies by the US military and is still controlled and operated by the US military, under agreement with the US department of transportation for the provision of GPS civil services. The dependency on US controlled satellite navigation systems has prompted the European Union (EU), to develop its own system which is called Galileo. The first two Galileo test satellites were launched in 2005 and 2008, the constellation currently consists of 10 satellites (ESA, 2015), and full operational capability is planned for 2020 (ESA, 2012). At the same time the GPS constellation, consisting of 31 satellites, is undergoing a modernization program (gps.gov, 2015); the Russians have revived their own system (GLONASS), consisting of 24 satellites (IAC, 2015), and the Chinese government is completing their GNSS BeiDou, with a current constellation of 17 satellites (beidou.gov.cn, 2015).

During the last three decades the differential GPS (DGPS), and subsequently DGNSS, technique has been the dominant operational mode for precise positioning for the geoscience, geospatial and navigation communities (Chris RIZOS et al. 2012). All DGNSS techniques are based on using more than one receiver to receive simultaneously the satellite signals, which takes more time and cost. Nowadays, a new technique is introduced to combine between the higher needed accuracy and the simplicity of the operational process, which is named Precise Point Positioning (PPP). It is a positioning approach that uses a stand-alone GNSS receiver for processing un-differenced carrier phase and pseudo-range measurements to compute positions which reaches, decimeter or centimeter accuracy (Zumberge et al. 1997).

The PPP technique turn out to be familiar in the research communities for applications that required high accuracy such as offshore positioning, aircraft navigation, high-precision farming and meteorology. Recently, PPP has become a valuable tool for some geodetic applications. It has the advantages for many reasons; simple field operation, cost-effectiveness, and improving positioning accuracy with no base stations (Changsheng Cai, 2009). Precise Point Positioning technique differs from other positioning methods, such as “Differential static, RTK etc.”, where PPP technique has advantage over traditional methods. What it is required, single receiver (at the user’s position) which makes it unnecessary to establish local reference station or to have access to observations from one (or more) reference station(s).

PPP is a precise geodetic point positioning approach that uses un-differenced dual frequency pseudo range and carrier phase observations along with precise satellite orbit and clock products. The main issue for precise point positioning to achieve high-accuracy positioning results is how to mitigate all potential errors involved in the space segment, signal propagation, ground environment, and receiver segment. Therefore, all errors must be handled in PPP in order to achieve centimeter-level accuracy.

These errors are classified as follows:

i. Satellite specific errors.
ii. Receiver specific errors.
iii. Atmospheric errors.

After handling these errors through dual-frequency observations, (atmospheric models, ocean loading corrections, and phase wind-up corrections… etc.,) this technique will have the potential to provide an equivalent positioning accuracy compared to relative technique. The success of this system will significantly improve the operational flexibility of precise positioning using GNSS, increase applications, and at the same time reduces the field operational costs. Currently PPP is capable of providing centimeter level accuracy in static mode and decimeter level accuracy in kinematic mode. This process requires the preliminary correction for different error sources that relates to the not perfectly modeled position of the GNSS satellites, the behavior of their atomic clocks, and the propagation delay introduced by ionosphere and troposphere…etc. However, several limitations still remain, primarily the long convergence times needed to resolve ambiguities, currently restricting the use of PPP for real-time applications (Thomas Grinter and Craig Roberts, 2013).

1.2 Research Objectives

The main objective of the research is to study and evaluate the PPP technique using single and dual frequency, un-differenced pseudorange and carrier phase, observations in both post processing static and kinematic modes. To achieve this objective, the following tasks are accomplished:

1. Recognizing the recent developments in the Global Navigation Satellite Systems.

2. Investigate the error sources of the signal travel from the satellite to the receiver and their mitigation strategies in PPP.

3. Accuracy assessment of the PPP technique in both post processing static and kinematic modes using single and dual frequency observations along with different types of precise ephemeris.

4. Performance evaluation of Precise Point Positioning (PPP) from GPS-Only and GPS+GLONASS satellites using CSRS-PPP Online Service.

5. Simple test for Real Time Precise Point Positioning (RT-PPP).

1.2 Thesis Outlines

The thesis consisted of five chapters:
In chapter 1, the main outlines of the research are given and a background of the PPP including the basic concept and current status is outlined. Also, the goal of the work and the thesis contents are summarized.

In chapter 2, an overview of precise point positioning, the history of PPP and recent performance and limitations of the technique are provided. Also, a brief description of error sources is shown and the handling strategies in PPP is highlighted.

In chapter 3, the mathematical model of the PPP technique and the required steps is described. All data types and formats needed, preprocessing processes, modelling, filtering and parameters estimation are illustrated.

Through chapter 4, the sources of data collection and the accuracy assessment results of PPP in both static and kinematic modes using single and dual frequency observations are clarified. Also, the performance of PPP in terms of accuracy and convergence time is assessed.

In chapter 5, summary, conclusions and recommendations for future work are itemized.

CHAPTER TWO

PRECISE POINT POSITIONING

2.1 History of PPP

Over the last decade of the 20th century, a lot of networks of Continuously Operating Reference Stations (CORS) were established in several areas around the world. These networks provide Global Navigation Satellite System (GNSS) data consisting of carrier phase and code range measurements in support of three dimensional positioning, meteorology, space weather, and geophysical applications throughout coverage areas (https://www.ngs.noaa.gov/). To keep the computational problem associated with the data analysis of such networks economically feasible, Zumberge et al. (1997) pioneered a novel technique called PPP in 1997.

The PPP technique is a one receiver approach. It depends mainly on determining precise satellite ephemeris and clock corrections from a global network of reference stations managed by the International GNSS Service (IGS), together with models for atmospheric correction, ocean loading, earth tides and other errors related to the signal travel from the satellite to the receiver. IGS uses its network, comprises of over 400 reference stations distributed around the world, to compute accurate satellite ephemeris and clock products through multiple global and regional analysis centers associated with it (http://www.igs.org/about/).

The concept of PPP technique is similar to some extent to the GPS Standard Point Positioning (SPP) that uses pseudo range measurement and real broadcast ephemeris to estimate receiver position and its accuracy is about meters. However, in PPP more precise satellite orbits and clock products provided by IGS are used instead of broadcast ephemeris in SPP. Moreover, PPP uses carrier phase measurements in its computational process and for high accuracy positioning results it uses dual frequency observations in order to overcome the ionospheric delay error through ionosphere free linear combinations. Zumberge et al. (1997) report a few-millimeter precision for a 24 hour period in horizontal components and centimeter precision in the vertical component. PPP differs from baseline processing in some modeling strategies. However, in baseline processing many effects such as earth tides, loading, and atmosphere canceled out by single differencing simultaneous observations from two receivers, which in PPP have to be taken into account explicitly.

Initially, precise satellite orbits and clock products have been available from the IGS since 1992 (Beutler et al., 1999) with a latency of about two weeks, limiting PPP to post-processing applications whereby the PPP solution is estimated afterwards (outside the receiver) after downloading orbits and clocks from the Internet. In PPP, for post processing, the receivers can both be static, resulting in station coordinates, or kinematic resulting in time-

series of receiver coordinates. Nowadays, IGS provides its users with ultrarapid and rapid precise products with smaller latencies but naturally with degraded accuracy opening the door for near real-time applications of PPP.

In spite of PPP technique was developed as a dual frequency one, it can also be used with only a single frequency. The biggest problem here is how to eliminate the ionosphere delay. Instead of the ionosphere free linear combination, single frequency PPP relies on either external ionosphere delay data or a linear combination of code and carrier phase data to eliminate the ionospheric delay. Global Ionosphere Models (GIM) computed by IGS analysis centers (Kouba, J., 2009a) are currently the global ionosphere models with the highest accuracy.

2.2 Performance and Limitations of PPP

As mentioned earlier, Zumberge et al. (1997) concluded that a few millimeter precision using PPP can be reached for a 24 hour period in horizontal components and centimeter precision in the vertical component. These results were reached after several initialization hours and so not acceptable for many applications, especially considering kinematic receivers. Along with the developments in all subjects related GNSS, PPP also took its luck from these developments and more improvements occurred in the IGS precise ephemeris and clock information. Therefore, the challenge for PPP is not only to improve the obtained accuracy to touch centimeters but also to shorten the time to reach this high results. Therefore, the convergence time of the PPP technique, the time the approach needs to reach a stable condition, has been investigated also.

Witchayangkoon and Segantine (1999) tested the PPP implementation of the Jet Propulsion Laboratory (JPL), using the precise IGS products and measurements from a static receiver, and found that the repeatability of the PPP solutions ranged from 10 to 20 cm after one hour of observations, and this decreased to a few centimeters after 12 hours, finally reaching 1 cm after 24 hours.

Kouba and Heroux (2001) report that the cm convergence is reached after processing 2-3 h of observations from an IGS station using precise IGS orbits and clocks products in static mode. Also, they mentioned that the convergence time can be decreased to only 30 minutes when high-rate satellite clock products are used. For kinematic positioning, Landau et al. (2008) report a final accuracy of 40 mm was achieved within a convergence time of 2 hours. Bisnath and Gao (2009 a,b) reached 10 cm accuracy after 20-25 minutes for an airborne platform in kinematic mode.

Melgard et al. (2010) report that 40 cm can be achieved from static PPP using GPS only dual frequency observations after 17 minutes of convergence time. Using single frequency GPS L1, van Bree and Tiberius (2012) concluded that 15 – 30 cm after 90 minutes of convergence time achieved in kinematic PPP. Monge et al. (2014) found that 2.5 cm can be achieved using GPS only static PPP after 2 hours of convergence time, improved to 1 cm after 10 hours and reached to 0.7 cm after 24 hours. Odijk et al. (2015) concluded that after 1 hour static PPP from dual GPS the accuracy was in the range of 7 – 18 cm.

Despite the improvements made in PPP the performance is still far removed from RTK performance which routinely achieving 10 – 20 mm accuracy (RMS) with average initialization times of 20 seconds or less (Landau et al., 2008). However, the development of PPP is not finished. A number of research groups work on the use of more than two frequencies and multiple systems for PPP as well as integer ambiguity resolution for PPP (De Bakker, P.F. 2015).

2.3 Modeling of Measurements in PPP

Generally the key issue for precise point positioning and navigation processes to achieve high accuracy positioning results is how to mitigate all potential errors involved in the satellite system. For PPP, all errors included in space segment, signal propagation, ground environmental conditions and receiver segment must be mitigated. In the differential GPS positioning, the reason that millimeter-level accuracy can be achieved is because some errors can be fully or partially removed by differencing observations between two stations. However, this differential technique can't be used in PPP due to the fact that only observations from a single receiver are available. Therefore, all errors must be handled in PPP in order to achieve centimeter-level accuracy.

Most of the PPP errors can be, to some extent, mitigated through modeling. While the receiver clock error and dry component of tropospheric delay are estimated as unknown parameters and the ionospheric delay can be removed through ionosphere-free observations combinations. In this chapter all errors related to PPP and modeling strategies will be discussed to overcome these errors.

2.3.1 Satellite Orbits/Clock Errors

The precise GNSS orbits and clocks, weighted according to their corresponding precision, are the key prerequisites for PPP, given that the proper measurements are made at the user site and the observation models are implemented correctly. The satellite orbital error may be defined as a difference between the actual satellite position and its computed value from

broadcast navigation message. Usually, this difference is expressed in three orbital elements: along-track, cross-track and radial. This error has a significant and direct impact on point positioning technique. On the other hand, the satellite clock error can be described by the satellite clock bias, drift and drift rate.

The satellite orbit and clock products can be classified into broadcast ephemeris and precise ephemeris. The broadcast ephemeris are available at the time of observation, at real time, with an accuracy of about 100 cm for satellites' orbits and 5 ns for clock corrections according to the International GNSS Service (IGS). However, the precise ephemeris are available with different latency times because of it is a post processed ones. Latency is due to the process of data collection, transmission, calculations and distribution of these products to all users around the world. These precise products are obtained from observations come through a global network of reference stations, whose coordinates are precisely determined, distributed around most of the world and equipped with high performance dual frequency receivers. After the process of data collection, these data are then go to global processing centers to generate the precise orbits and clock products using different sophisticated software packages. Finally, these precise ephemeris are transmitted to users via Internet or geostationary communication satellites.

The key role of precise orbits and clock products is back to the International GNSS Service (IGS). It is a civilian organization that has ensured open access for high-quality GNSS data products since 1994 (Kouba and Héroux, 2001) to support scientific earth science research, educational and commercial applications and a wide variety of applications that touch millions of users in virtually all segments of the global economy. The IGS collects, archives, and freely distributes GPS observation data sets of sufficient accuracy to satisfy the objectives of a wide range of applications and experimentation. These data sets are used by the IGS to generate the data products which are made available to interested users through IGS website.

Current official IGS products include (http://www.igs.org/products/):

- Tracking station data, coordinates and velocities
- GPS satellite ephemerides
- GLONASS satellite ephemerides
- Earth rotation parameters
- GPS satellite and IGS tracking station clock information
- Zenith tropospheric path delay estimates
- Global ionospheric maps

These products support the analysis of earth sciences and other efforts such as enhancing of the International Terrestrial Reference Frame (ITRF), earth deformation monitoring, monitoring earth rotation, the troposphere and ionosphere delays, determining orbits of scientific satellites, and other applications.

The IGS is a voluntary collaboration of over 200 self-funding agencies, universities, and research institutions in more than 100 countries (Dow, J.M., Neilan, R. E., and Rizos, C.,). Figure (2.1) shows the IGS organizational diagram. The global tracking network of IGS as shown in Figure (2.2) consists of more than 400 Continuously Operating Reference Stations (CORS) that provides a rich data set to the IGS Analysis Centers (AC), which formulate and freely provide precise products such as satellite ephemeris and clock corrections.

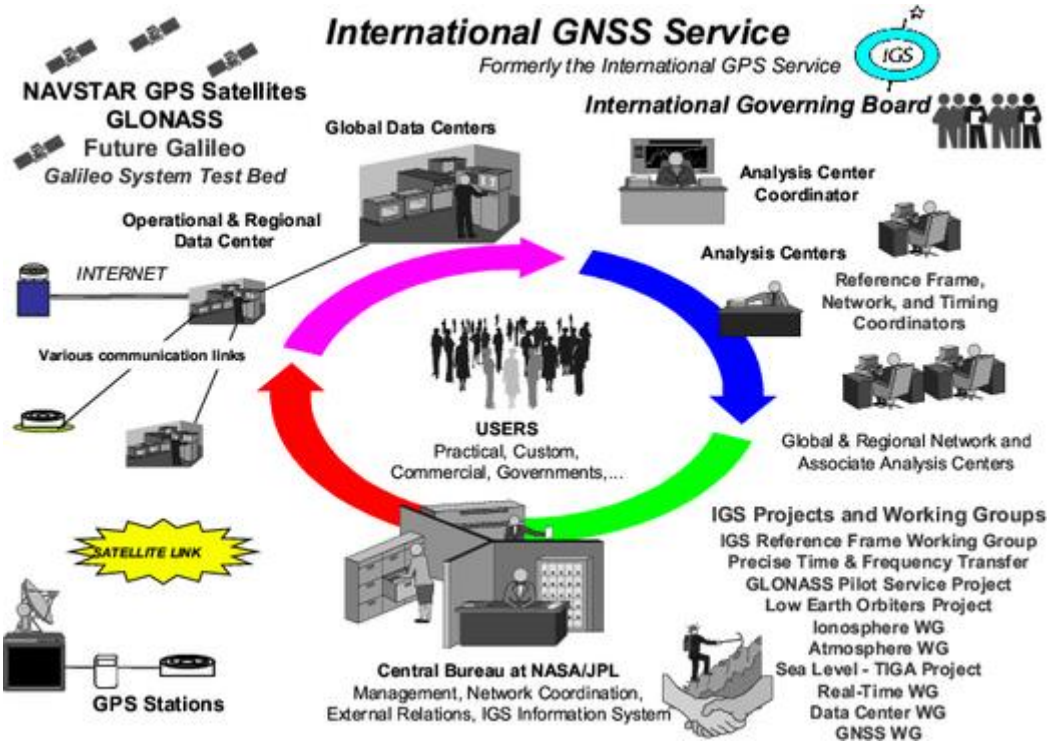

Figure (2.1) The IGS organizational diagram (http://www.igs.org/).

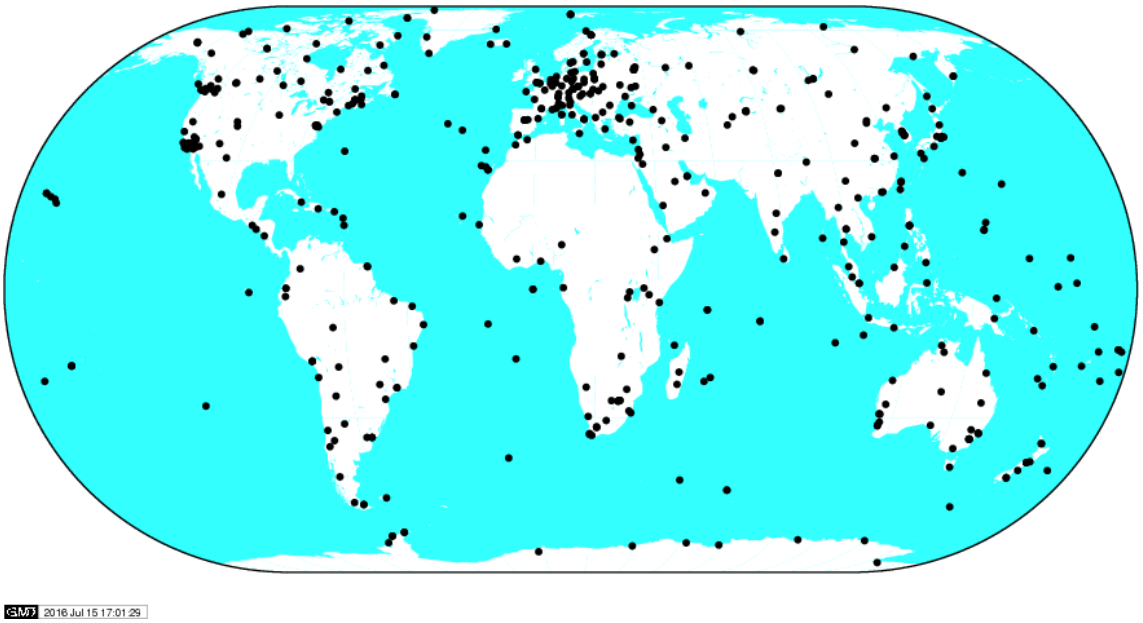

Figure (2.2) The IGS tracking network (from http://www.igs.org/).

Currently, there are up to ten IGS Analysis Centers (AC) which provide us with different categories of precise orbits and clock solutions. Tables (2.1) and (2.2) show accuracy, latency and sample interval of different types of GPS and GLONASS ephemeris respectively. From the Table (2.1), it is clearly observed that the accuracy is increasing from the IGS ultra-rapid to IGS final products but the latency becomes longer.

Table (2.1) Types of available GPS satellite ephemeris and clocks (from http://www.igs.org/).

Type		Accuracy	Latency	Updates	Sample Interval
Broadcast	orbits	~100 cm	real time	--	daily
	Sat. clocks	~5 ns RMS ~2.5 ns SDev			
Ultra-Rapid (predicted half)	orbits	~5 cm	real time	at 03, 09, 15, 21 UTC	15 min
	Sat. clocks	~3 ns RMS ~1.5 ns SDev			
Ultra-Rapid (observed half)	orbits	~3 cm	3 - 9 hours	at 03, 09, 15, 21 UTC	15 min
	Sat. clocks	~150 ps RMS ~50 ps SDev			
Rapid	orbits	~2.5 cm	17 - 41 hours	at 17 UTC daily	15 min

	Sat. & Stn. clocks	~75 ps RMS ~25 ps SDev			5 min
Final	orbits	~2.5 cm	12 - 18 days	every Thursday	15 min
	Sat. & Stn. clocks	~75 ps RMS ~20 ps SDev			Sat.: 30s Stn.: 5 min

Table (2.2) Available GLONASS satellite ephemeris (from http://www.igs.org/).

Type	Accuracy	Latency	Updates	Sample Interval
Final	~3 cm	12 - 18 days	every Thursday	15 min

In addition to the above ephemeris and after several years of pilot project operation, on April 1, 2013, the IGS Real Time Service (RTS) has been officially launched, providing precise orbit/clocks products in real time. The ultra-rapid and RTS products have become useful to many other real-time and near real-time applications.

2.3.2 Ionospheric Error

Since Selective Availability (SA) has switched off, the ionospheric error has become the dominant error source in GNSS positioning applications which can reach tens of meters at zenith. The ionosphere is a region of the earth's upper atmosphere, from about 50 km to 1,000 km altitude. It is a shell of electrons and electrically charged atoms and molecules that surrounds the earth. It owes its existence primarily to ultraviolet radiation from the Sun. These free electrons in the ionosphere have a great influence on the electromagnetic waves, including refraction, reflection and absorption. The GNSS signal flight affected by these electrons, existed in the ionosphere, causing a change of propagation speed of the signal and so the measured range between the receiver and satellite will be corrupted by an ionospheric error. For high performance positioning applications, the ionospheric effect must be removed from all observations.

The ionosphere is a dispersive medium (i.e., the wave propagation speed and thence, the refractive index depends on the frequency) and the refractive index is almost the important element to be characterized. The propagation speed of the GNSS electromagnetic signals in the ionosphere depends on its electron density, which is typically driven by two main processes: during the day, sun radiation causes ionization of neutral atoms producing free electrons and ions. During the night, the recombination process prevails, where free

electrons are recombined with ions to produce neutral particles, which leads to a reduction in the electron density.

In GNSS, there are different frequencies on which signals are transmitted and therefore the ionosphere layer will cause different delays on these frequencies. The phase refractive index (n_p) of the ionosphere can be approximated by (Seeber, 1993):

$$n_p = 1 - \frac{40.3 \cdot N_e}{f^2} \tag{2.1}$$

Where N_e is the total electron density (el/m3);
f is the radio wave frequency (Hz).

At the frequency of GNSS signals, the previous approximation accounts for more than the 99.9% of the refractivity (first order ionospheric effect). Similarly, the group refractive index (n_g) (first order approximation) can be expressed as:

$$n_g = 1 + \frac{40.3 \cdot N_e}{f^2} \tag{2.2}$$

The group delay of the ionosphere can be expressed in the unit of length as (Liao, 2000):

$$\Delta g = \int (n_g - 1) dl \tag{2.3}$$

Substituting from equation (2.2) into equation (2.3):

$$\Delta g = \frac{40.3}{f^2} \int N_e dl = \frac{40.3}{f^2} \cdot TEC \tag{2.4}$$

where TEC (Total Electron Content) is the total number of electrons along the path between a station and a satellite. Similarly, the carrier phase advance ($\Delta\Phi$) may be written as:

$$\Delta\Phi = \int (n_p - 1) dl = -\frac{40.3}{f^2} \int N_e dl = -\frac{40.3}{f^2} \cdot TEC \tag{2.5}$$

Therefore, from equations (2.4) and (2.5) phase measurements suffer advancement when crossing the ionosphere, i.e., a negative delay, and the code measurements suffer a positive delay. Therefore the phase ranges are measured shorter than the true geometric range between the satellite and the

receiver whereas the code pseudo ranges are measured longer than the true geometric range.

The ionospheric delay error can be eliminated for dual frequency receivers through linear combinations of observations on L1 and L2 due to the dispersive property of ionosphere layer. For precise point positioning, the ionosphere-free observation combinations are used which can remove the first order (up to 99.9 %) ionospheric effect. Equations (2.6) and (2.7) represent the traditional ionosphere-free combinations (Kouba and Héroux, 2001).

$$P_{IF} = \frac{f_{L1}^2}{(f_{L1}^2 - f_{L2}^2)} P_{L1} - \frac{f_{L2}^2}{(f_{L1}^2 - f_{L2}^2)} P_{L2} \tag{2.6}$$

$$\phi_{IF} = \frac{f_{L1}^2}{(f_{L1}^2 - f_{L2}^2)} \phi_{L1} - \frac{f_{L2}^2}{(f_{L1}^2 - f_{L2}^2)} \phi_{L2} \tag{2.7}$$

Where P_{IF} and ϕ_{IF} are the ionosphere-free code and phase observations
ϕ_{L1} and ϕ_{L2} are the carrier phase observations at L1 and L2
P_{L1} and P_{L2} are the code observations at L1 and L2
f_{L1} and f_{L2} are the carrier frequencies at L1 and L2

Single frequency receivers need to apply a model to remove the ionospheric refraction, which can reach up to few tens of meters, depending on the elevation of rays and the ionospheric conditions. The GPS users can use the Klobuchar ionospheric model to overcome the ionospheric effect whose parameters broadcasted at the time of observation with the navigation message. It can only eliminate (50-60) % of the total ionospheric error (Klobuchar, 1996). An alternative way to single frequency receivers, better than Klobuchar model, is to use Global Ionospheric Models (GIM) to eliminate the ionospheric delay. These models are available through IGS which produce final and rapid ionospheric models with different accuracy and latency as shown in Table (2.3). The results from (Chen and Gao, 2005) indicate that the global ionospheric models provided by IGS offer better performance than Klobuchar model.

Table (2.3) Global Ionospheric Models (GIM) (from IGS - http://www.igs.org/).

Type	Accuracy	Latency	Updates	Sample Interval
Final ionospheric TEC grid	2-8 TECU	~11 days	weekly	2 hours; 5 deg (lon) x 2.5 deg (lat)
Rapid ionospheric TEC grid	2-9 TECU	<24 hours	daily	2 hours; 5 deg (lon) x 2.5 deg (lat)

2.3.3 Tropospheric Error

Troposphere is the atmospheric layer placed between the earth's surface and an altitude of about 40 km (Hofmann, 2001). It is the lowest portion of the earth's atmosphere and is also where all weather takes place. The effect of the troposphere on the GNSS signals appears as an extra delay in the measurement of the signal traveling from the satellite to receiver. This delay depends on many factors such as the satellite elevation angle, atmospheric pressure, temperature and water vapor pressure as well as the location of transmitter and receiver antennas.

The troposphere, unlike the ionosphere, is a nondispersive medium with respect to radio waves and so the signal propagation is frequency independent through it. Consequently, its effect cannot be eliminated using linear combination from dual frequency observations. Hopfield (1969) shows the possibility of separating the tropospheric effect into dry and wet components as shown in Figure (2.3). The dry component is caused by the higher portion of the troposphere, due to dry gases (mainly N_2 and O_2), and accounts for about 90% of the total tropospheric delay. On the other side, the wet component is caused by the lower portion of the troposphere, due to water vapor, and accounts for about 10% of the total tropospheric delay.

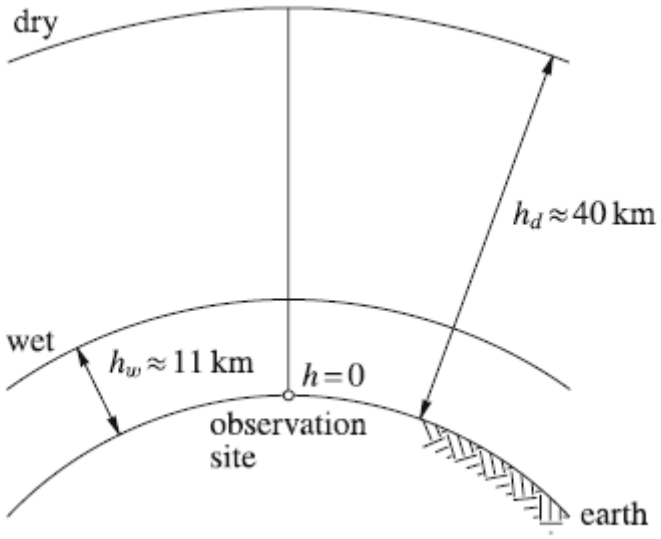

Figure (2.3) The dry and wet components of troposphere.

According to (Misra and Enge, 2001), the tropospheric delay of the dry component can be easily modeled whereas the wet component is difficult to be modeled due to the irregular variations of the liquid water and water vapor over space and time in the troposphere. The tropospheric delay depends on the signal path through the neutral atmosphere, and then can be modeled as a function of the satellite elevation angle, so it can be approximated (about 90%-95%) as following (Black and Eisner, 1984):

$$T\ (elev.) = T_{dry} * M_{dry}\ (elev.) + T_{wet} * M_{wet}\ (elev.) \quad (2.8)$$

where $T\ (elev.)$ is the tropospheric delay error

T_{dry} and T_{wet} are the tropospheric dry and wet nominal components

M_{dry} and M_{wet} are the tropospheric dry and wet mappings

The tropospheric nominal components, which corresponds to the vertical delay, can be calculated from two different methods. The simple nominal approach, which does not require any surface meteorological data, can be expressed as:

$$T_{dry} = 2.3 * \exp(-0.116 * 10^{-3} * h) \quad (2.9)$$

$$T_{wet} = 0.1 \quad (2.10)$$

Where h is the receiver height over the ellipsoid

The second method is the UNB-3 nominal approach. In this one, the tropospheric nominal obtained from the receiver's height and estimates of

five meteorological parameters: pressure, temperature, water vapor pressure, temperature lapse rate and water vapor lapse rate.

Regarding to tropospheric mapping M_{dry} and M_{wet}, which are the slant factors in order to project the vertical delay in the direction of the satellite observation for the dry and wet components, there is a simple mapping model depends only on satellite elevation and uses a common way for both dry and wet components as following (Black and Eisner, 1984):

$$M_{dry} = M_{wet} = 1.001 / \text{sqrt}\,(0.002001 + \sin^2(\text{elev})) \qquad (2.11)$$

Where elev is the satellite elevation angle and this method is valid for satellite elevation angles over 5 degrees. The other method is the Niell mapping model which does not require surface meteorological measurements and provides comparable accuracy and precision. It uses only the location of the user receiver and time of measurement and involves different obliquity factors for the wet and dry components.

There are many common global tropospheric models used to overcome the tropospheric delay such as Hopfield and Saastamoinen. The dry tropospheric component, in precise point positioning, is mitigated using a tropospheric model whereas the wet component is estimated as an unknown parameter along with the three-dimension coordinates, receiver clock offset, and ambiguities.

2.3.4 Satellite and Receiver Antenna Phase Center offset

The measurements in GNSS positioning are referred to the so-called antenna phase center. The position of the antenna phase center is not necessarily the geometric center of the antenna. Indeed, it is not constant, but it depends on the direction the radio signal coming in, elevation and azimuth and also depends on the frequency of the signal. Information from the broadcast navigation message refers to the satellite's antenna phase center and therefore, no corrections applied when using the broadcast ephemeris. Nevertheless, this correction is of paramount importance when doing precise point positioning using precise orbits and clock products.

The offset in the satellite antenna phase center arises from the distance between the mass center of the satellite and the satellite antenna phase center. Unlike the orbit ephemeris in the GPS broadcast navigation message which refers to the satellite antenna phase center, the IGS precise satellite orbits and clock products refer to the satellite center of mass due to the fact that force

models used for satellite orbit modeling refer to the satellite center of mass. Not all satellites need to consider the satellite antenna phase center offset because of the consistency of the two centers in modern satellites as in block IIR satellites in GPS. Figure (2.4) shows an example of the satellite antenna phase center offset in the satellite body fixed reference frame.

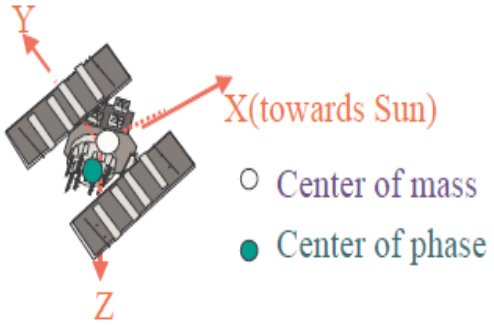

Relative GPS antenna phase center offsets adopted by IGS in satellite body fixed reference frame (m)

	X	Y	Z
Block II/IIA:	0.279	0.000	1.023
Block IIR :	0.000	0.000	0.000

Figure (2.4) Satellite antenna phase center offsets in satellite body fixed reference frame.

Since the electrical phase center of a receiver antenna that the measurements refer to is different from the center of the physical mark, the receiver antenna phase center offset needs to be taken into account in PPP. For any given GNSS receiver antenna, its phase center varies with the changing direction of the received satellite signal. The magnitude of the variation usually depends on the satellite elevation angle. The inherent azimuth has a very small effect on the phase center variation, which is usually caused by the local environment around the antenna site. Antenna calibrations may be divided into two parts (Czopek and Mader, 2002). One is the calibration for an average phase center offset with respect to a physical feature of the antenna. The other is the calibration for the phase center variation (PCV) with the elevation angel or possibly azimuth. Both parts must be conducted in the antenna calibrations. Figure (2.5) illustrates a layout of a permanent receiver site with indication of the Monument Marker (MM), Antenna Reference Point (ARP) and Antenna Phase Centre (APC).

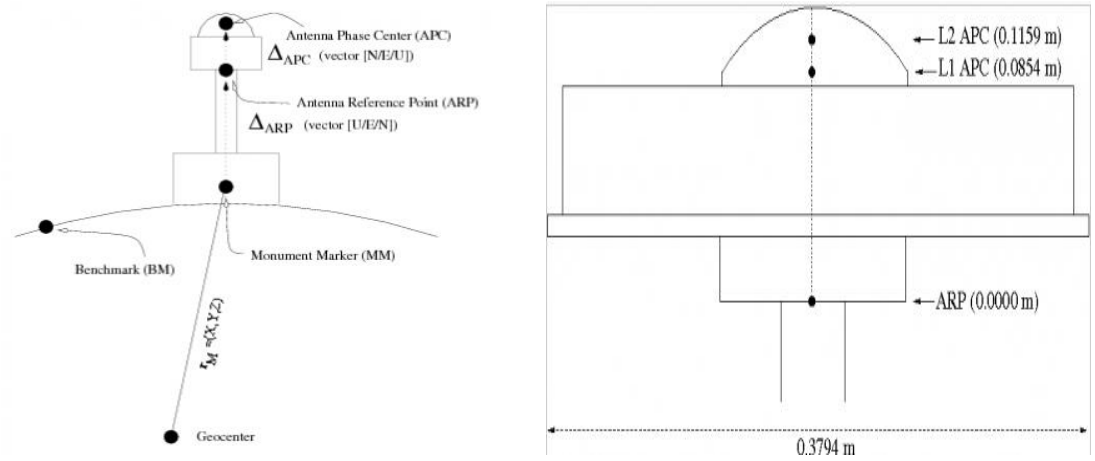

Figure (2.5) Layout of a permanent receiver site with indication of the Monument Marker, Antenna Reference Point and Antenna Phase Centre.

2.3.5 Phase Wind Up

Phase wind up correction affects only the carrier phase measurements. It is originated from the nature of the GNSS signals. The electromagnetic waves of the GNSS signals characterized by its right-handed circularly polarized feature. In differential positioning, this correction is negligible but required in high accuracy positioning as in precise point positioning as it may change the observed carrier phase up to one cycle.

The phase wind up depends on the orientation of the receiver and satellite antennas and the direction of the line-of-sight as shown in Figure (2.6). It is due to the rotation of the line-of-sight in relation to the antenna. Usually, while the receiver antenna is kept fixed in static mode or move slowly in kinematic mode, the satellite moves along its path performing a continuous reorientation to keep its solar panels pointing towards the sun direction for obtaining the maximum energy while the satellite antenna keeps pointing to the earth. This reorientation causes a phase variation that the receiver misunderstands as a range variation.

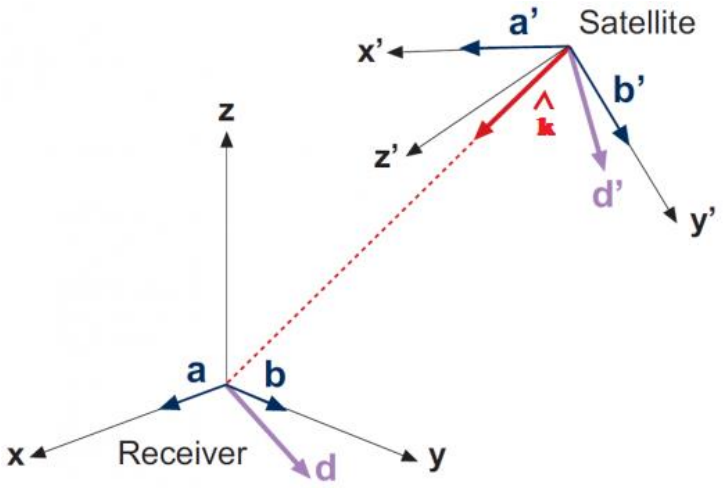

Figure (2.6) Phase wind up.

2.3.6 Solid Earth Tides

Solid earth tides affect the earth's crust movement (and thus the receiver location coordinates) due to gravitational attracting forces imposed by external bodies, mainly the sun and the moon. It produces periodic vertical and horizontal displacements on the earth that can be represented by spherical harmonics expansion. The correction of the solid earth tides which depends on site location, tide frequency and sidereal time may reach about 30 cm in the radial direction and 5 cm in the horizontal plane (Kouba and Héroux, 2001). For precise point positioning, this correction must be taken into account whereas for differential positioning over short baseline (<100 km), both stations have almost identical tidal displacements and so the relative positions will be largely unaffected by the solid earth tides.

2.3.7 Ocean Loading

Ocean loading effect is similar largely to the solid earth tides. It results from the load of the ocean tides on the underlying crust caused by the redistribution of seawater under gravitational force. It is due to the elastic response of the earth's crust to ocean tides which deformed the sea floor causing a surface displacement to adjacent lands. It is more localized and comprises of diurnal and semi diurnal components with magnitude smaller than solid earth tides. For high accuracy static and kinematic point positioning, its effect must be taken into account near the sea regions, while it can be neglected for stations far away (> 1000 km) from ocean coast lines.

2.3.8 Polar Tides

The changes of the earth’s spin axis with respect to earth’s crust, i.e. the polar motion, causes periodical deformations due to changes in the earth

centrifugal potential. This has an effect smaller than 2.5 cm in vertical and 0.7 cm in horizontal, but must be taken into account if the observations are carried out over periods longer than two months.

2.3.9 Relativistic Clock Correction

Measuring the signal flight time from the satellite to receiver is the basis of satellite positioning which depends significantly on the clocks carried on them. The rate of advance of two identical clocks, one placed in the satellite and the other on the terrestrial surface, will differ due to the difference of the gravitational potential (general relativity) and to the relative speed between them (special relativity).

The special relativity, in which the satellite clock speed appears slower than the clock on the ground due to their relative motion, can be divided into constant and periodical components. The constant component depends only on the nominal value of the semi-major axis of the satellite orbit, which is adjusted (in factory) modifying the clock oscillating frequency of the satellite. The periodical component is due to the orbit eccentricity and can be corrected as (GPS ICD, 2000):

$$\Delta_{rel} = -2\,\frac{\mathbf{r}^{sat}\cdot\mathbf{v}^{sat}}{c^2} \tag{2.12}$$

Where

Δ_{rel} is the periodical component of the special relativity effect
$\mathbf{r}^{sat}$ is the instantaneous position vector of the satellite
$\mathbf{v}^{sat}$ is the instantaneous velocity vector of the satellite
c is the speed of light

On the other hand, the general relativity in which the clock of the satellite appears to run faster than the one on the ground due to their difference in gravitational potential, can be eliminated by the following equation (Rothacher and Beutler, 2002):

$$\Delta t_p = \frac{2GM}{c^2}\ln\left(\frac{r^s + r_r + r_r^s}{r^s + r_r - r_r^s}\right) \tag{2.13}$$

Where

Δt_p is the general relativity error
G is the gravitational constant
M is the mass of the Earth
r^s is the distance between the satellite and the Earth center

r_r is the distance between the receiver and the Earth center
r_r^s is the distance from the receiver to the satellite
c is the speed of light

2.3.10 Relativistic Path Range Correction

For high accuracy satellite positioning, for PPP, all errors despite its diminutive value must be taken into consideration. The relativistic path range effect is a secondary effect which affects the range by an error less than 4 cm and therefore, for most purposes it can be neglected. This effect is named the Shapiro signal propagation delay and introduces a general relativistic correction to the geometric range due to the space-time curvature produced by the gravitational field. Consequently, the geometric range must be corrected by an amount given by the expression:

$$\Delta\rho_{rel} = \frac{2\mu}{c^2} ln \frac{r^{sat} + r_{rcv} + r_{rcv}^{sat}}{r^{sat} + r_{rcv} - r_{rcv}^{sat}} \quad (2.14)$$

Where

r^{sat} is the geocentric distance of the satellite
r_{rcv} is the geocentric distance of the receiver
r_{rcv}^{sat} is the distance between the satellite and the receiver
c is the speed of light
μ is a gravitational constant

A summary of the previous mentioned observation errors, their magnitudes and mitigation strategies is provided in Table (2.4).

Table (2.4) Error sources, magnitudes and corresponding mitigation methods in PPP (Junbo Shi, 2012).

	Error terms	**Magnitude**	**Mitigation methods**
Satellite Related Errors	Satellite orbit and clock	~ 100 cm orbit ~ 2.5 ns clock	Precise IGS satellite orbit/clock products
	Relativistic effect	Up to 13 m	Model correction
	Satellite antenna phase center correction	~ 3 m offset ~ 5 mm variation	IGS ANTEX file
	Phase wind-up	2 ~ 4 cm Sometimes up to one cycle	Model correction

Propagation Related Errors	Troposphere	~ 2.3 m zenith delay	- Zenith hydrostatic delay modeling - Zenith wet delay estimation
	Ionosphere	up to 14 m zenith delay	- Precise IGS IONEX models - Ionosphere free Linear combination
	Relativistic Path Range Correction	Up to 4 cm	Model correction
Receiver Related Errors	Receiver antenna phase center correction	up to 20 cm offset ~ 4 mm variation	IGS ANTEX file
	Receiver clock error	up to 1 ms	Estimation for each epoch
	Solid earth tides	up to 12 cm radial and 5 cm north directions	Model correction
	Polar tides	up to 25 mm vertical and 7 mm horizontal directions	Model correction
	Ocean loading	up to 5 cm radial and 2 cm horizontal directions	Model correction
	Earth rotation parameters	~ 3 cm	Model correction

After talking about different sources of errors in PPP with techniques to overcome, chapter 3 will describe how to incorporate these mitigation methods in the PPP processing procedure.

CHAPTER THREE

PROCESSING STRATEGY OF PRECISE POINT POSITIONING (PPP)

3.1 PPP Mathematical Model

The goal of PPP technique is to determine the receiver coordinates, receiver clock offset and other unknown parameters using single receiver from pseudo range and carrier phase observations. The precise point positioning principle is based on solving a geometric problem from the measured ranges and carrier phases to the satellites, with precise known coordinates of the satellites and modelling imperfect path between receiver and satellite as shown in Figure (3.1).

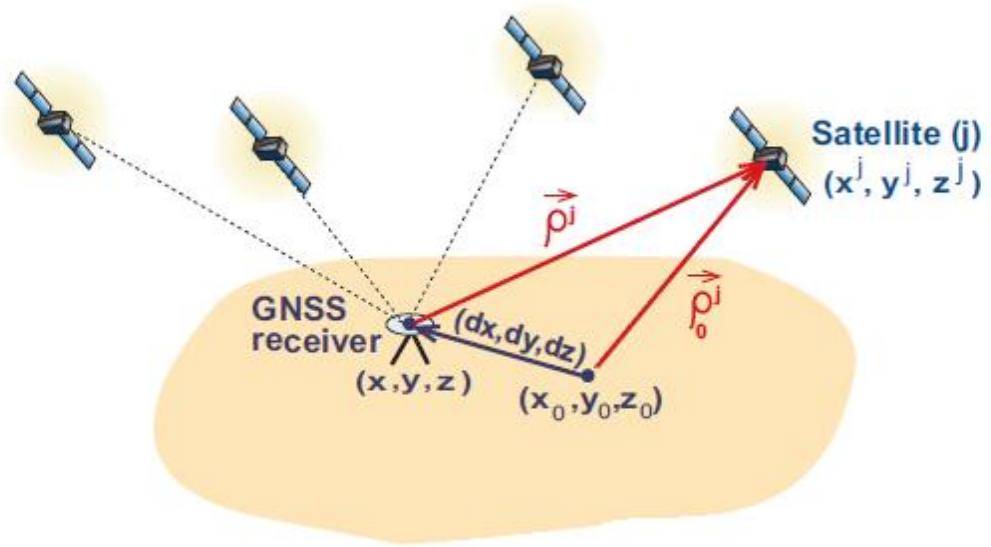

Figure (3.1) Geometric problem in PPP technique (J. Sanz Subirana et al, 2013).

In general, the code pseudo range and carrier phase observations on L1 and L2 between a receiver and a satellite can be described as following in equation (3.1) (Changsheng Cai, 2009):

$$P_i = \rho + c\,.dt - c\,.dT + d_{orb} + d_{trop} + d_{ion/P_i} + d_{mult/P_i} + \varepsilon_{P_i}$$
$$\Phi_i = \rho + c\,.dt - c\,.dT + d_{orb} + d_{trop} - d_{ion/\Phi_i} + \lambda_i.N_i + d_{mult/\Phi_i} + \varepsilon_{\Phi_i} \quad (3.1)$$

where,

P_i is the measured pseudo range on L_i (m)
Φ_i is the measured carrier phase on L_i (m)
ρ is the true geometric range (m)
c is the speed of light (m/s)
dt is the receiver clock error (s)

dT is the satellite clock error (s)
d_{orb} is the satellite orbit error (m)
d_{trop} is the tropospheric delay (m)
d_{ion} is the ionospheric delay on L_i (m)
λ_i is the wavelength on L_i (m/cycle)
N_i is the integer phase ambiguity on L_i (cycle)
d_{mult/P_i} is the multipath effect in the measured pseudo range on L_i (m)
d_{mult/Φ_i} is the multipath effect in the measured carrier phase on L_i (m)
ε is the measurement noise (m)

On the other hand, the observation PPP model uses the ionosphere-free combinations between code measurements from L1 and L2 data as well as between carrier phase observations on L1 and L2 which are the most popular form used in PPP to mitigate the effect of the ionosphere error (Changsheng Cai, 2009). So, the PPP model has the form of the ionosphere-free code and phase observation combinations as expressed below in the unit of length (Shen, 2002):

$$P_{IF} = \frac{f_1^2 .\ P_1 - f_2^2 .\ P_2}{f_1^2 - f_2^2} = \rho + c(dt - dT) + d_{orb} + d_{trop} + d_{mult/P_i} + \varepsilon_{P_i}$$

$$\Phi_{IF} = \frac{f_1^2 . \Phi_1 - f_2^2 . \Phi_2}{f_1^2 - f_2^2} = \rho + c(dt - dT) + d_{orb} + d_{trop} + \frac{c\, f_1\, N_1 - c\, f_2\, N_2}{f_1^2 - f_2^2} + d_{mult/\Phi_i} + \varepsilon_{\Phi_i} \qquad (3.2)$$

Where P_{IF} and Φ_{IF} are the ionosphere free code and carrier phase combinations and f_1 and f_2 are frequency of carriers L_1 and L_2 respectively. The parameters estimated in the PPP model include three dimensional position coordinate, one receiver clock offset, one zenith wet tropospheric delay error, and the combined ambiguity parameters associated with each observed satellites.

3.2 PPP Strategy

The Precise Point Positioning (PPP) technique depends on a sequential steps as shown in Figure (3.2). The technique needs at first the RINEX observation file, ANTEX, precise Differential Code Bias (DCB) file as well as the precise orbits and clock products. The second step includes the preprocessing process in which the elevation mask is predefined, RINEX observation file is edited and quality checked and cycle slips are detected. The modelling of not perfect conditions obstruct the

signal travel path is the third step. Filtering and adjustment is the most critical one in PPP technique at which the Kalman filter procedure is implemented. Finally outputs are assessed and analyzed relative to a reference solution.

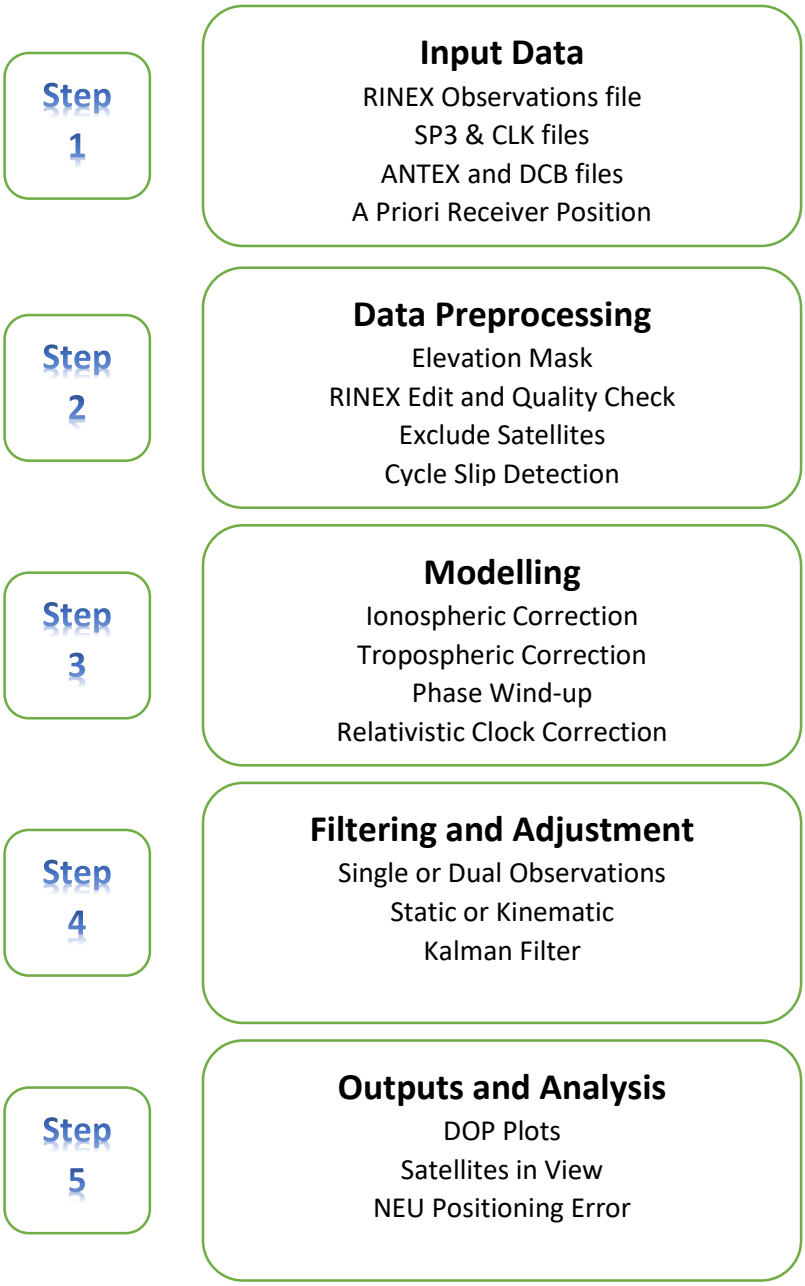

Figure (3.2) PPP processing strategy.

3.3 Input Data

In this part we will discuss most of allowable input files needed to do PPP in both static and kinematic modes. These inputs can be a variety of standard formats like RINEX, ANTEX, SP3, SINEX and IONEX files.

3.3.1 RINEX observation file

In 1989, W. Gurtner of the Astronomical Institute of the University of Berne, Switzerland, outlined the RINEX, Receiver Independent Exchange, format to facilitate the exchange of the GPS data of different receiver types (ftp://ftp.unibe.ch/aiub/rinex/). The observation and navigation files are the most commonly used RINEX (ASCII) file types. The observation file, basically used for precise point positioning, contains the carrier phases, code ranges, Doppler measurements, and signal-to-noise ratios, while the navigation file used for Standard Positioning Service contains the ephemeris data of the satellites. Observations from different GNSS are entitled using a character such as 'G' for GPS, 'R' for GLONASS, 'E' for Galileo, and 'S' for SBAS satellites. Temporarily, RINEX has been updated several times adapting to different developments in GNSS signals and also applications. The most common version at present is 2.11 (https://en.wikipedia.org/wiki/RINEX), which enables storage of measurements from GPS (including GPS modernization signals e.g. L5 and L2C), GLONASS, Galileo, Beidou, along with data from EGNOS and WAAS satellite based augmentation systems (SBAS), QZSS, simultaneously. The current recent version is RINEX 3.03 published in July 2015.

3.3.2 SP3 and CLK files

The SP3 and CLK files contain the orbits and clocks of the satellites at specific times. The SP3 includes the most precise orbital information for the satellites which provided by the IGS, while the CLK file provides a higher rate of the clocks and a higher rate processing steps. The precise ephemeris consists of satellite positions and velocities at equidistant epochs and typical spacing of the data is 15 minutes (Bernhard Hofmann-Wellenhof et al., 2008). The position and velocity data between the given epochs are achieved by interpolation where, as an example, the Lagrange interpolation based on polynomial base functions is used. IGS provides its users free of charge different categories of clock file. It can be 15 or 5 minutes and also provides clocks with higher rate like 30 and 5 seconds (derived by CODE analysis center) clock data for a higher update rate of station observations.

3.3.3 ANTEX and IONEX files

Satellite and receiver antenna phase center corrections are provided in the Antenna Exchange (ANTEX) format which is defined in a separate format specification. It contains the absolute IGS phase center corrections for satellite and receiver antennas to be used with the IGS08 terrestrial reference frame which is closely related to, but not identical with ITRF2008 because the latter is based on igs05.atx antenna phase center corrections (ftp://igs.org/pub/station/general/). The latest version is

symbolically linked to the generic filename 'igs08_1890.atx' where 1890 is the current GPS week. The IGS network was used to extract information about the Total Electron Content (TEC) of the ionosphere on a global scale. Since 1998, IGS associate analysis centers have provided products containing ionosphere vertical total electron content maps derived from the dual-frequency GPS data. These ionosphere products are available in a rapid solutions with a latency of less than 24 hours, a final solution with a latency of approximately 11 days, and a predicted solution, available both one and two days prior. Ionosphere products are provided in IONEX (IONosphere ECchange) format. IONEX files is basically needed for precise point positioning where only single frequency observations are available.

3.3.4 A Priori Receiver Position

A priori receiver position is the initial receiver position used for linearizing the filter and to obtain the values for the models. As an example, we will take about different options available for this a priori position in the glab software. Firstly, we can get a priori receiver position using the APROX POSITION XYZ field of the RINEX observation file as shown in Figure (3.3). Secondly, the receiver position in XYZ components in meters can be specified if we know it. Thirdly, when using IGS sites, a priori receiver position can be found for the IGS site from a SINEX (Solution Independent Exchange) file where matching takes place between the observation RINEX header record MARKER NAME with the marker position present in the SINEX file. In case of kinematic positioning no a priori receiver position is required as it is calculated automatically in the Kalman filter computations.

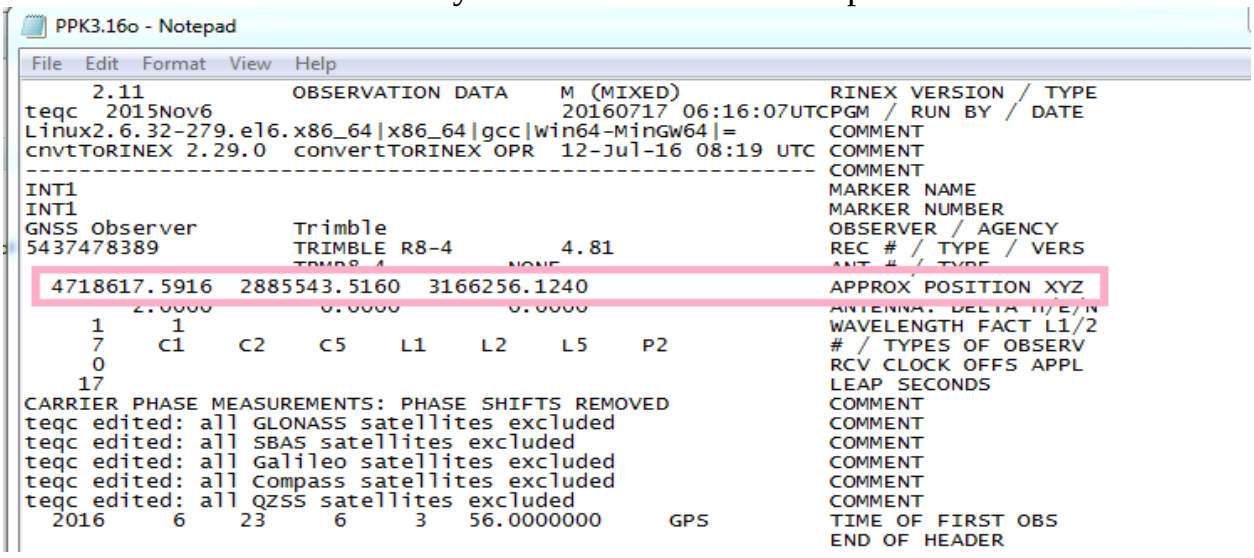

Figure (3.3) Approximate receiver position from RINEX observation file.

3.3.5 Differential Code Biases (DCB)

Differential Code Biases (DCB) are the delays due to electronic, antennas and cables of receiver and transmitter devices which directly affect the measurements with a bias. In Precise Point Positioning, this effect can be corrected using the information extracted from Precise DCB files distributed for free from the IGS organization.

3.4 Data Preprocessing

In this part explanation of some preprocessing options will be given for the input data discussed in earlier section. In particular, these options include changing the decimation rate, the elevation mask, the cycle-slip detection and selecting individual satellites for the processing. The data decimation option allows to decimate the input data at a specified rate at which every time an epoch is found in the input RINEX observation file, all the processing takes place. Even in decimated data, all the epochs are used for cycle slip detection, and arc length computations, but the process is stopped just before the modeling. This option is intended to be used to reduce computation time.

One of the most important parameters in data preprocessing options is the elevation mask. It is used to discard all the satellites below a specified elevation angle where low elevation satellites should be discarded for geodetic processing as they may contain increased errors due to low signal-to-noise ratio and multipath. In the next part a quick look will be taken on the preprocessing software, TEQC, and some methods for cycle slip detection.

3.4.1 TEQC

TEQC is a simple powerful toolkit for resolving many preprocessing problems with GNSS data. It can read GNSS native receiver files and translate the data to other formats, edit and/or correct of RINEX header metadata records as well as cut/splice of RINEX files (L. H. Estey and C. M. Meertens, 1999). One of its capabilities is quality checking of GPS and/or GLONASS data (native binary, BINEX, or RINEX observation files, with or without navigation files). TEQC is provided at no cost by UNAVCO (https://www.unavco.org/software/), as executable binaries for common processors. It is a command line program and not a GUI as shown in Figure (3.4).

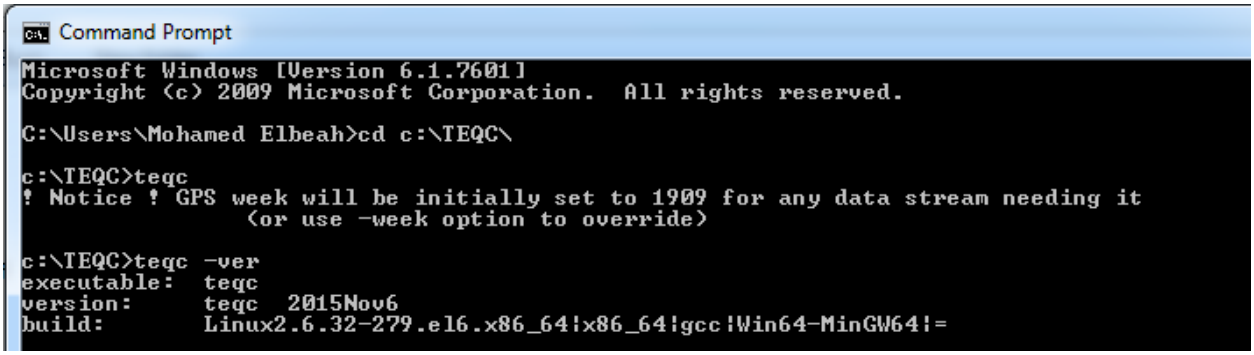

Figure (3.4) TEQC command line.

Figure (3.5) shows how to use TEQC to get a summary of how many observations are in a RINEX file. It is cleared in the figure which SVs are tracked, the types of observations (such as L1 and L2) and a count of the observables for each type for each SV.

```
c:\TEQC>teqc -O.sum . PPK31750.16o
! Notice ! change of antenna topocentric correction
! Notice ! change of monument name from 'INT1' to 'INT11' in 'PPK31750.16o'
! Notice ! change of monument number from 'INT1' to 'INT11' in 'PPK31750.16o'
          C1     C2     C5     L1     L2     L5     P2
         ----   ----   ----   ----   ----   ----   ----
   G05   6706   6585      0   6599   6585      0   6384
   G07   2266   2249      0   2249   2249      0   2245
   G13  13652      0      0  13593  12910      0  12910
   G15  16827  16795      0  16800  16796      0  16584
   G17  13623  13514      0  13546  13516      0  13156
   G19  17379      0      0  17344  16890      0  16890
   G20   6100      0      0   6049   5955      0   5955
   G28   9908      0      0   9833   8819      0   8819
   G30   6634   6572   6576   6587   6572   6576   6403
   G24  18690  18655  18655  18655  18655  18655  18650
   G12  16532  16526      0  16526  16526      0  16503
   G06  14918  14751  14748  14758  14753  14748  14603
   G02  12272      0      0  12232  12166      0  12166
   G25   9581   9414   9433   9434   9423   9433   9284
   G29   7907   7853      0   7868   7862      0   7776
   G32   6167   5865   5926   5929   5893   5926   5608
   G14   4227      0      0   3894   3279      0   3279
   R06   3865   3865      0   3865   3865      0   3858
   R07   7938   7928      0   7928   7919      0   7926
   R08  10876  10835      0  10845  10833      0  10840
   R09  14554  14259      0  14522  14497      0  14517
   R16   4995   4353      0   4941   4849      0   4841
   R18   4630   4610      0   4622   4599      0   4610
   R19  11102  11065      0  11073  11052      0  11056
   R20  17123  17034      0  17054  17022      0  17030
   R01   8141   8081      0   8095   8060      0   8077
   R21  13986  13980      0  13983  13976      0  13980
   R11  13049      0      0  13021      0      0      0
   R22   8401   8385      0   8385   8383      0   8384
   R12   3436   1895      0   3176   3163      0   3175
   R23   1715   1650      0   1670   1642      0   1623
```

Figure (3.5) Summary of how many observations are in a RINEX file using TEQC.

Figure (3.6) displays, as an example, the results of a quality check of a RINEX observation file using TEQC. Shown in Figure (3.6), the release date of the TEQC version, a time plot displays signal quality indicators by time for each SV in the data file, the top of the plot shows time bin divisions and labels the column which has SV PRN numbers and a corresponding time scale with start and end time values at the bottom of the plot. The symbols presented in the time plot point to successes or problems. Each symbol refers to a specific indication such as symbol I indicates to an ionospheric phase slip, symbol N refers to no qc done although existed data and symbol o indicates normal good dual frequency GPS data with phase and code pseudo range.

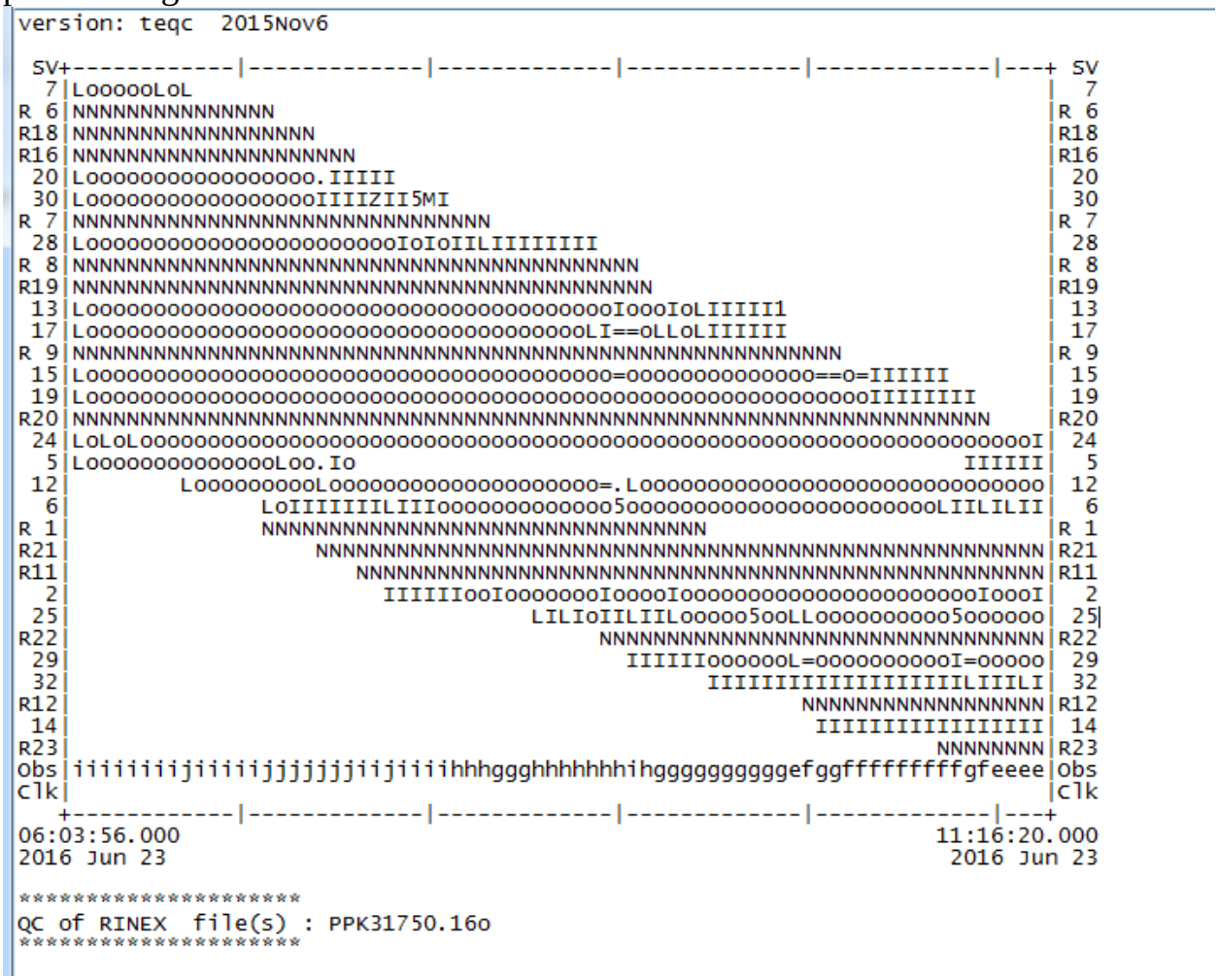

Figure (3.6) Output of a quality check of a sample RINEX observation file using TEQC.

3.4.2 Cycle Slip Detection

Cycle slips occur when receiver losses of signal lock causing discontinuities in the phase measurements which are seen as jumps of integer numbers of wavelengths and so the integer ambiguity N changes by an arbitrary integer value. These jumps

are restricted to phase measurements. According to (Bernhard Hofmann-Wellenhof et al., 2008), Figure (3.7) shows a schematic representation of a cycle slip. There are many sources for cycle slips that can be distinguished like those caused by obstructions of the satellite signal due to buildings, trees, mountains, bridges, etc. This source is the most common one particularly for kinematic activities based upon the carrier phase. Another source for cycle slips is a low signal to noise (S/N) ratio due to bad ionospheric conditions, high receiver dynamics and multipath or low satellite elevation. Cycle slips could also be caused due to a failure in the receiver software which leads to incorrect signal processing. As shown in Figure (3.7), detection and repair of cycle slip requires the location of the jump and the determination of its size. Detection is accomplished by a testing quantity and repairs of cycle slips are made by correcting all subsequent phase observations for this satellite and this carrier by a fixed integer number of cycles.

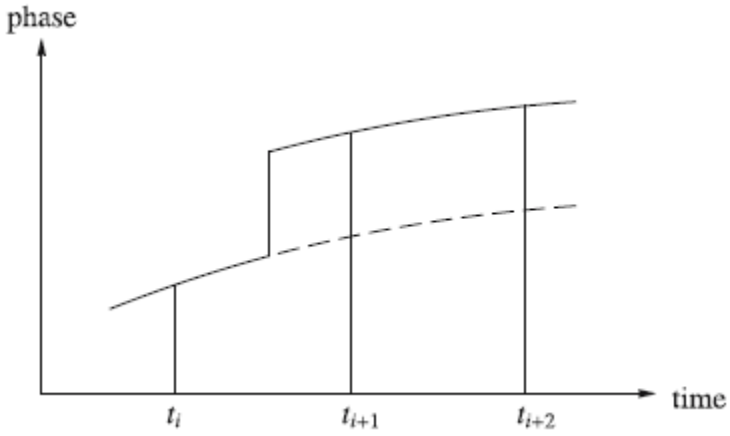

Figure (3.7) A schematic representation of a cycle slip (Hofmann-Wellenhof et al., 2008).

Different empirical methods are used for cycle-slip detection, operating over undifferenced, single differenced or double differenced measurements between pairs of satellites and receivers. In this part we will present methods that are related to single receiver positioning, and thus do not require any differencing of data between receivers, being suitable for implementation in real time. Additionally, they are based on using only combinations of measurements at different frequencies, or just one frequency measurements.

3.4.2.1 The Geometry-Free Carrier Phase Combination

This cycle slip detector is implemented for dual-frequency receivers using only carrier phase measurements. It forms a geometric-free combination which shall be affected by ionosphere and will follow its shape with a second order interpolator. In this type, carrier phase measurements of signals at two different frequencies are

subtracted in order to remove the geometry, including clocks, and all non-dispersive effects. This detector, in non-disturbed conditions with very low noise, gives a very precise test signal and provides a reliable detection even for small jumps although it is affected by the ionospheric refraction. Though, this effect varies as a smooth function and can be modelled by a low-degree polynomial fit but, high ionospheric activity conditions can reduce the performance of this detector, mainly with low sampling rate data.

According to (J. Sanz Subirana et al., 2013), for easier way to build a cycle-slip detector, it is important to consider the differences in time of consecutive samples as shown in Figure (3.8). An enhancement of this process is the use of nth-order differences to take benefit of the jump amplitude enlargement produced by the differencing process.

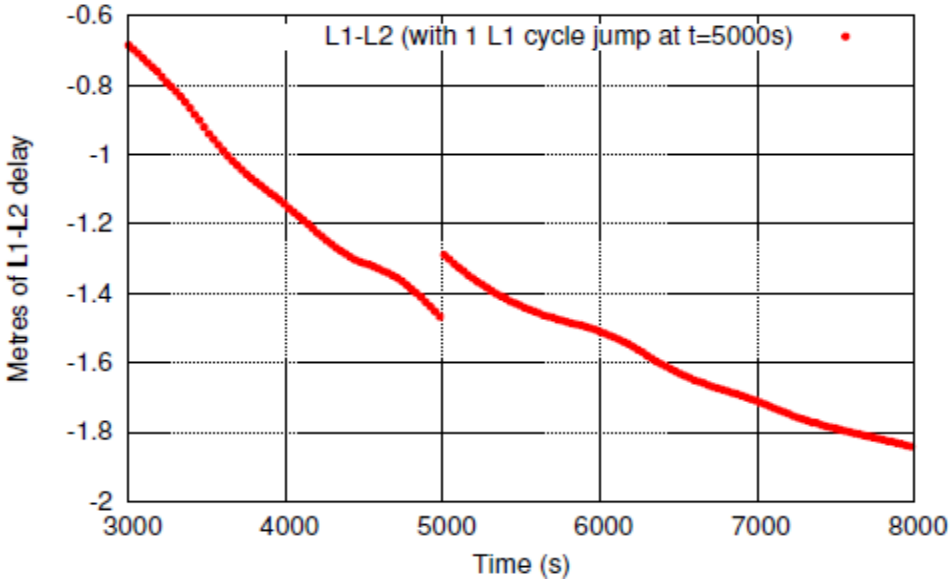

Figure (3.8) Effect of a cycle slip in the carrier phase measurements (J. Sanz Subirana et al., 2013).

Table (3.1) illustrates a computational scheme of such differences between consecutive carrier phase measurements. This approach lets us to make a realistic enough detector for many applications. Nevertheless, it must be considered that, as the jumps are enlarged, also the signal noise is amplified, which can lead to incorrect detections in some scenarios (for instance, with low signal-to-noise ratios, large ionospheric gradients, etc.). One way to mitigate the impact of these effects is to use a low-order polynomial fit, reducing the test signal noise.

Table (3.1) A computational scheme of differences between consecutive carrier phase measurements: a jump in amplitude ε happens at time t_4 (Hofmann-Wellenhof et al., 2008).

t_i	$y(t_i)$	Δy	$\Delta^2 y$	$\Delta^3 y$	$\Delta^4 y$
t_1	0				
		0			
t_2	0		0		
		0		ϵ	
t_3	0		ϵ		-3ϵ
		ϵ		-2ϵ	
t_4	ϵ		$-\epsilon$		3ϵ
		0		ϵ	
t_5	ϵ		0		$-\epsilon$
		0		0	
t_6	ϵ		0		
		0			
t_7	ϵ				

3.4.2.2 L1-C1 Difference

This cycle slip detector is used for single frequency receivers. It is based only on data measurements of a single receiver and uses the difference between L1 and C1. This difference encloses basically sudden jumps coming from cycle-slips, noise coming from C1 and an ionospheric divergence with time, due to the different effects that the ionosphere causes in carrier phase and pseudo range measurements. It is a simple approach suitable for running in real time, but with a worse performance than the two frequency detectors. This detector is based on computing the mean and standard deviation of the code pseudo range and carrier phase (L1-C1) difference along the epochs, proving a window to limit the divergence. A cycle slip is declared when the expected mean value is compared against the obtained one and if it is higher than a specific threshold.

3.5 Modelling

The PPP technique allows centimeter level accuracy to be attained for static positioning and decimeter level, or better, for kinematic positioning. This high accuracy necessitates precise measurement modelling, where all model terms described in the previous chapter must be taken into account up to centimeter level or better. Most of PPP errors, except for troposphere, receiver clock and ionosphere delay, can to some extent be mitigated through modeling. The receiver clock error and tropospheric delay can be estimated as unknown parameters, while ionospheric delay can be removed through ionosphere-free observations combinations.

3.6 Parameter Estimation for PPP in glab Tool

This part is devoted to estimating the receiver's position along with other unknown parameters in PPP technique. As the measurements are noisy (receiver noise, multipath) and the applied models are not perfect, adjustment and filtering

techniques are required for parameter estimation. The Kalman filter can be used to solve the PPP observation model taking into account the carrier phase biases as constant along continuous phase arcs and as white noise at those instants when cycle slips occurs.

For instance, there are three configuration options in glab tool for all unknown parameters, Phi, Q, and P_0 (Sanz, J. et al., 2012). Phi sets the propagation of parameters between epochs. The value of 1 means that the value estimated in the epoch i+1 is used as apriori value in the epoch i and the value of 0 means that the apriori value is always 0. The process noise parameter Q sets the stability of a parameter along time. The process noise of 0 means that the parameter is a constant. While, P_0 sets the initial values for all parameters**.** Figures (3.9) and (3.10) display the configuration options for all unknown parameters in PPP using Kalman filter procedure in static and kinematic modes respectively in glab software.

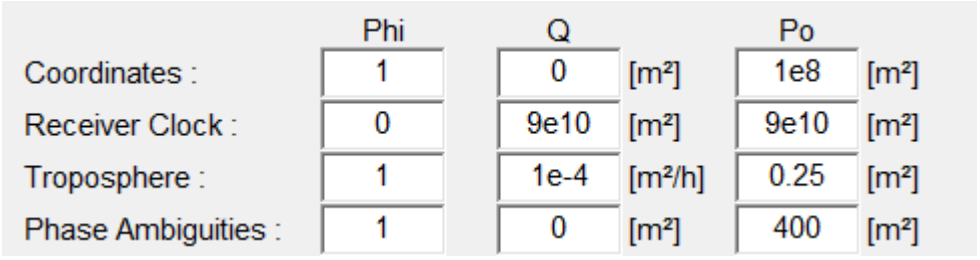

Figure (3.9) Configuration options for unknown parameters in static PPP in glab software.

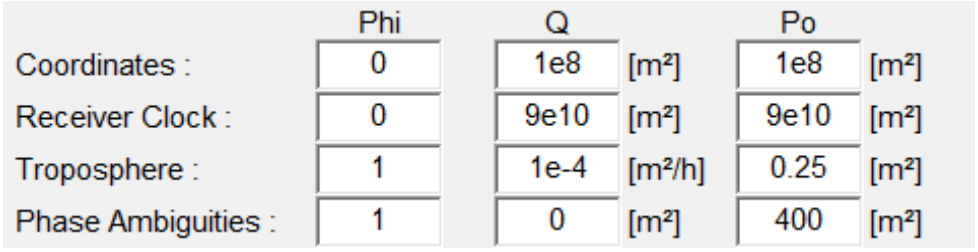

Figure (3.10) Configuration options for unknown parameters in kinematic PPP in software.

For static PPP the coordinates are taken as constants, whereas for kinematic PPP the coordinates are taken as white noise process. The above solution method is called floating ambiguity procedure that the ambiguities are estimated by the filter as real numbers. Generally, expected errors at the decimeter level, or better, in kinematic positioning and at the centimeter level in static PPP can be after a best part of one observation hour.

3.7 Outputs & Analysis

Outputs gained after filtering and adjustment step can be assessed and analyzed relative to a reference solution. With the glab tool we can use configured templates to display the quality of the results for a specific condition. As for example, the NEU position error template at which the three components (North, East and Up) of the error of the receiver position obtained by the filter can be displayed as in Figure (3.11). Also, Figures (3.12) and (3.13) display the DOP values and the number of satellites in view respectively during the time of observations.

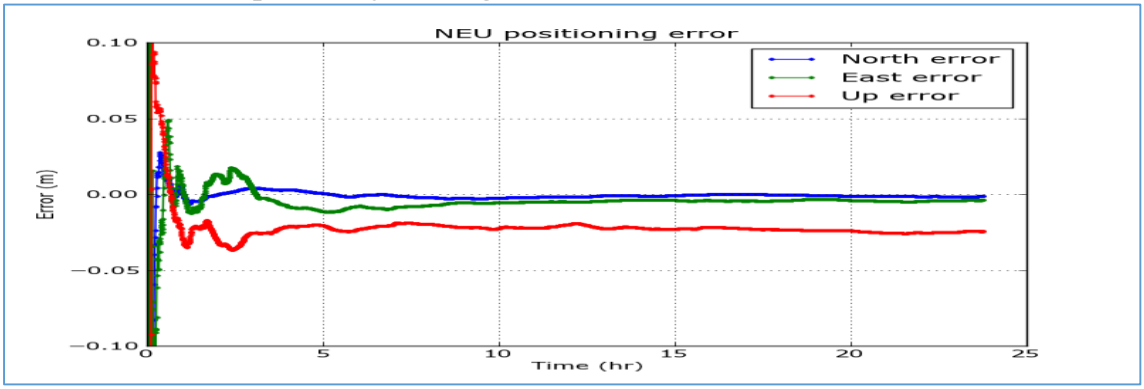

Figure (3.11) Positioning error results in NEU components in static PPP using glab.

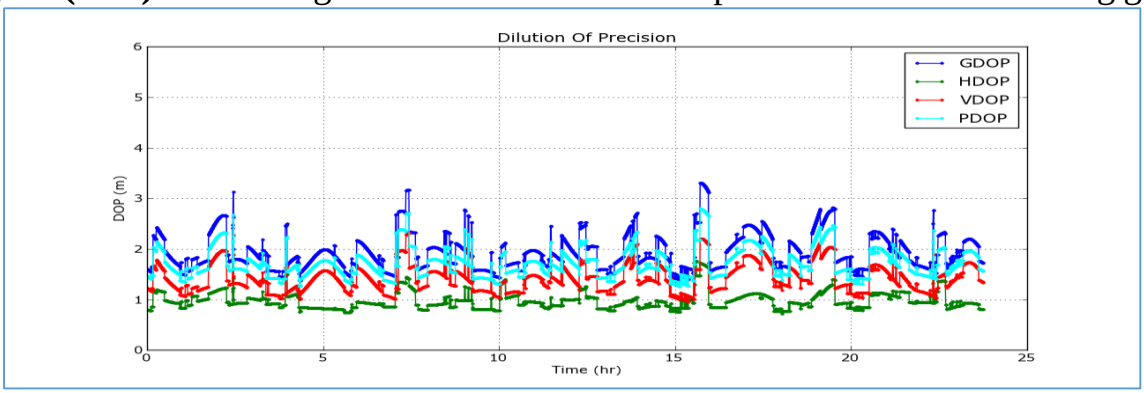

Figure (3.12) Dilution of Precision (DOP) values in glab.

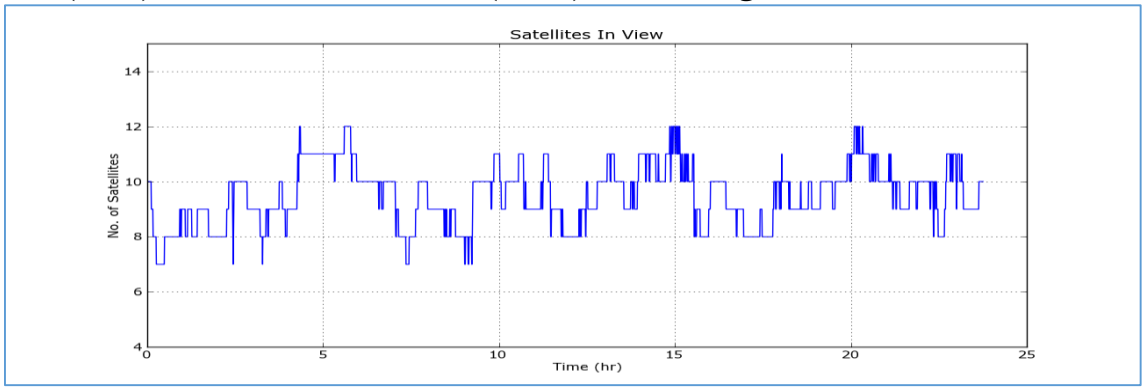

Figure (3.13) Number of GPS satellites in view in glab.

After what we listed earlier in this chapter about the processing strategy of PPP from input files, preprocessing options, modeling, adjustment to potential outputs, Figure (3.14) displays a flow chart for different processing routes of static and kinematic PPP achieved in the research.

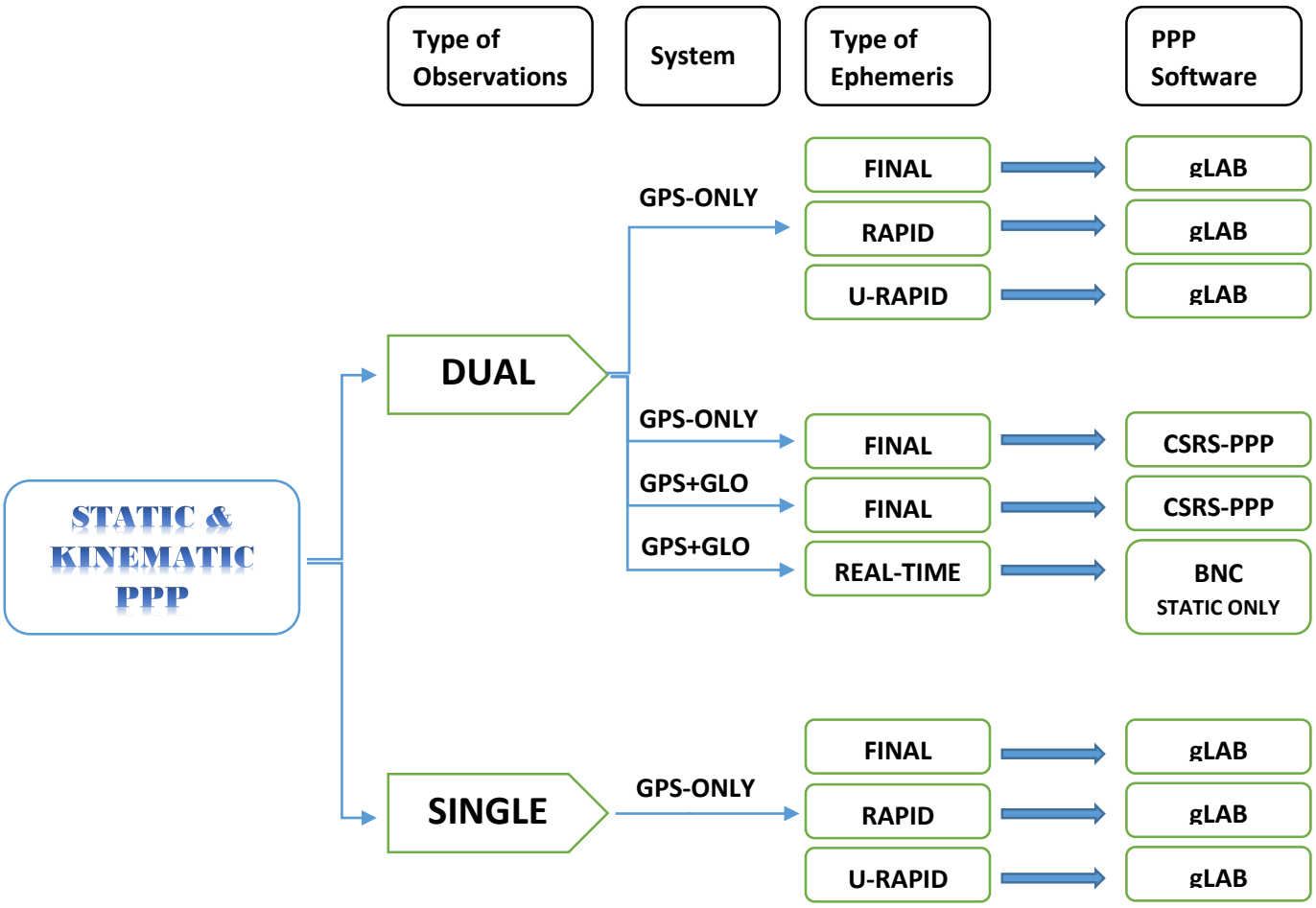

Figure (3.14) Flow chart of different processing routes for static and kinematic PPP.

In the next chapter, the different routes will be described in details. Different types of observations such as dual and single ones will be used. Static and kinematic data will be processed in post processing using glab software and CSRS-PPP online service. Also, PPP will be assessed using various categories of precise ephemeris, final, rapid and ultra-rapid ephemeris.

CHAPTER FOUR

RESULTS AND ANALYSIS

In this chapter, the performance of PPP technique in static and kinematic modes will be assessed using different types of precise ephemeris (orbits & clock products) through different types of observations, single and dual frequency measurements, in post processed mode. Also, we will do an experiment of Real-Time Precise Point Positioning (RT-PPP). Several computations were conducted and their results are presented in this chapter. Performance assessment has been done using different types of ephemeris products such as:

i. **IGS Final products (IGS)** The IGS Final products have the highest quality and internal consistency of all IGS products. They are made available on a weekly basis, by each Friday, with a delay up to 13 (for the last day of the week) to 20 (for the first day of the week) days (http://www.igs.org/). The IGS Final products are the basis for the IGS reference frame and are intended for those applications demanding high consistency and quality.

ii. **IGS Rapid products (IGR)** The IGS Rapid products have a quality nearly comparable to that of the Final products. They are made available on a daily basis with a delay of about 17 hours after the end of the previous observation day; i.e., the IGS Rapid products are released daily at about 17:00 UTC (http://www.igs.org/).

iii. **IGS Ultra-rapid products (IGU)** The Ultra-rapid products are available for real time and near real time use. The ultra-rapid observed half products will be used in PPP processing. They released four times per day, at 03:00, 09:00, 15:00, and 21:00 UTC (http://www.igs.org/).

Table (4.1) explains accuracy, latency and sample interval of different types of GPS satellite ephemerides and satellite clocks provided by the International GNSS Service (IGS) that were used in the research. Besides products presented in Table (4.1), the IGS launched Real-Time Service (RTS) to support applications requiring real-time access to IGS products. RTS is a GNSS orbit and clock correction service that enables precise point positioning (PPP) and related applications at worldwide scales.

4.1 The PPP Software

Three different PPP software packages were applied to complete all practical work. The first one is gLAB tool which developed by the research group of Astronomy and Geomatics (gAGE) from the Universitat Politecnica de Catalunya (UPC), Spain (http://gage.upc.edu/). The second is NRCan-PPP software through CSRS-PPP online service operated by the Geodetic Survey

Division of Natural Resources, Canada (http://www.nrcan.gc.ca/). The BKG Ntrip Client (BNC), Germany, is the third software used in our research. It is an Open Source multi-stream client program designed for a variety of real-time GNSS applications (https://igs.bkg.bund.de/ntrip/bnc). In the coming sections we will give a brief description on each software and all processing results from each one.

Table (4.1) GPS Satellite Ephemerides / Satellite & Station Clocks (from IGS [http://www.igs.org/]).

Type		Accuracy	Latency	Updates	Sample Interval
Broadcast	orbits	~100 cm	real time	--	daily
	Sat. clocks	~5 ns RMS ~2.5 ns SDev			
Ultra-Rapid (observed half)	orbits	~3 cm	3 - 9 hours	at 03, 09, 15, 21 UTC	15 min
	Sat. clocks	~150 ps RMS ~50 ps SDev			
Rapid	orbits	~2.5 cm	17 - 41 hours	at 17 UTC daily	15 min
	Sat. clocks	~75 ps RMS ~25 ps SDev			5 min
Final	orbits	~2.5 cm	12 - 18 days	every Thursday	15 min
	Sat. clocks	~75 ps RMS ~20 ps SDev			Sat.: 30s

4.2 Data Collection

For static assessment, GNSS observation datasets collected on Wednesday, March 11, 2015 at GPS week 1835 from twelve IGS permanent stations, including GLPS, NICO, KIRU, ALIC, IRKJ, ISPA, KOKB, LHAZ, PDEL, STHL, UNBJ and YSSK, were used for the numerical computations for static PPP assessment. These stations are equipped with dual frequency receivers. In addition to these sites, a station SFE1 established at the roof of Faculty of Engineering at Shoubra, Cairo, Egypt and continuous observations were taken from this site at the same previous time span over the GPS week 1835 (7 days of observations). Table (4.2) shows a list of these stations as well as the receiver and antenna types. Figure (4.1) shows the geographic locations of stations used in this analysis.

In this study, daily GPS datasets at 30 second sampling interval were used in processing. The precise satellite orbit and clock products generated by the analysis center at CDDIS (Crustal Dynamics Data Information System) were used to eliminate the satellite orbit and clock errors. The elevation cut-off angle was set to 7°. Daily PPP coordinates were estimated for each station

and compared with the reference position of each station. The reference coordinates were obtained from the IGS weekly reference frame solutions for each station in SINEX format.

Table (4.2) List of reference stations and their receiver and antenna types used in static PPP assessment.

Station	Receiver type	Antenna type
GLPS	JAVAD TRE_G3TH DELTA	ASH701945B_M SCIT
NICO	LEICA GR25	LEIAR25.R4 LEIT
KIRU	SEPT POLARX4	SEPCHOKE_MC SPKE
SFE1	TRIMBLE R8	TRMR8_GNSS3
ALIC	LEICA GR25	LEIAR25.R3 NONE
IRKJ	JPS LEGACY	JPSREGANT_SD_E NONE
ISPA	ASHTECH UZ-12	ASH701945E_M SCIT
KOKB	ASHTECH UZ-12	ASH701945G_M NONE
LHAZ	TPS E_GGD	ASH701941.B SNOW
PDEL	LEICA GRX1200GGPRO	LEIAT504GG NONE
STHL	TPS NET-G3A	TPSCR.G3 SCIS
UNBJ	TPS LEGACY	TRM57971.00 NONE
YSSK	ASHTECH Z-XII3	ASH701933B_M

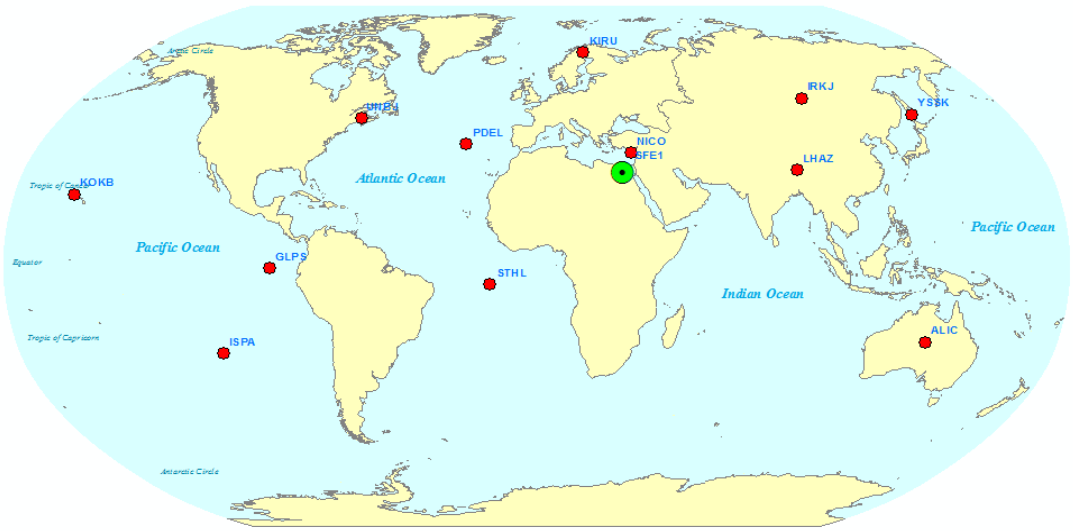

Figure (4.1) Geographic locations of stations used in static PPP analysis.

Regarding station SFE1 that created at the roof of Faculty of Engineering at Shoubra, the fixed coordinates for this site come from fixing it with three nearby IGS stations RAMO, DRAG and NICO as shown in Figure (4.2). The observation process at station SFE1 continued seven days at GPS week 1835 and then every day was processed individually with the IGS sites as displayed in Figure (4.3). The GPS network as in Figure (4.3) adjusted with

fixing only two control stations, RAMO and DRAG, while leaving station NICO to be as a check point for adjustment results.

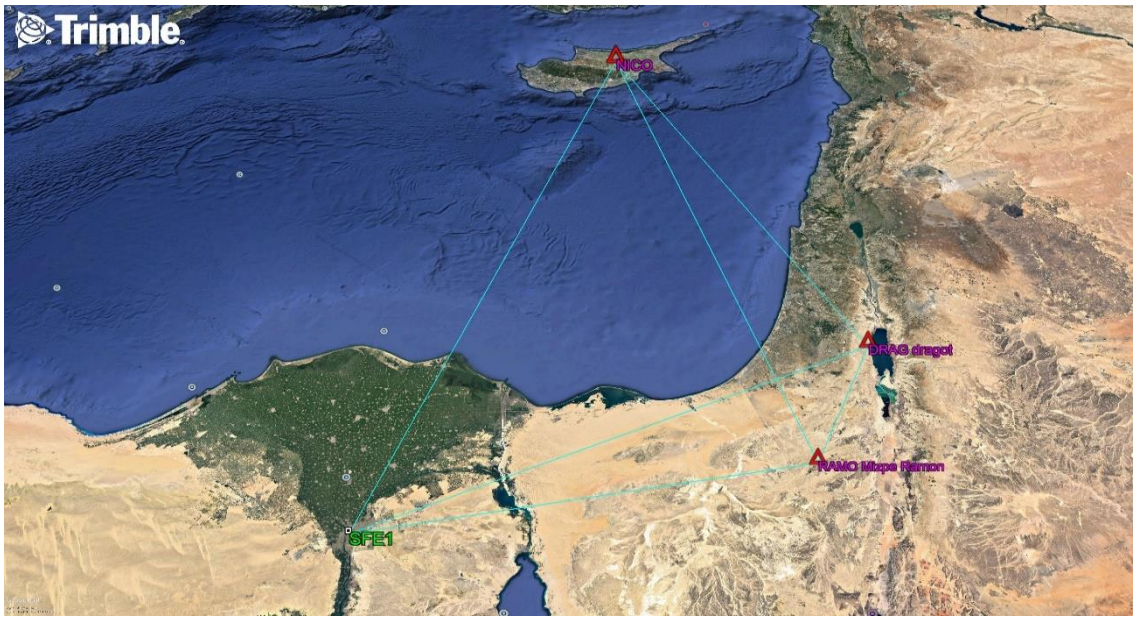

Figure (4.2) Geographic locations of stations SFE1, RAMO, DRAG and NICO.

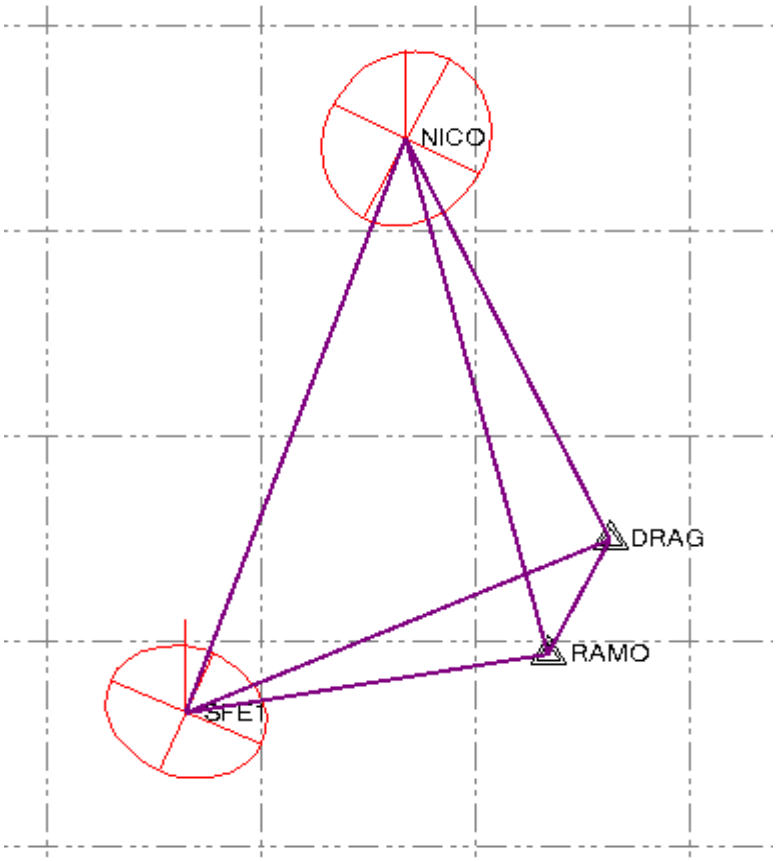

Figure (4.3) Network processed of stations SFE1, RAMO, DRAG and NICO.

Table (4.3) shows the control points constrained during adjustment process and Table (4.4) displays the difference between coordinates of station NICO resulted from adjustment process and its known coordinates.

Table (4.3) Control point constraints during network adjustment for station SFE1.

Point ID	Type	East σ (Meter)	North σ (Meter)	Height σ (Meter)
DRAG	Global	Fixed	Fixed	Fixed
RAMO	Global	Fixed	Fixed	Fixed

Table (4.4) Control coordinate comparisons between adjusted coordinates and known coordinates of station NICO after network adjustment of station SFE1.

Point ID	Δ Easting (Meter)	Δ Northing (Meter)	Δ Height (Meter)
NICO	0.001	-0.008	0.009

The adjusted Earth Centered Earth Fixed (ECEF) coordinates with their standard errors from one day of observations are shown in Table (4.5) and the error ellipse components for stations NICO and SFE1 are illustrated in Table (4.6).

Table (4.5) Adjusted ECEF coordinates for one day of observations for network connecting RAMO, DRAG, NICO and SFE1 stations.

Point ID	X (Meter)	X Error (Meter)	Y (Meter)	Y Error (Meter)	Z (Meter)	Z Error (Meter)	3D Error (Meter)	Constraint
DRAG	4432980.450	--	3149432.231	--	3322110.655	--	--	LLh
NICO	4359415.520	0.003	2874117.176	0.002	3650777.959	0.003	0.004	
RAMO	4514721.643	--	3133507.981	--	3228024.890	--	--	LLh
SFE1	4722585.044	0.003	2865173.220	0.002	3178234.851	0.002	0.004	

Table (4.6) Error ellipse components for stations NICO and SFE1 resulted from network adjustment.

Point ID	Semi-major axis (Meter)	Semi-minor axis (Meter)	Azimuth
NICO	0.0030	0.0026	28°
SFE1	0.0026	0.0021	114°

After processing seven days of observations, XYZ solution for station SFE1 resulted from each day. The weighted mean for cartesian X, Y and Z coordinates were calculated as shown in Tables (4.7), (4.8) and (4.9) and used as reference solution for PPP technique.

Table (4.7) Calculation of weighted mean for X coordinate of station SFE1.

Time		X (Meter)	σ (Meter)	Weight	W*X	Mean (cm)
GPS Week 1835	Day 1	4722585.044	0.003	11.111	52473167.16	
	Day 2	4722585.044	0.006	2.778	13118291.79	
	Day 3	4722585.052	0.006	2.778	13118291.81	
	Day 4	4722585.042	0.007	2.041	9637928.657	4722585.045
	Day 5	4722585.044	0.005	4.000	18890340.18	
	Day 6	4722585.044	0.003	11.111	52473167.16	
	Day 7	4722585.046	0.003	11.111	52473167.18	
				44.930		

Table (4.8) Calculation of weighted mean for Y coordinate of station SFE1.

Time		Y (Meter)	σ (Meter)	Weight	W*Y	Mean (cm)
GPS Week 1835	Day 1	2865173.220	0.002	25.000	71629330.5	
	Day 2	2865173.220	0.006	2.778	7958814.5	
	Day 3	2865173.226	0.006	2.778	7958814.517	
	Day 4	2865173.221	0.007	2.041	5847292.288	2865173.220
	Day 5	2865173.221	0.006	2.778	7958814.503	
	Day 6	2865173.221	0.003	11.111	31835258.01	
	Day 7	2865173.219	0.003	11.111	31835257.99	
				57.596		

Table (4.9) Calculation of weighted mean for Z coordinate of station SFE1.

Time		Z (Meter)	σ (Meter)	Weight	W*Z	Mean (cm)
GPS Week 1835	Day 1	3178234.851	0.002	25.000	79455871.28	
	Day 2	3178234.850	0.006	2.778	8828430.139	
	Day 3	3178234.854	0.006	2.778	8828430.15	
	Day 4	3178234.858	0.006	2.778	8828430.161	3178234.854
	Day 5	3178234.856	0.005	4.000	12712939.42	
	Day 6	3178234.855	0.003	11.111	35313720.61	
	Day 7	3178234.860	0.003	11.111	35313720.67	
				59.556		

To examine PPP in kinematic mode, PPK continuous trajectory collected on Wednesday, October 12, 2016 in an open area near the road of Cairo – Ain El Sokhna were used to evaluate the accuracy of kinematic PPP solution. In order to make true analysis, we need a reference solution for better results. So, a base station was created near the area of interest and was fixed related to a control station named SFE1 located at the roof of Faculty of Engineering at Shoubra. Figure (4.4) shows the baseline between SFE1 and this base station used for kinematic work. Fixing of Base station was done using Trimble Business Center software version 3.61. After getting true coordinates for the Base station, kinematic datasets were processed using TBC software to obtain accurate coordinates of continuous data to be used as a reference solution for comparison process.

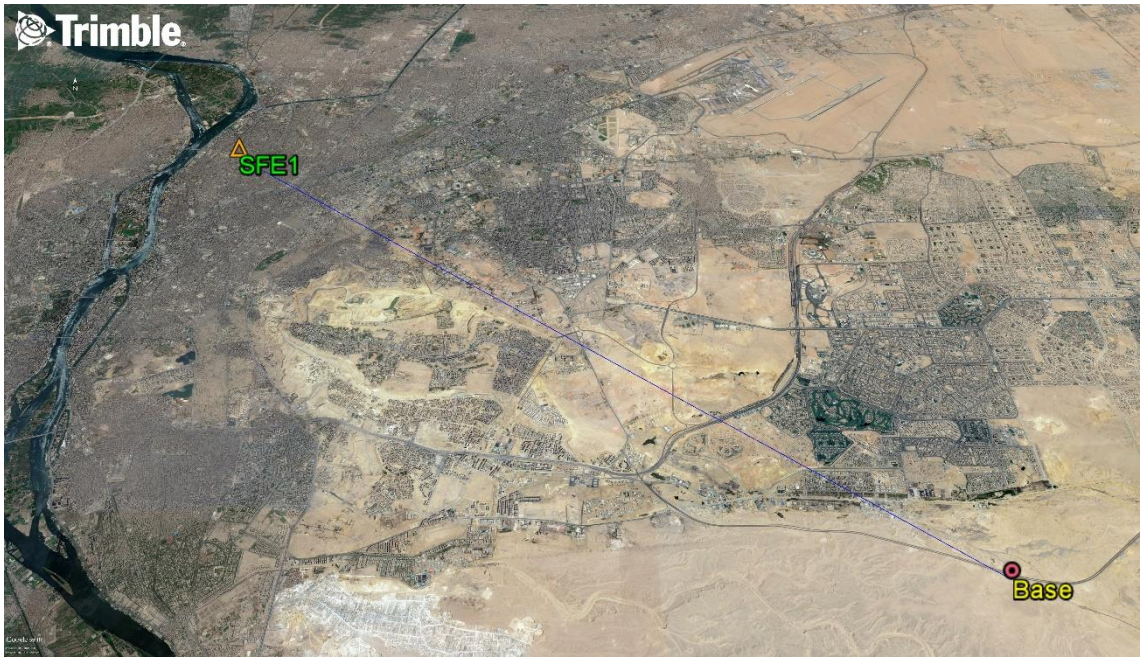

Figure (4.4) Baseline between SFE1 and Base station for kinematic work.

Table (4.10) shows the processing summary of the baseline between SFE1 and the Base station. The baseline was processed using dual frequency observations and final precise ephemeris to obtain accurate results for Base station as indicated, in Table (4.11), in the standard error for the processed vector between the two stations.

Table (4.10) Baseline processing summary between SFE1 and Base stations.

Baseline Observation:	SFE1 --- Base (B1)
Solution Type:	Fixed
Frequency used:	Dual Frequency (L1, L2)
Horizontal Precision:	0.002 m
Vertical Precision:	0.012 m
RMS (cm):	0.007 m
Max (cm)imum PDOP:	4.720
Ephemeris used:	Precise
Antenna Model:	NGS Absolute
Processing Duration:	05:31:43
Processing interval:	1 second

Table (4.11) Standard Error for the processed vector SFE1 --- Base.

σ ΔEasting	0.001 m	**σNS Fwd Azimuth**	0°00'00"	**σ ΔX**	0.004 m
σ ΔNorthing	0.001 m	**σEllipsoid Dist.**	0.001 m	**σ ΔY**	0.003 m
σ ΔElevation	0.006 m	**σ ΔHeight**	0.006 m	**σ ΔZ**	0.003 m

The PPK dataset used for PPP assessment in kinematic technique was observed in continuous kinematic mode using dual frequency receiver mounted in a rod and moved with a person. The kinematic observations started with 1 hour static initialization followed by about 4 hours of continuous kinematic trajectory. Table (4.12) indicates the observation details of the kinematic dataset and Figure (4.5) shows an image for the observed continuous trajectory.

Table (4.12) Observation details of the kinematic dataset.

Start Time:	10/12/2016 6:07:41 AM (UTC)
End Time:	10/12/2016 11:00:33 AM (UTC)
Duration:	04:52:52
Epochs Observed:	11322
Update Rate:	1 sec
Survey Mode:	continuous kinematic
Receiver Type:	Trimble R8-4
Antenna Type:	TRMR8-4
Satellites Observed:	20 (GPS only)

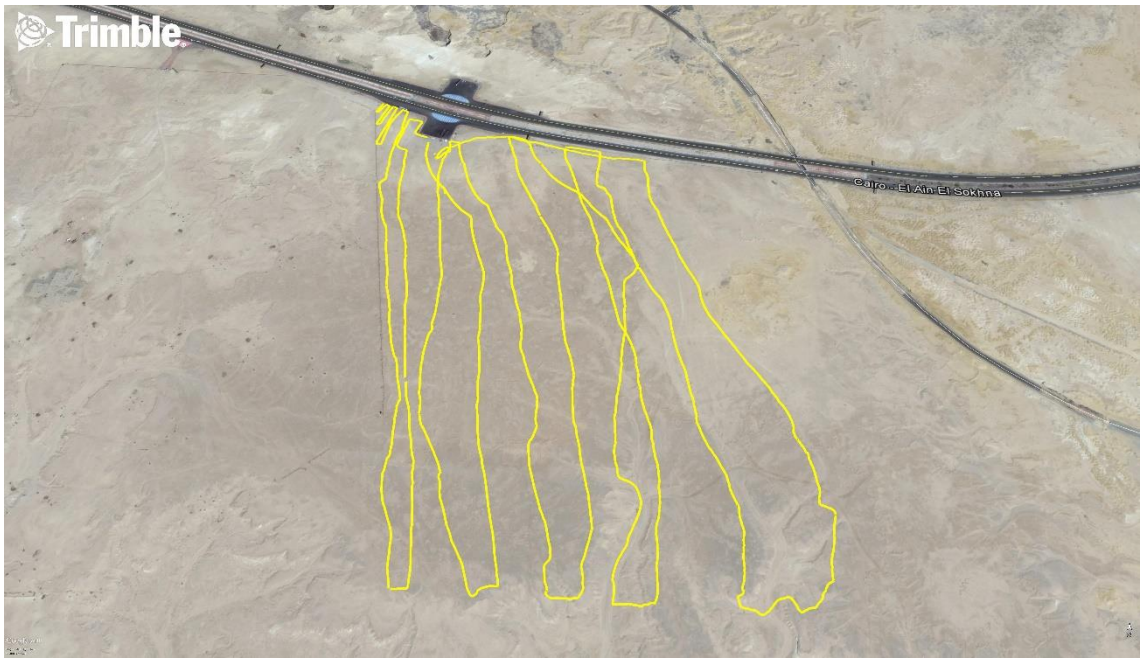

Figure (4.5) Image for the observed continuous kinematic trajectory.

To evaluate the kinematic PPP solution, the relative solution of the continuous trajectory computed using differential TBC software will be used as a reference solution. In kinematic PPP solution, final IGS precise orbits and final precise clock products of 5 seconds sample rate obtained from CODE analysis center were used for processing. In addition to final ephemeris, rapid precise orbits and clock products of 5 minutes sample rate were used for rapid kinematic PPP. For consistency with final clocks, rapid clock products were interpolated to get a solution every 5 seconds.

4.3 Results from gLAB Software

In this section we will present all processing results from gLAB software. It can process observations from GPS-Only satellites. Single and dual frequency observations will be processed with gLAB tool along with final, rapid and ultra-rapid precise products.

4.3.1 The ESA/UPC GNSS-Lab Tool (gLAB)

gLAB, developed under ESA Contract by the research group of Astronomy and Geomatics (gAGE) from the Universitat Politecnica de Catalunya (UPC), is a multipurpose package to process and analyze GPS data. gLAB performs precise modeling of GPS observables (pseudo range and carrier phase) at the centimetre level, allowing both standalone GPS positioning and PPP (Sanz, J. et al., 2012). The gLAB software tool is provided free of charge by ESA to universities and GNSS professionals. Figure (4.6) shows an example for one of the results that we can get from the software.

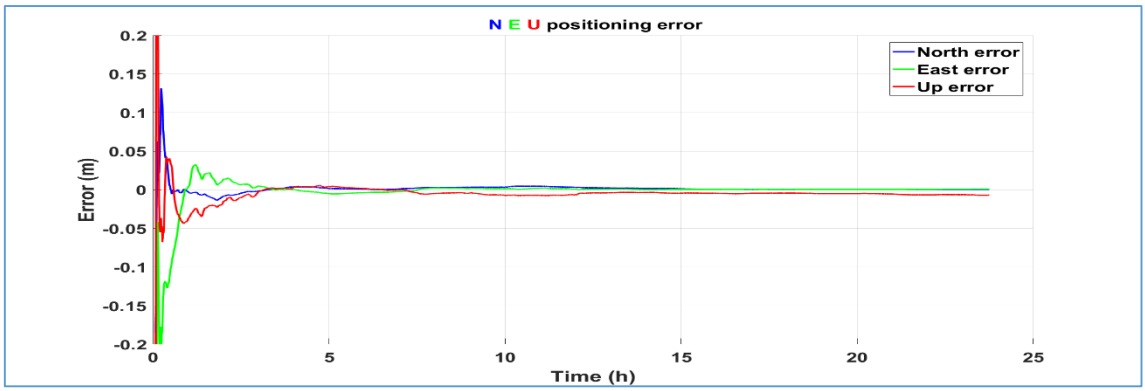

Figure (4.6) Sample of static PPP results

4.3.2 Assessment of Static PPP In gLAB

To analyze the results from static PPP technique in gLAB tool, we used different types of precise orbits and clocks such as final, rapid and ultra-rapid precise products throughout different types of observations such as single and dual frequency observations. Assessment of static PPP will depend on the accuracy and the convergence time of the solution.

At first, there are two factors affecting final results for GPS processing. The first one is the satellite geometry (DOP) which indicates to status of distribution of satellites at the time of observation. The second is the satellites number in view during observation process. As shown in Figure (4.7) the number of satellites used in the data processing for three IGS stations and station SFE1.

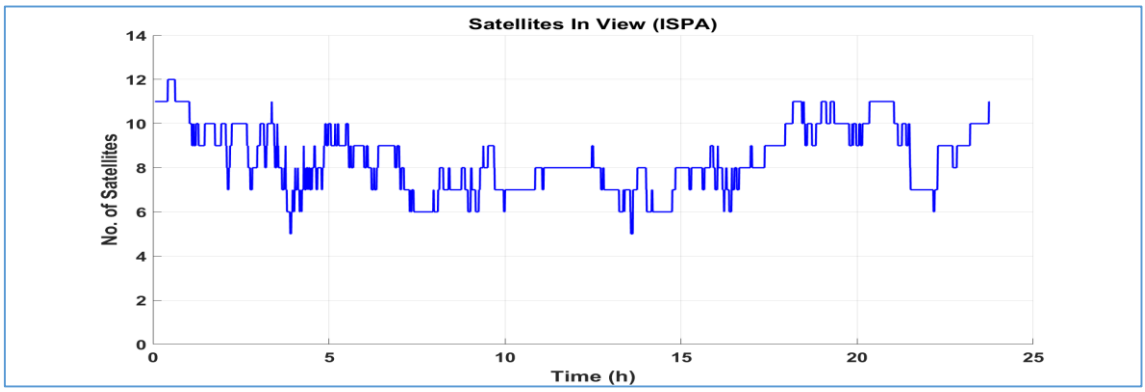

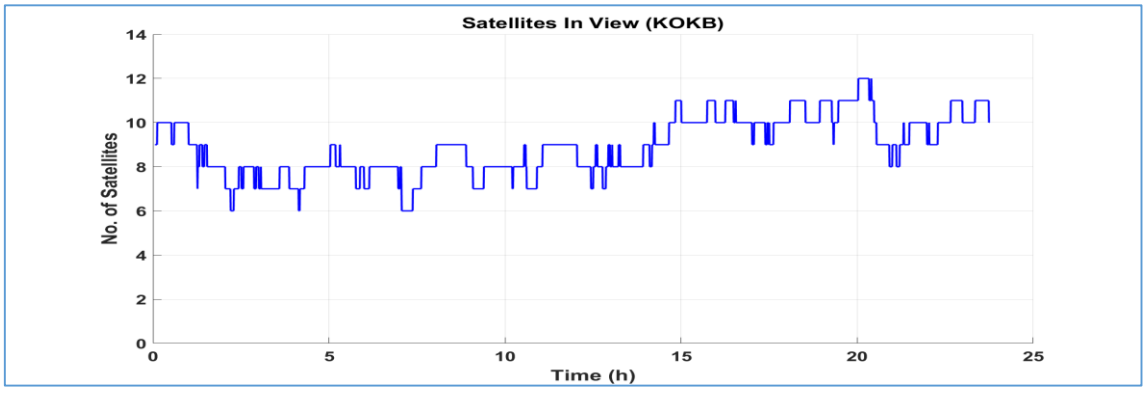

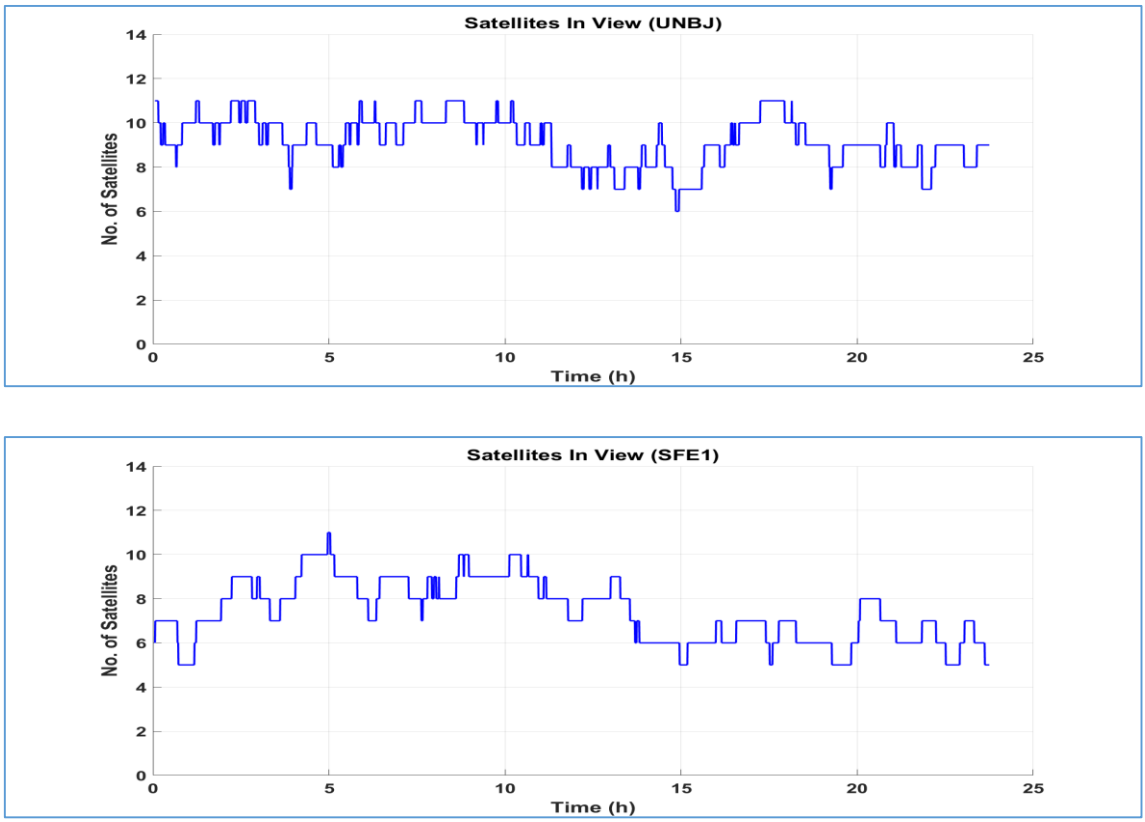

Figure (4.7) Number of satellites in view for stations ISPA, KOKB, UNBJ and SFE1.

Besides, the number of satellites in view, the satellite geometry (DOPs) shown in Figure (4.8) affects greatly the estimated position.

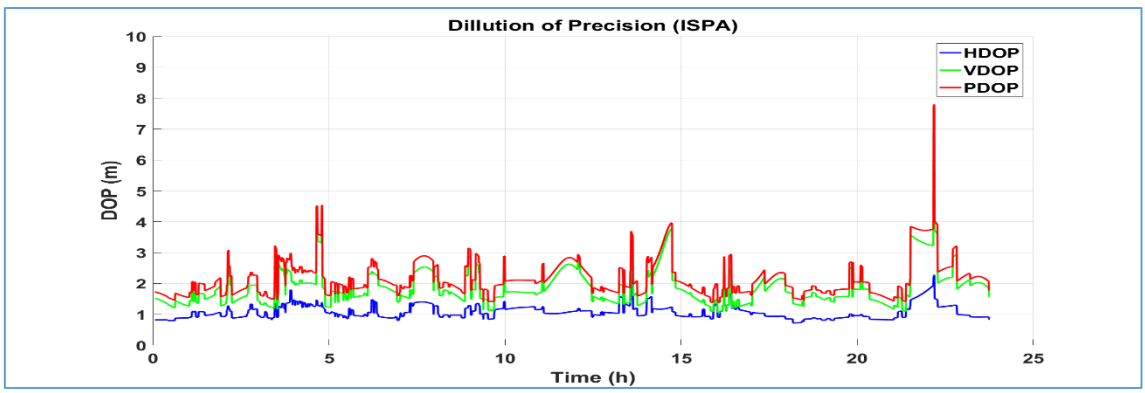

Figure (4.8) Satellite geometry (DOP) for stations ISPA, KOKB, UNBJ and SFE1.

The number of satellites at each epoch and the satellite geometry as illustrated by the DOPs can provide valuable information for the analysis, especially when problems occur. During the entire test period, the number of satellites used ranges between four and fourteen in the GPS-only processing. The observations from approximately nine GPS satellites on average are processed with respect to IGS sites. Moreover, approximately 7-8 GPS satellites on average were processed related to station SFE1 due to surroundings of the station. Assessment of performance of PPP in static mode will depend on 24-hour dataset to estimate the accuracy of station position. GPS datasets from twelve IGS permanent stations were used for this assessment besides station SFE1.

4.3.2.1 Case 1 Assessment of Static PPP Using Dual Frequency Observations and Final Precise Ephemeris

In this case, dual frequency observations were considered from GPS-Only satellites and final precise ephemeris. The site coordinates from International GNSS Service and fixed coordinates of station SFE1 were used as true coordinates to assess the accuracy of PPP. The estimated three-dimension coordinate from PPP solution have been converted to position discrepancies in north, east, and up components with respect to the true coordinates.

Figure (4.9) shows the processing results of four stations ISPA, KOKB, UNBJ and SFE1 using dual frequency observations and IGS final precise orbits and clock products, including the positioning errors in east, north and up directions with respect to the true station coordinates obtained from IGS and fixed coordinates of station SFE1. These graphs represent the accuracy of PPP solution which reflect how different the PPP position estimate is from its true coordinates over the day.

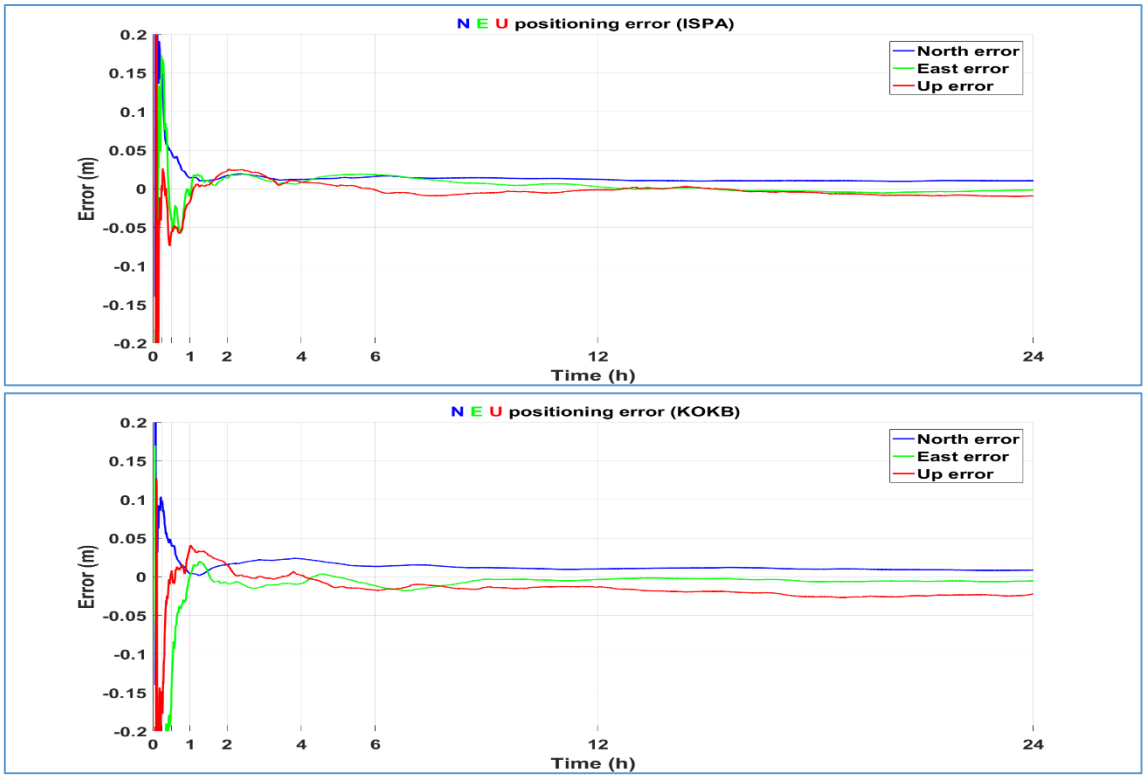

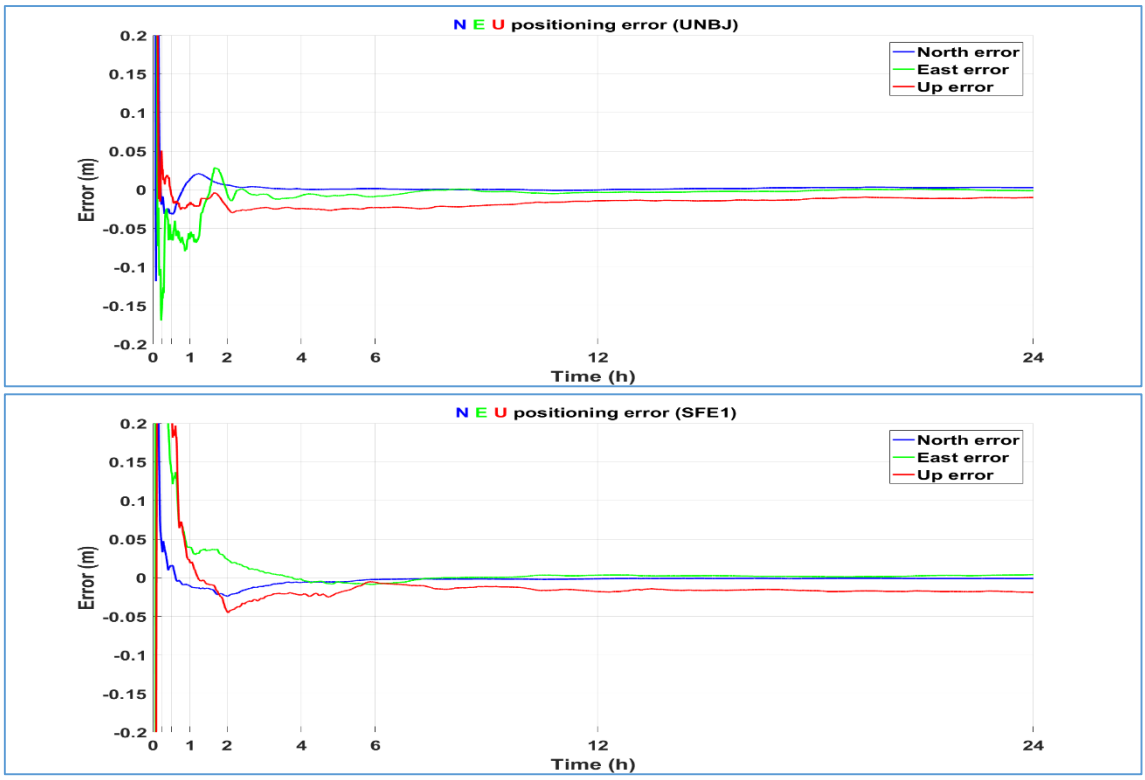

Figure (4.9) Processing results from static PPP using dual frequency observations and IGS final ephemeris over the day (DOY 70, 2015) for stations ISPA, KOKB, UNBJ and SFE1.

For focusing on convergence time for PPP solution in static mode which means how long it takes a position filter to reach a stable condition, Table (A.1), in Appendix A, shows the processing results for all twelve IGS stations at different time spans over the day in north, east and up directions. Time spans were at 0.25, 0.5, 1, 2, 4, 6, 12 and 24 hours. While Table (A.2), in Appendix A, shows the processing results for station SFE1 from all seven days of observation.

The statistical analysis for the absolute positioning errors of static PPP from the twelve IGS sites is illustrated in Table (4.13). In this table the maximum and minimum value for absolute error at each time span are shown besides mean and RMS (cm) error at 95% confidence level. For a clear view, Figure (4.10) illustrates the mean errors at each time span at 95% confidence level.

Table (4.13) The statistical analysis for the absolute positioning errors of static PPP from the twelve IGS sites using dual frequency observations and final precise ephemeris over the day (DOY 70, 2015) at 95% confidence level.

	Time (hr.)	Max (cm)	Min (cm)	Mean (cm)	RMS (cm)
North	0.25	15.96	0.88	7.84	9.18
	0.5	5.67	0.10	2.92	3.37
	1	3.24	0.07	1.15	1.55
	2	1.99	0.15	0.85	1.05
	4	1.21	0.11	0.57	0.67
	6	1.61	0.02	0.62	0.83
	12	1.01	0.02	0.31	0.43
	24	0.88	0.06	0.21	0.31
East	0.25	49.62	8.74	22.08	25.31
	0.5	27.67	1.49	11.63	14.33
	1	7.99	0.04	2.52	3.57
	2	2.07	0.02	1.02	1.18
	4	1.28	0.04	0.58	0.69
	6	1.83	0.05	0.87	1.01
	12	0.69	0.01	0.34	0.41
	24	0.60	0.04	0.24	0.30
Up	0.25	23.79	0.34	9.98	13.06
	0.5	26.87	0.21	8.86	12.62
	1	4.43	1.62	3.04	3.21
	2	3.81	1.37	2.31	2.45
	4	3.12	0.11	1.23	1.55
	6	3.62	0.15	1.42	1.84
	12	2.55	0.03	1.26	1.58
	24	3.19	0.16	1.35	1.70

From Table (4.13), it is clearly observed that the static PPP solution from dual frequency observations and final precise ephemeris can reach less than 3 cm of mean error after one hour of observation in horizontal direction and about 3 cm in vertical direction at 95% confidence level. After 2 hours the solution can reach about 1 cm in horizontal and less than 3 cm in vertical direction. Also, the PPP solution become millimeters in horizontal direction and less than 2 cm after 4 hours of observation. These results are more sufficient for a lot of applications that demands precise outputs.

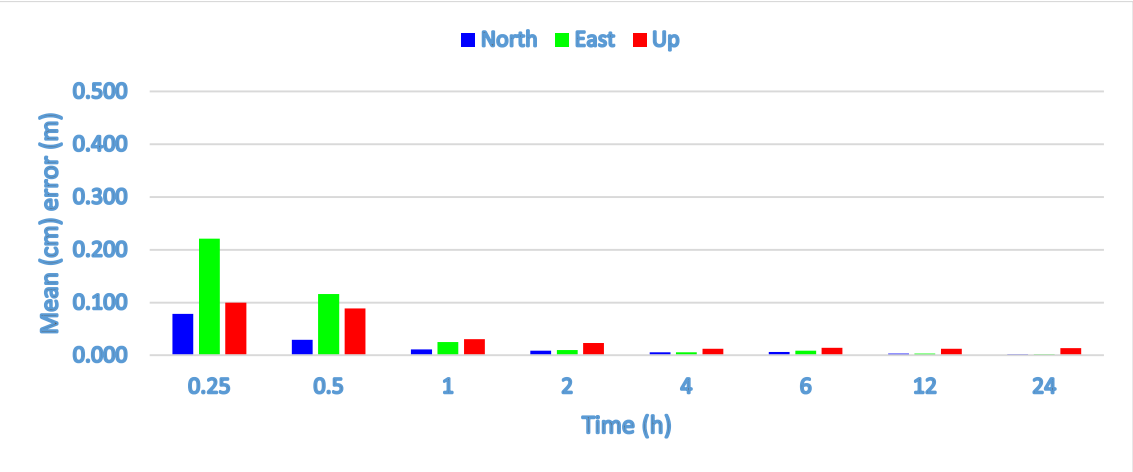

Figure (4.10) Absolute mean error of static PPP from the twelve IGS sites using dual frequency observations and final precise ephemeris over the day (DOY 70, 2015) at 95% confidence level.

On the other hand, the statistical analysis for the absolute positioning errors of static PPP from SFE1 is demonstrated in Table (4.14). These results were done from the seven days of observations at the station. For a clear view, Figure (4.11) illustrates the mean errors at each time span at 95% confidence level.

From Table (4.14), it is seen that the static PPP solution from dual observations and final precise ephemeris from SFE1 station was almost close to the results from IGS sites. The static PPP solution from SFE1 reaches about 3 cm in horizontal and 4 cm in vertical after 2 hours. While after 4 hours the solution reaches millimeters in horizontal direction and less than 3 cm in vertical direction. The results from SFE1 station was less accurate than from IGS sites can be interpreted due to two reasons. The first reason is that true coordinates for SFE1 was calculated from fixing it with three IGS sites around us and the final solution was carried with error resulted from long processed baselines between SFE1 and IGS sites. The second reason was that cut off angle at SFE1 was 15^{o} due to surroundings and it was cleared that for better results for PPP solution the cut off angle should be between 5^{o} and 10^{o}.

Table (4.14) The statistical analysis for the absolute positioning errors of static PPP from station SFE1 over the seven days using dual frequency observations and final precise ephemeris at 95% confidence level.

	Time (hr.)	Max (cm)	Min (cm)	Mean (cm)	RMS (cm)
North	0.25	13.99	1.63	6.46	7.44
	0.5	5.60	0.82	2.27	2.82
	1	2.25	0.43	1.52	1.64
	2	2.38	1.48	1.82	1.84
	4	0.84	0.00	0.38	0.49
	6	0.48	0.03	0.25	0.28
	12	0.37	0.04	0.17	0.21
	24	0.27	0.01	0.12	0.14
East	0.25	48.68	20.86	39.38	40.27
	0.5	28.17	10.64	18.81	19.67
	1	9.37	2.11	5.30	5.74
	2	4.25	2.06	2.96	3.07
	4	1.90	0.11	0.68	0.90
	6	0.82	0.01	0.36	0.45
	12	0.71	0.34	0.52	0.53
	24	0.93	0.37	0.57	0.60
Up	0.25	37.73	1.67	27.73	30.05
	0.5	27.77	1.53	15.79	17.62
	1	8.29	0.13	2.67	3.67
	2	7.22	2.02	4.21	4.58
	4	3.23	2.21	2.80	2.81
	6	1.40	0.58	1.02	1.05
	12	2.08	1.41	1.64	1.65
	24	2.13	1.37	1.74	1.76

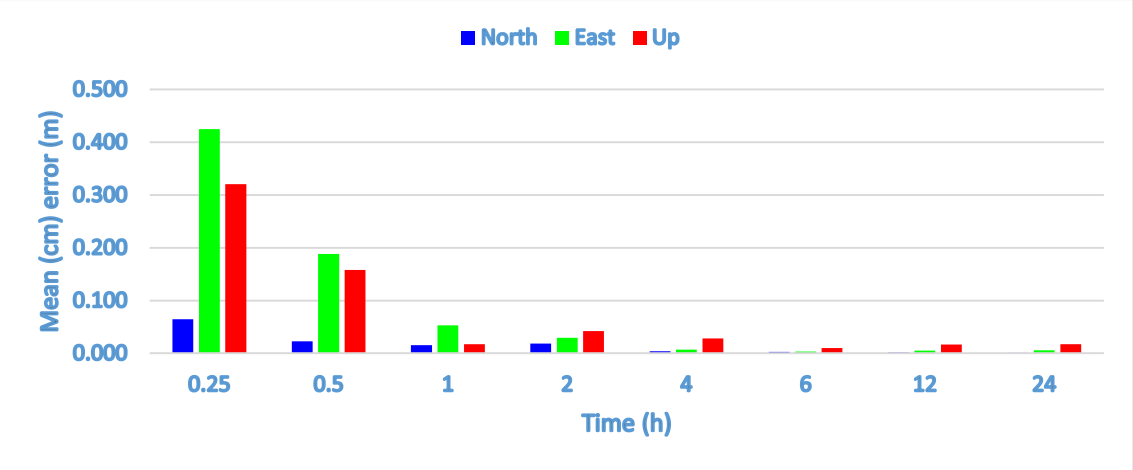

Figure (4.11) Absolute mean error of static PPP from station SFE1 using dual frequency observations and final precise ephemeris over the seven days at 95% confidence level.

4.3.2.2 Case 2 Assessment of Static PPP Using Dual Frequency Observations and Rapid Precise Ephemeris

In this case, rapid precise ephemeris were used along with dual frequency observations from GPS-Only satellites. Figure (4.12) displays the processing results of the four stations ISPA, KOKB, UNBJ and SFE1 including the positioning errors in east, north and up directions with respect to the true station coordinates. Figure (4.12) presents the accuracy of the PPP solution over the day.

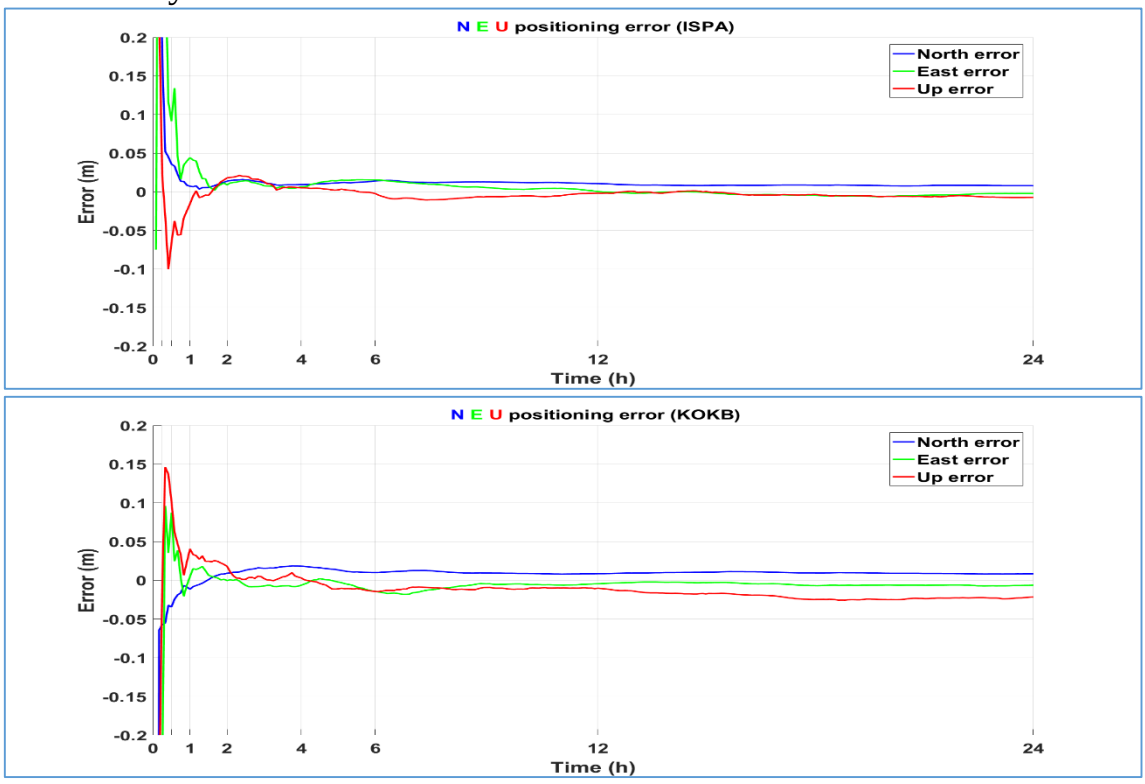

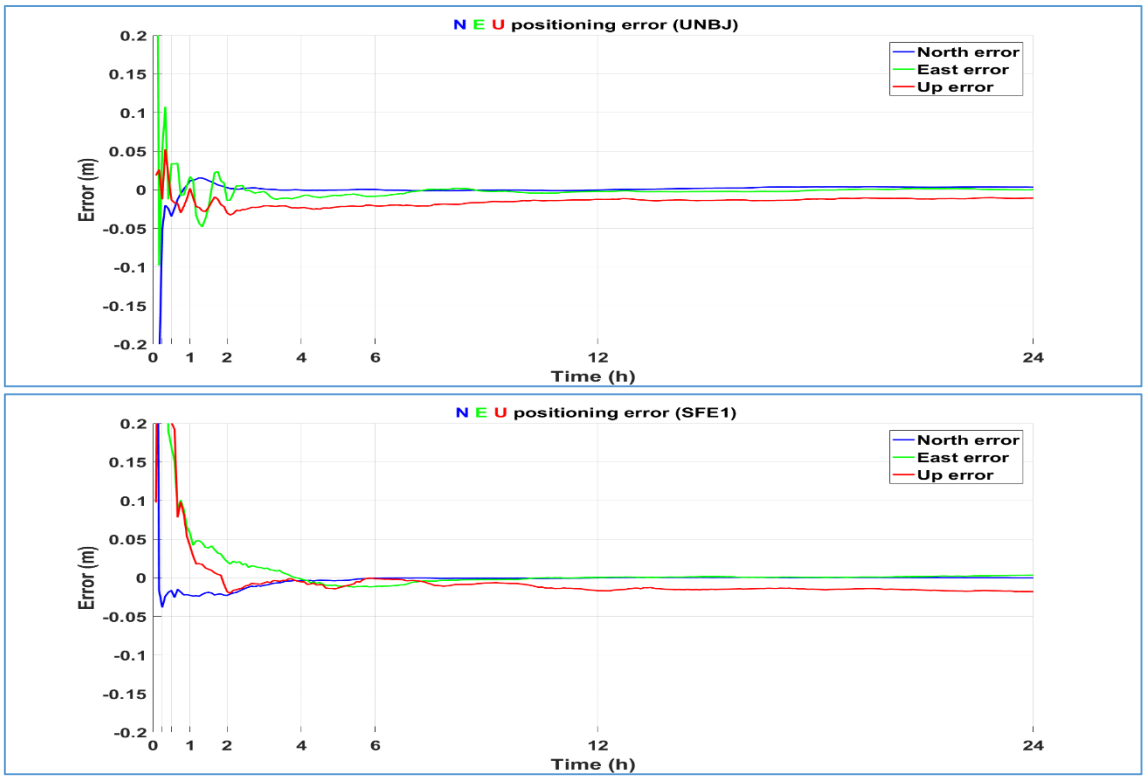

Figure (4.12) Processing results from static PPP using dual frequency observations and IGS rapid ephemeris over the day (DOY 70, 2015) for stations ISPA, KOKB, UNBJ and SFE1.

To assess the static PPP solution from dual frequency observations and rapid precise ephemeris in terms of convergence time, Table (A.3), in Appendix A, shows the processing results for all twelve IGS stations at different time spans over the day (DOY 70, 2015) in north, east and up directions. While Table (A.4), in Appendix A, indicates to the processing results for station SFE1 from all seven days of observations. The absolute positioning errors, maximum, minimum, mean and RMS (cm) errors, of static PPP from the twelve IGS sites at 95% confidence level are shown in Table (4.15). Additionally, Figure (4.13) illustrates the mean errors at each time span at 95% confidence level.

Table (4.15) The statistical analysis for the absolute positioning errors of static PPP from the twelve IGS sites over the day (DOY 70, 2015) using dual observations and rapid precise ephemeris at 95% confidence level.

	Time (hr.)	Max (cm)	Min (cm)	Mean (cm)	RMS (cm)
North	0.25	17.78	3.88	8.56	9.85
	0.5	5.62	0.27	2.60	3.05
	1	2.65	0.03	1.03	1.33
	2	2.23	0.03	0.76	0.97
	4	1.22	0.01	0.55	0.65
	6	1.42	0.00	0.56	0.76
	12	0.86	0.02	0.28	0.38
	24	0.79	0.00	0.20	0.29
East	0.25	42.01	2.84	18.13	21.61
	0.5	16.45	1.88	8.70	9.65
	1	4.43	0.28	1.87	2.29
	2	3.66	0.03	1.28	1.58
	4	1.18	0.12	0.66	0.74
	6	1.56	0.08	0.81	0.96
	12	0.77	0.01	0.32	0.42
	24	0.67	0.01	0.28	0.37
Up	0.25	47.90	0.74	9.80	16.76
	0.5	21.50	1.30	7.39	9.63
	1	7.91	0.19	3.72	4.35
	2	4.71	1.08	2.89	3.11
	4	3.54	0.30	1.33	1.64
	6	4.27	0.15	1.59	2.07
	12	2.50	0.09	1.14	1.44
	24	2.92	0.06	1.29	1.56

Table (4.15) shows that the static PPP solution from dual observations and rapid precise ephemeris can be close to the results from using final precise ephemeris. The PPP solution can reach less than 3 cm of mean error after one hour of observation in horizontal direction about 4 cm in vertical direction at 95% confidence level. After 2 hours the solution can reach about 2 cm in horizontal and less than 3 cm in vertical direction. Also, the PPP solution become millimeters in horizontal direction and less than 2 cm after 4 hours of observation. These results using rapid precise ephemeris, available

after 17-41 hours, taking us not to wait for final precise ephemeris available after 14-18 days.

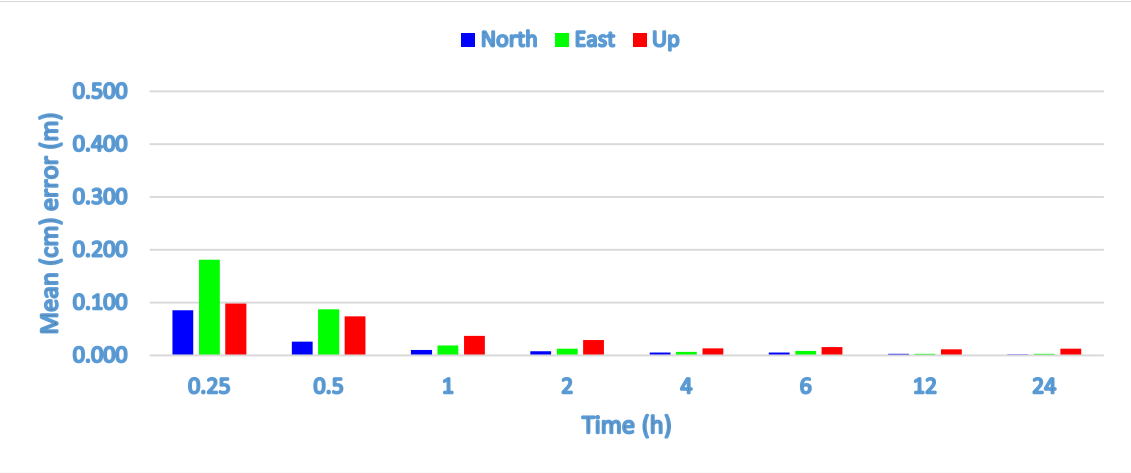

Figure (4.13) Absolute mean error of static PPP from the twelve IGS sites using dual frequency observations and rapid precise ephemeris over the day (DOY 70, 2015) at 95% confidence level.

On the other hand, the statistical analysis for the absolute positioning errors of static PPP from SFE1 is presented in Table (4.16). For a clear view, Figure (4.14) illustrates the mean errors at each time span at 95% confidence level. From Table (4.16), it is seen that the static PPP solution from dual observations and rapid precise ephemeris from SFE1 station was far to a small extent to the results from IGS sites. The static PPP solution from SFE1 reaches about 2 cm in north, 7 cm in east and less than 5 cm in up direction after 1 hour. While after 2 hours the solution reaches 2 cm, 4 cm and 3 cm in north, east and up directions respectively. The PPP solution can be millimeters in horizontal direction and less than 2 cm in vertical direction after 4 hours.

Table (4.16) The statistical analysis for the absolute positioning errors of static PPP from station SFE1 from the seven days using dual frequency observations and rapid precise ephemeris at 95% confidence level.

	Time (hr.)	Max (cm)	Min (cm)	Mean (cm)	RMS (cm)
North	0.25	4.27	0.69	2.34	2.69
	0.5	4.51	0.21	1.81	2.44
	1	4.32	0.13	2.14	2.42
	2	2.39	1.87	2.14	2.14
	4	0.97	0.22	0.43	0.51

	6	0.27	0.01	0.11	0.14
	12	0.31	0.00	0.16	0.19
	24	0.32	0.00	0.14	0.17
East	0.25	77.50	15.90	44.90	50.86
	0.5	40.75	10.81	20.77	23.08
	1	13.00	2.75	6.77	7.59
	2	4.46	2.10	3.36	3.45
	4	2.22	0.16	0.89	1.17
	6	1.13	0.10	0.36	0.52
	12	0.71	0.07	0.40	0.46
	24	0.55	0.25	0.41	0.42
Up	0.25	81.76	1.13	42.02	49.26
	0.5	45.00	7.07	23.21	25.79
	1	5.89	1.52	4.15	4.39
	2	5.29	0.31	2.27	2.81
	4	2.45	0.51	1.76	1.87
	6	1.10	0.13	0.54	0.64
	12	1.67	0.87	1.28	1.30
	24	1.79	1.14	1.54	1.55

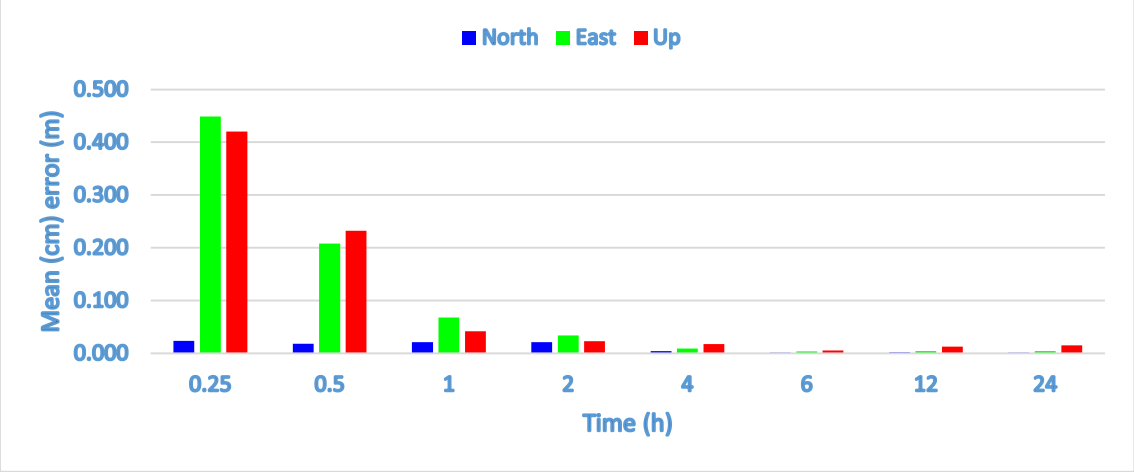

Figure (4.14) Absolute mean error of static PPP from station SFE1 using dual frequency observations and rapid precise ephemeris over the seven days at 95% confidence level.

4.3.2.3 Case 3 Assessment of Static PPP Using Dual Frequency Observations and Ultra-Rapid Precise Ephemeris

In this case, we used ultra-rapid precise ephemeris along with dual frequency observations from GPS-Only satellites. Figure (4.15) shows the processing results obtained from four stations ISPA, KOKB, UNBJ and SFE1 including the positioning errors over the day in east, north and up directions with respect to the true station coordinates.

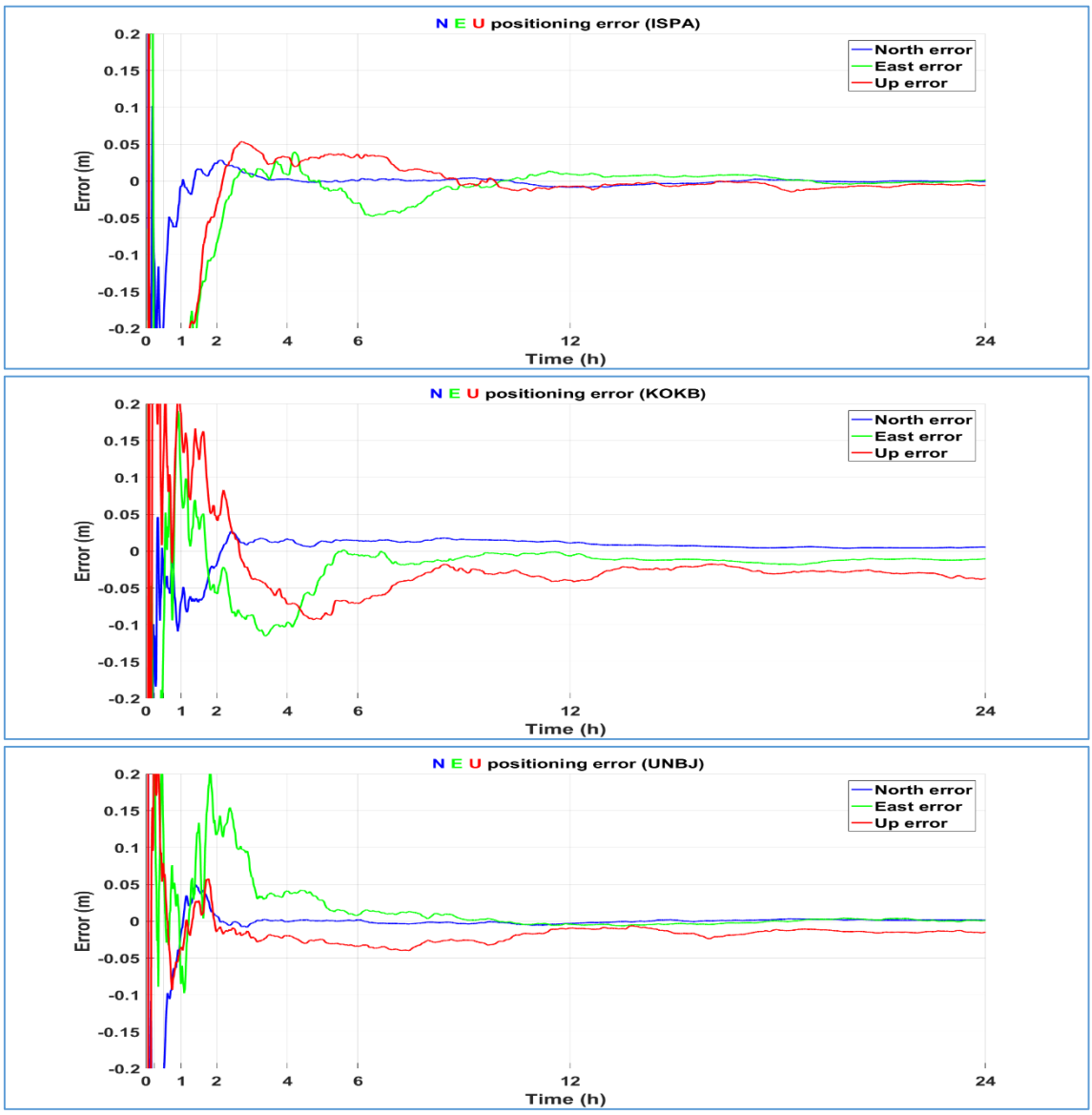

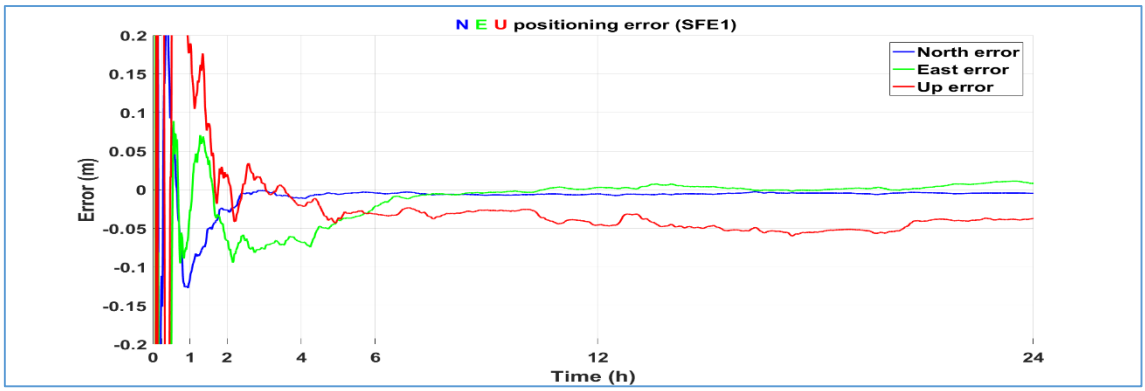

Figure (4.15) Processing results from static PPP using dual frequency observations and IGS ultra-rapid ephemeris over the day (DOY 70, 2015) for stations ISPA, KOKB, UNBJ and SFE1.

In according to convergence time of the PPP solution, Table (A.5), in Appendix A, demonstrates the processing results for all twelve IGS stations at different time sessions all the day in north, east and up directions. However, Table (A.6), in Appendix A, indicates to the processing results for station SFE1 from all seven days of observations. The statistical results, maximum, minimum, mean and RMS (cm) errors, for the absolute positioning errors of static PPP from the twelve IGS sites at 95% confidence level are shown in Table (4.17). Furthermore, Figure (4.16) illustrates the mean errors at each time span at 95% confidence level.

Table (4.17) The statistical analysis for the absolute positioning errors of static PPP from the twelve IGS sites using dual frequency observations and ultra-rapid precise ephemeris over the day (DOY 70, 2015) at 95% confidence level.

	Time (hr.)	Max (cm)	Min (cm)	Mean (cm)	RMS (cm)
North	0.25	50.09	1.12	20.33	25.38
	0.5	23.11	0.94	11.29	13.10
	1	13.33	0.72	5.87	7.37
	2	4.01	0.50	2.11	2.39
	4	1.93	0.05	0.99	1.16
	6	2.09	0.04	0.87	1.09
	12	1.25	0.00	0.59	0.70
	24	0.84	0.03	0.35	0.42
East	0.25	74.69	4.17	35.24	40.73
	0.5	48.70	4.23	22.92	27.69
	1	31.86	1.84	10.21	13.05
	2	13.19	0.13	6.30	7.25

	4	8.16	0.58	3.07	3.75
	6	3.49	0.22	1.52	1.82
	12	1.78	0.09	0.64	0.78
	24	0.74	0.05	0.30	0.40
Up	0.25	185.53	23.42	86.84	101.98
	0.5	38.41	1.81	18.84	22.19
	1	27.61	0.31	11.04	14.56
	2	6.83	0.91	3.11	3.50
	4	4.90	0.51	2.62	2.92
	6	3.89	0.56	2.30	2.61
	12	3.95	0.34	1.80	2.19
	24	2.30	0.36	1.19	1.32

From Table (4.17), it is noticed that the static PPP solution of the twelve IGS sites from dual observations and ultra-rapid precise ephemeris at 95% confidence level needs 4 and 6 hours to reach less than 2 cm error in horizontal direction and need 12 hours to reach the same accuracy in vertical direction. The PPP solution can reach about 2, 1 and less than 1 cm after 2, 4 and 6 hours respectively in north direction. In east component, the solution reaches 3 and less than 2 cm after 4 and 6 hours respectively and close to millimeters after 12 hours. While the solution in the vertical component was less than 3 cm after 4 hours and need 12-24 hours to be less than 2 cm. Briefly, the PPP solution needs 12 hours to be millimeters in horizontal direction and less than 2 cm in vertical direction.

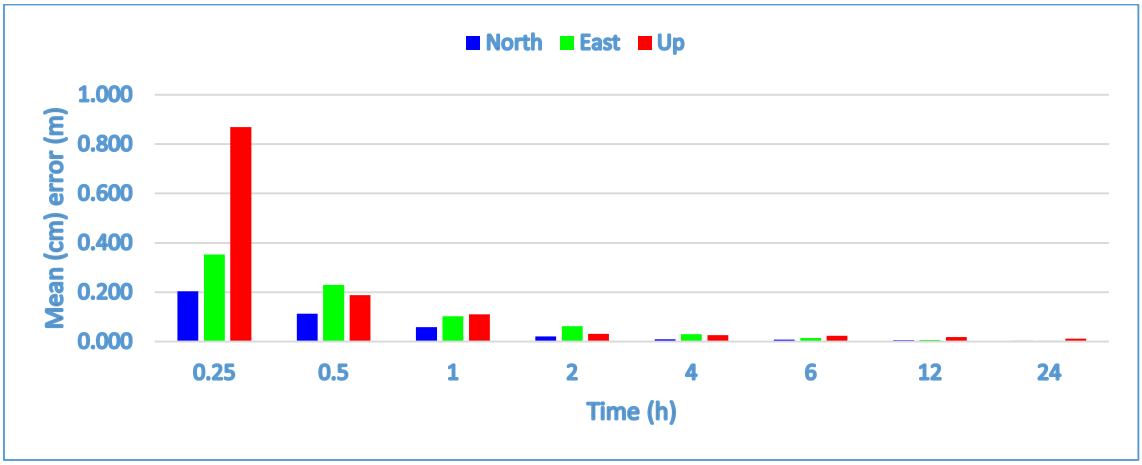

Figure (4.16) Absolute mean error of static PPP from the twelve IGS sites using dual frequency observations and ultra-rapid precise ephemeris over the day (DOY 70, 2015) at 95% confidence level.

Additionally, the statistical analysis for the absolute positioning errors of static PPP from station SFE1 is presented in Table (4.18). Also, Figure (4.17) illustrates the mean errors at each time span at 95% confidence level.

Table (4.18) The statistical analysis for the absolute positioning errors of static PPP from station SFE1 using dual frequency observations and ultra-rapid precise ephemeris over the seven days at 95% confidence level.

	Time (hr.)	Max (cm)	Min (cm)	Mean (cm)	RMS (cm)
North	0.25	25.23	15.14	19.55	19.86
	0.5	11.06	0.52	6.14	7.21
	1	11.48	0.65	5.89	6.88
	2	5.09	0.06	2.05	2.70
	4	2.62	0.06	1.03	1.31
	6	1.46	0.28	0.69	0.79
	12	0.94	0.05	0.43	0.51
	24	0.46	0.00	0.25	0.30
East	0.25	26.85	3.87	14.31	17.00
	0.5	61.99	6.62	33.26	39.48
	1	39.35	2.58	21.06	24.21
	2	10.87	6.52	9.25	9.36
	4	6.79	0.99	4.25	4.71
	6	4.22	0.13	1.70	2.25
	12	0.83	0.30	0.47	0.50
	24	1.14	0.14	0.75	0.81
Up	0.25	182.69	23.56	82.17	98.33
	0.5	86.81	10.99	36.12	44.87
	1	67.03	10.68	31.31	35.87
	2	9.42	2.01	5.22	6.04
	4	6.31	2.01	3.53	3.83
	6	8.24	0.20	2.97	4.13
	12	4.70	0.17	2.54	3.12
	24	4.61	1.08	3.27	3.47

From Table (4.18), it is observed that the static PPP solution from dual observations and ultra-rapid precise ephemeris at 95% confidence level from station SFE1 was little more than the results from IGS sites. The static PPP solution from SFE1 was close to 2 cm in north direction after 2 hours and reach less than 1 cm after 6 hours. In east direction, it was about 2 cm after

6 hours and less than 1 cm after 12 hours. The vertical component need 4 hours to be less than 5 cm and 12 hours to be about 3 cm and did not improve than 3 cm.

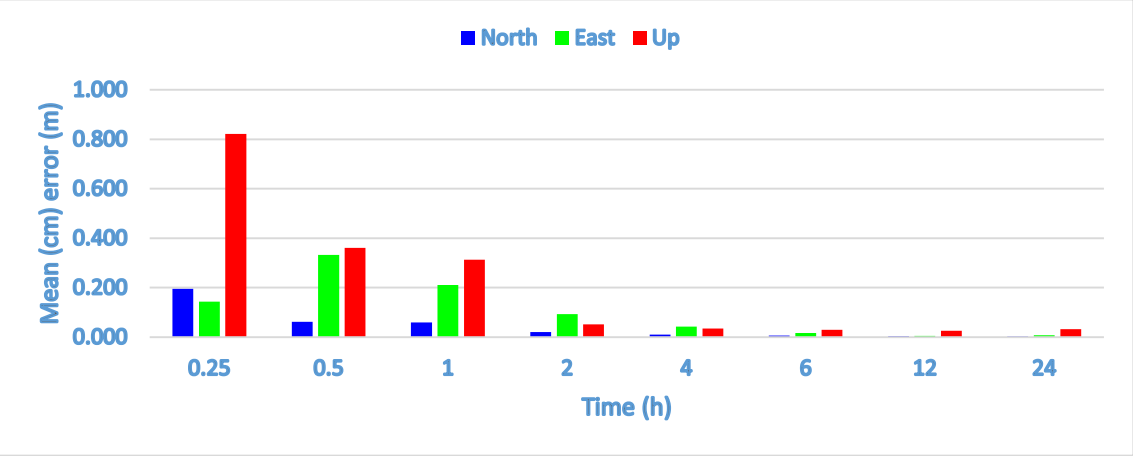

Figure (4.17) Absolute mean error of static PPP from station SFE1 using dual frequency observations and ultra-rapid precise ephemeris over the seven days at 95% confidence level.

4.3.2.4 Case 4 Assessment of Static PPP Using Single Frequency Observations and Final Precise Ephemeris

In this case, single frequency observations were considered from GPS-Only satellites and final precise orbits and clock products. The big different when processing with single observations is how to overcome ionospheric delay that removed through ionosphere free linear combinations in processing dual observations. In this section we will use precise ionospheric model from IGS service to get rid of ionospheric delay error in processing of single observations.

Figure (4.18) shows the processing results of four stations ISPA, KOKB, UNBJ and SFE1 using single frequency observations and IGS final precise orbits and clock products, including the positioning errors in east, north and up directions with respect to the true station coordinates. These graphs reflect how different the PPP position estimate is from its true coordinates over the day.

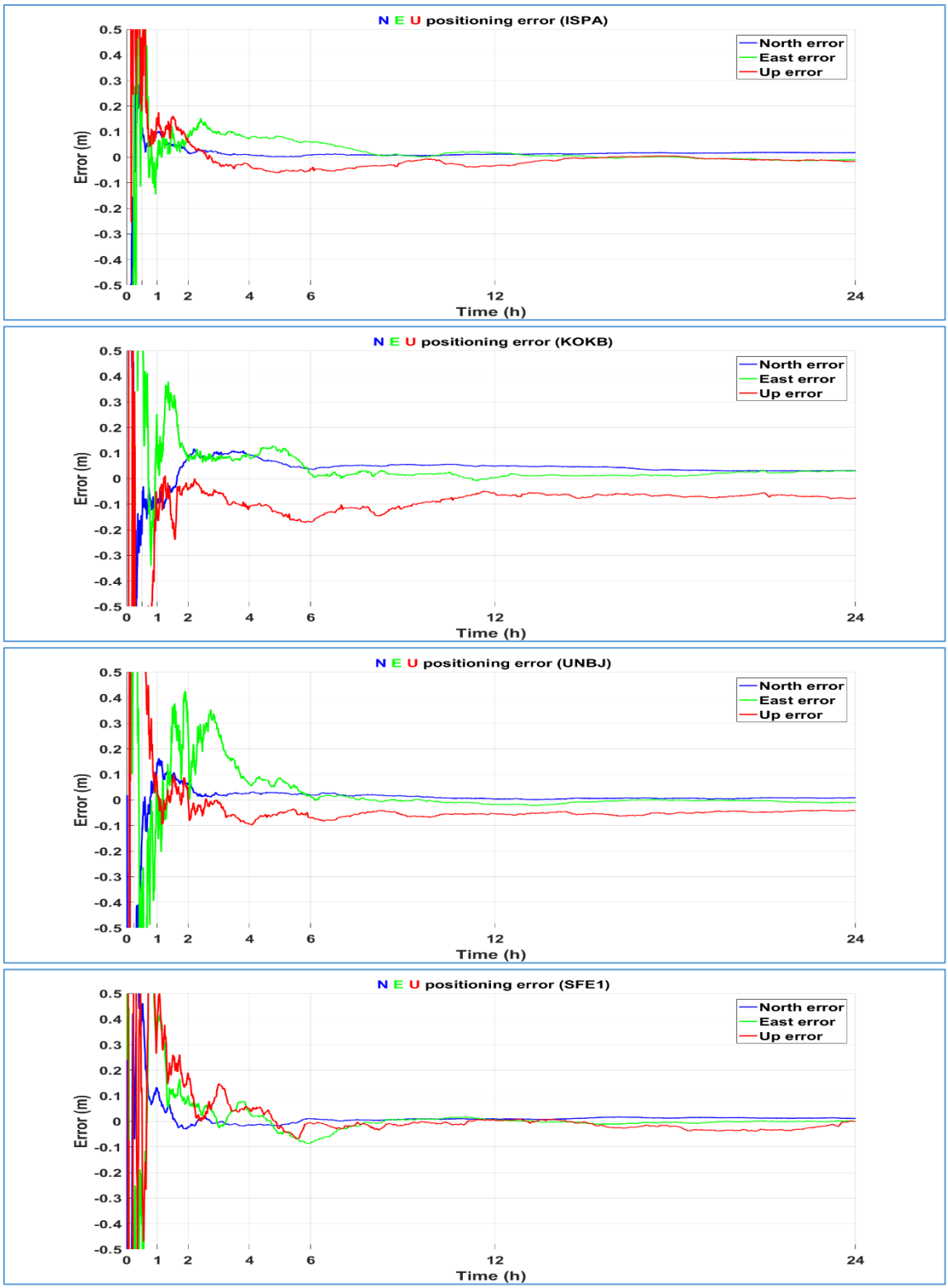

Figure (4.18) Processing results from static PPP using single frequency observations and IGS final ephemeris over the day (DOY 70, 2015) for stations ISPA, KOKB, UNBJ and SFE1.

Regarding convergence time of PPP solution in static mode, Table (A.7), in Appendix A, shows the processing results for all twelve IGS stations at different time spans over the day, in north, east and up directions. Table

(A.8), in Appendix A, shows the processing results for station SFE1 from all seven days of observation. Furthermore, Table (4.19) illustrates the statistical analysis, maximum, minimum, mean and RMS (cm) errors, for the absolute positioning errors of static PPP from the twelve IGS sites at 95% confidence level. Figures (4.19) explains the mean errors at each time span at 95% confidence level.

Table (4.19) The statistical analysis for the absolute positioning errors of static PPP from the twelve IGS sites using single frequency observations and final precise ephemeris over the day (DOY 70, 2015) at 95% confidence level.

	Time (hr.)	Max (cm)	Min (cm)	Mean (cm)	RMS (cm)
North	0.25	120.73	2.22	38.50	51.80
	0.5	28.81	6.79	14.71	16.33
	1	14.86	0.05	6.31	7.70
	2	14.77	0.05	5.27	7.12
	4	4.02	0.44	1.75	2.08
	6	2.96	0.21	1.10	1.38
	12	1.67	0.13	0.94	1.09
	24	1.97	0.16	1.02	1.20
East	0.25	325.64	0.30	114.52	162.57
	0.5	71.84	1.33	27.46	34.65
	1	32.88	1.92	12.97	15.60
	2	37.07	0.16	12.05	16.79
	4	9.25	0.23	5.25	6.02
	6	8.26	0.62	2.53	3.43
	12	3.43	0.07	1.49	1.75
	24	2.92	0.39	1.35	1.59
Up	0.25	208.41	15.24	94.82	117.53
	0.5	96.42	0.15	38.02	48.21
	1	78.03	1.38	29.70	39.57
	2	16.45	0.86	7.56	9.15
	4	15.03	1.73	8.10	9.09
	6	16.80	0.08	6.11	7.59
	12	7.38	0.35	4.05	4.53
	24	7.85	1.19	4.21	4.78

From Table (4.19), it is noticed that the static PPP solution from single frequency observations and final precise ephemeris needs more time to reach more accurate results, less than 2 cm, in contrast to results from dual frequency observations. In this case the mean error of the PPP solution in north direction was less than 6 cm, 2 cm and 1.5 cm after 2, 4 and 6 hours respectively. In east direction, the mean error was 12 cm after 2 hours and reaches less than 3 cm after 6 hours. The results in the vertical direction were also not so good. The solution reaches less than 8 cm after 2 hours and needs a lot of time, 12 hours, to be less than 5 cm. The major limitation with single-frequency PPP is due to the ionospheric delay error. The Ionospheric delay here estimated from agencies such as the IGS can overcome only 50-60 of the ionospheric error.

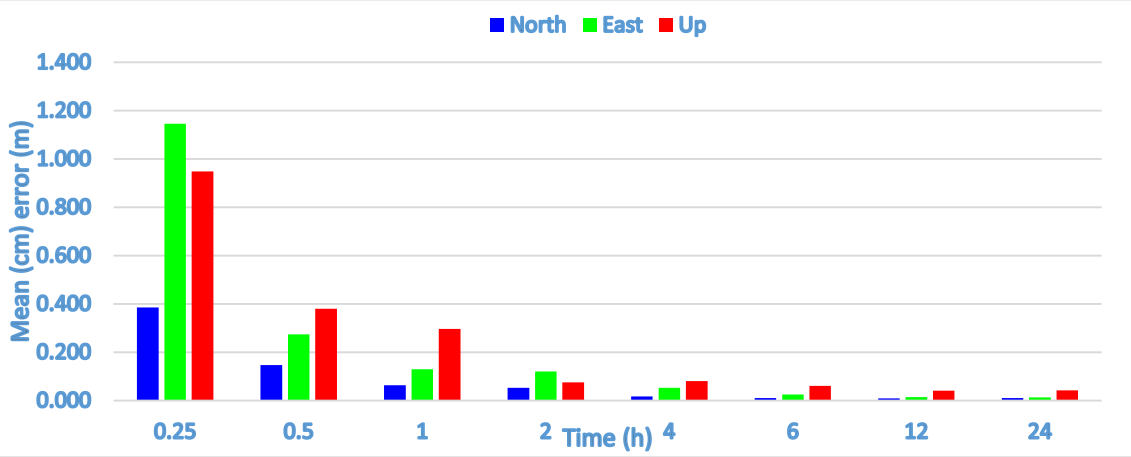

Figure (4.19) Absolute mean error of static PPP from the twelve IGS sites using single frequency observations and final precise ephemeris over the day (DOY 70, 2015) at 95% confidence level.

On the other hand, the statistical analysis for the absolute positioning errors of static PPP from SFE1 is shown in Table (4.20). Figure (4.20) illustrates the mean errors at each time span at 95% confidence level. The results of the PPP solution at SFE1 station is very close to that from IGS sites. The solution needs 4 hours to be less than 2 cm in north direction. However, it needs 6 hours to still below 3 cm in east direction. Also, in the vertical direction the PPP solution reaches less than 5 cm after 12 hours.

Table (4.20) The statistical analysis for the absolute positioning errors of static PPP from station SFE1 using single frequency observations and final precise ephemeris over the seven days at 95% confidence level.

	Time (hr.)	Max (cm)	Min (cm)	Mean (cm)	RMS (cm)
North	0.25	83.96	13.30	47.00	55.06
	0.5	42.80	7.97	21.28	25.59
	1	18.34	0.64	7.94	9.82
	2	6.15	1.43	3.83	4.10
	4	1.59	0.60	0.91	0.99
	6	2.06	0.31	1.06	1.19
	12	1.75	0.77	1.33	1.37
	24	1.54	0.89	1.22	1.23
East	0.25	269.24	25.45	122.54	141.22
	0.5	48.45	5.98	28.04	31.56
	1	73.34	12.74	42.33	46.57
	2	17.11	7.43	11.66	12.13
	4	9.28	3.39	5.46	5.82
	6	4.15	0.20	2.17	2.53
	12	3.65	0.18	2.12	2.51
	24	2.47	0.00	1.18	1.45
Up	0.25	146.78	2.76	60.24	74.03
	0.5	71.34	9.42	35.79	43.83
	1	75.66	29.32	54.07	56.17
	2	19.02	14.32	16.00	16.09
	4	8.24	4.95	6.06	6.16
	6	3.67	0.51	2.08	2.37
	12	7.49	0.50	2.59	3.58
	24	1.98	0.05	0.87	1.09

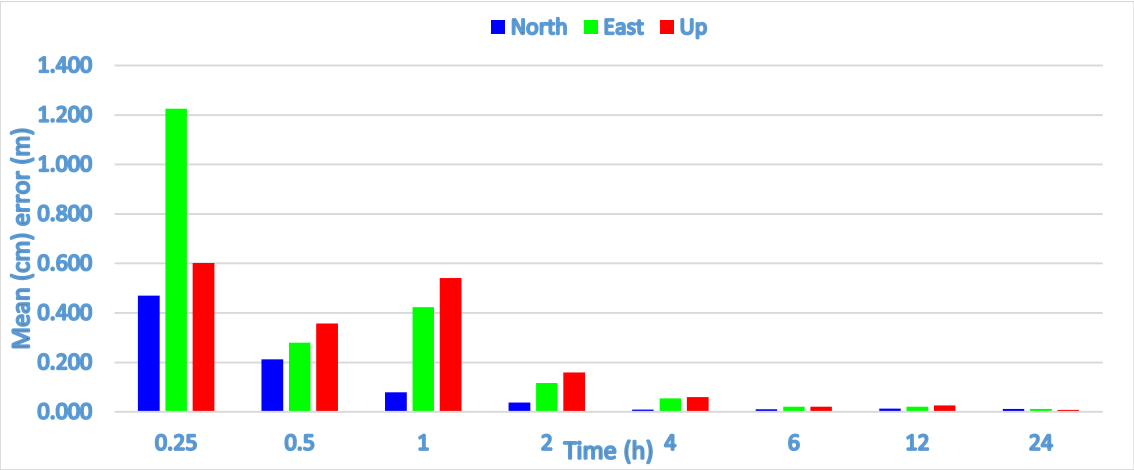

Figure (4.20) Absolute mean error of static PPP from station SFE1 using single frequency observations and final precise ephemeris over the seven days at 95% confidence level.

4.3.2.5 Case 5 Assessment of Static PPP Using Single Frequency Observations and Rapid Precise Ephemeris

In this case, rapid precise ephemeris was used along with single frequency observations from GPS-Only satellites. Figure (4.21) shows the processing results of the four stations ISPA, KOKB, UNBJ and SFE1 including the positioning errors in east, north and up directions with respect to the true station coordinates

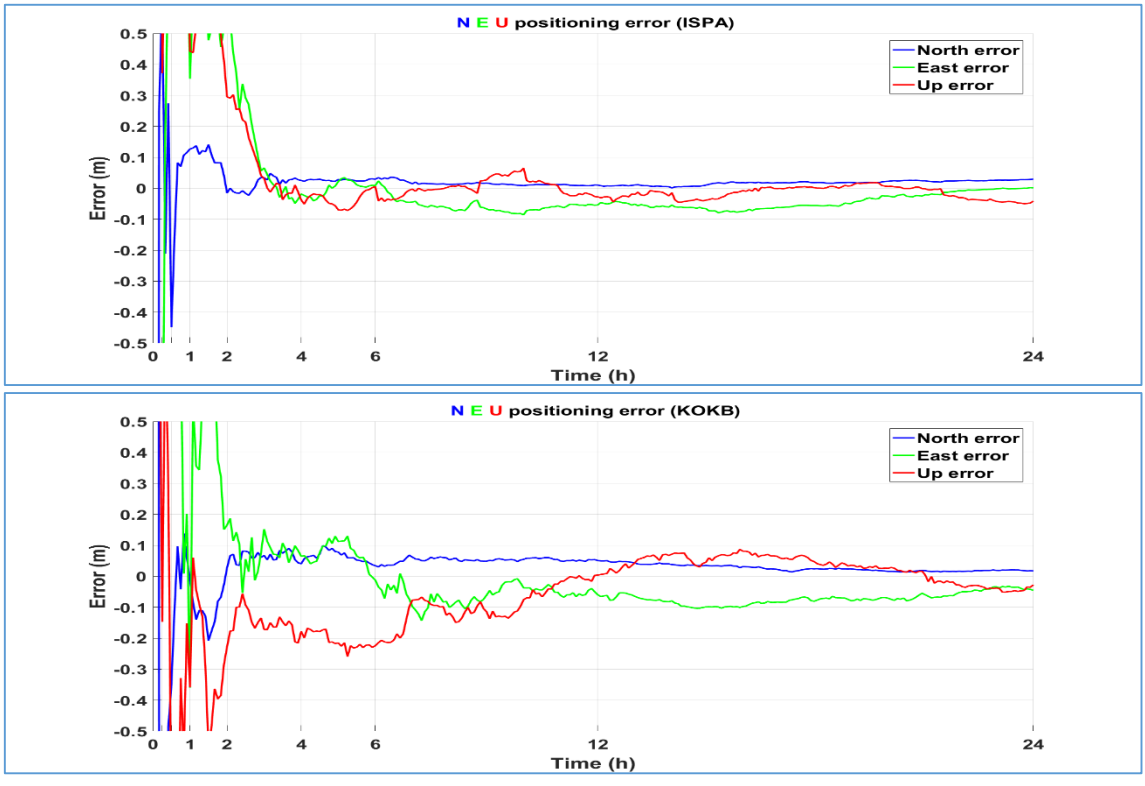

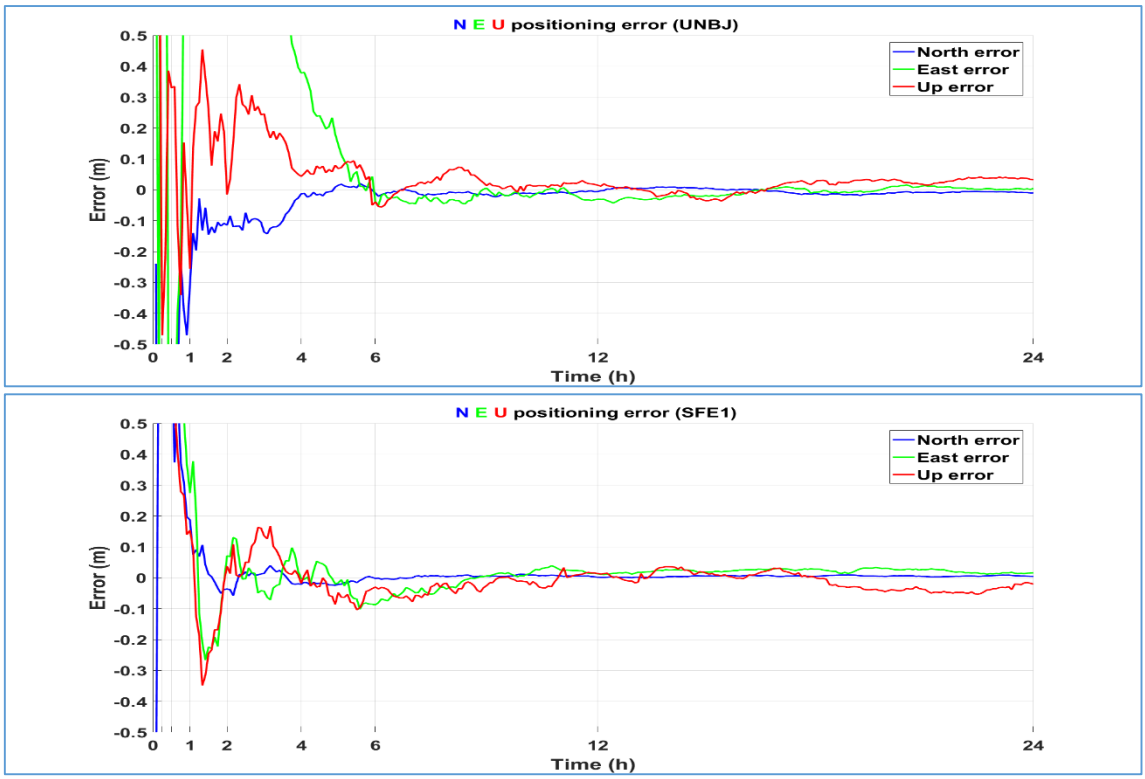

Figure (4.21) Processing results from static PPP using single frequency observations and IGS rapid ephemeris over the day (DOY 70, 2015) for stations ISPA, KOKB, UNBJ and SFE1.

Table (A.9), in Appendix A, demonstrates the processing results of static PPP using single frequency observations and rapid ephemeris for all twelve IGS stations at different time spans over the day in north, east and up directions. Whereas, Table (A.10), in Appendix A, indicates to the processing results for station SFE1 from all seven days of observations. The absolute positioning errors, maximum, minimum, mean and RMS (cm) errors, of static PPP from single observations and rapid ephemeris for the twelve IGS sites at 95% confidence level are shown in Table (4.21). Furthermore, Figure (4.22) illustrates the mean errors at each time span at 95% confidence level.

Table (4.21) The statistical analysis for the absolute positioning errors of static PPP from the twelve IGS sites using single frequency observations and rapid precise ephemeris over the day (DOY 70, 2015) at 95% confidence level.

	Time (hr.)	Max (cm)	Min (cm)	Mean (cm)	RMS (cm)
North	0.25	287.92	5.53	126.86	149.79
	0.5	87.86	4.82	37.58	45.21
	1	17.26	1.08	10.68	11.98
	2	14.89	1.53	6.18	7.54
	4	5.62	0.59	2.75	3.12
	6	3.72	0.43	1.78	2.13
	12	4.88	0.46	1.46	1.90
	24	2.97	0.16	1.27	1.49
East	0.25	358.95	1.06	118.43	171.27
	0.5	181.55	3.12	71.55	92.43
	1	141.93	1.84	39.50	62.45
	2	88.63	0.17	29.42	40.90
	4	37.81	0.28	8.39	13.17
	6	13.11	0.50	3.48	5.02
	12	5.95	0.75	2.75	3.19
	24	4.55	0.13	1.89	2.44
Up	0.25	264.16	14.69	152.69	174.47
	0.5	202.19	1.71	64.63	85.43
	1	45.72	3.22	29.39	32.29
	2	40.29	1.49	19.46	23.10
	4	32.97	2.14	11.45	14.56
	6	22.41	0.54	9.76	12.30
	12	10.62	0.38	4.30	5.27
	24	8.93	1.00	4.04	4.78

From Table (4.21), the static PPP solution from single observations and rapid precise ephemeris also needs more time to reach more accurate results. In this case the mean error of the PPP solution in north direction was less than 7 cm, 3 cm and 2 cm after 2, 4 and 6 hours respectively. In east direction, the mean error was 30 cm after 2 hours and reaches less than 10 cm after 4 hours up to less than 5 cm after 6 hours. The results in the vertical direction reaches less than 12 cm after 4 hours and needs a lot of time, 12 hours, to be less than 5 cm.

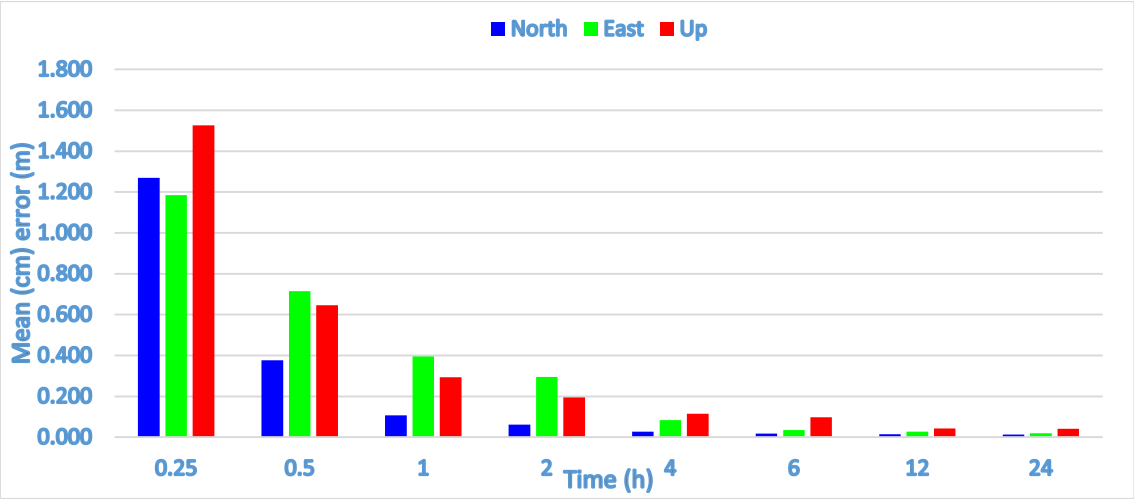

Figure (4.22) Absolute mean error of static PPP from the twelve IGS sites using single frequency observations and rapid precise ephemeris over the day (DOY 70, 2015) at 95% confidence level.

The statistical analysis for the absolute positioning errors of static PPP from station SFE1 is presented in Table (4.22). For a clear view, Figure (4.23) illustrates the mean errors at each time span at 95% confidence level. From Table (4.22), it is seen that the static PPP solution from single observations and rapid precise ephemeris from SFE1 station was close to a small extent to the results from IGS sites. The static PPP solution from SFE1 reaches about 3 cm in north, 7 cm in east and less than 6 cm in up direction after 4 hours. While after 6 hours the solution reaches less than 2 cm and 5 cm in north and east directions respectively. The PPP solution can reach less than 5 cm in the vertical direction after 12 hours.

Table (4.22) The statistical analysis for the absolute positioning errors of static PPP from station SFE1 over the seven days using single frequency observations and rapid precise ephemeris at 95% confidence level.

	Time (hr.)	Max (cm)	Min (cm)	Mean (cm)	RMS (cm)
North	0.25	178.07	6.14	59.75	85.67
	0.5	82.86	17.55	53.38	57.99
	1	36.36	3.47	17.54	20.57
	2	9.61	0.43	5.84	6.88
	4	5.69	0.72	2.30	3.03
	6	2.27	0.16	0.96	1.20
	12	2.68	0.22	1.31	1.61
	24	2.17	0.06	0.94	1.23

East	0.25	504.63	0.88	193.64	245.07
	0.5	232.37	19.74	140.78	157.58
	1	71.43	3.19	35.79	41.47
	2	43.83	0.57	18.81	23.62
	4	19.73	0.20	6.47	9.13
	6	8.75	1.37	3.82	4.56
	12	9.42	0.73	4.62	5.74
	24	5.51	1.03	2.98	3.36

Up	0.25	674.49	47.21	255.65	325.41
	0.5	228.69	7.41	91.36	118.52
	1	53.08	7.73	25.57	29.55
	2	43.26	3.78	24.05	28.96
	4	11.35	1.77	5.78	6.44
	6	15.00	0.38	5.22	7.04
	12	5.85	0.97	2.96	3.52
	24	9.14	0.39	5.44	6.26

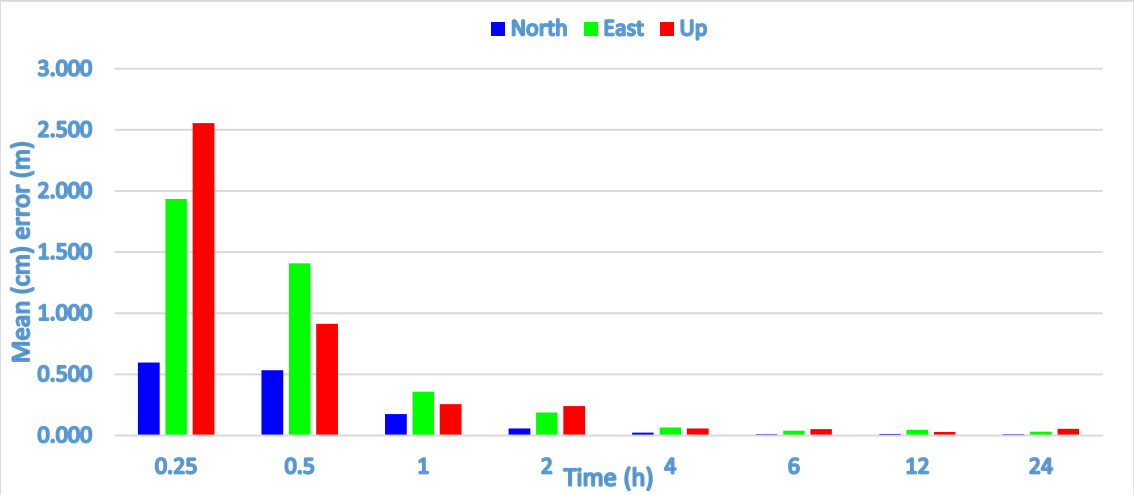

Figure (4.23) Absolute mean error of static PPP from station SFE1 over the seven days using single frequency observations and rapid precise ephemeris at 95% confidence level.

4.3.2.6 Case 6 Assessment of Static PPP Using Single Frequency Observations and Ultra-Rapid Precise Ephemeris

In this case, single frequency observations were considered from GPS-Only satellites and ultra-rapid precise ephemeris. We used klobuchar (GPS) model, broadcasted with the navigation message, to eliminate ionospheric delay error in processing of single observations as there is no ultra-rapid

ionospheric model. The processing results of the four stations ISPA, KOKB, UNBJ and SFE1 using single frequency observations and ultra-rapid precise ephemeris are shown in Figure (4.24), including the positioning errors in east, north and up directions with respect to the true station coordinates.

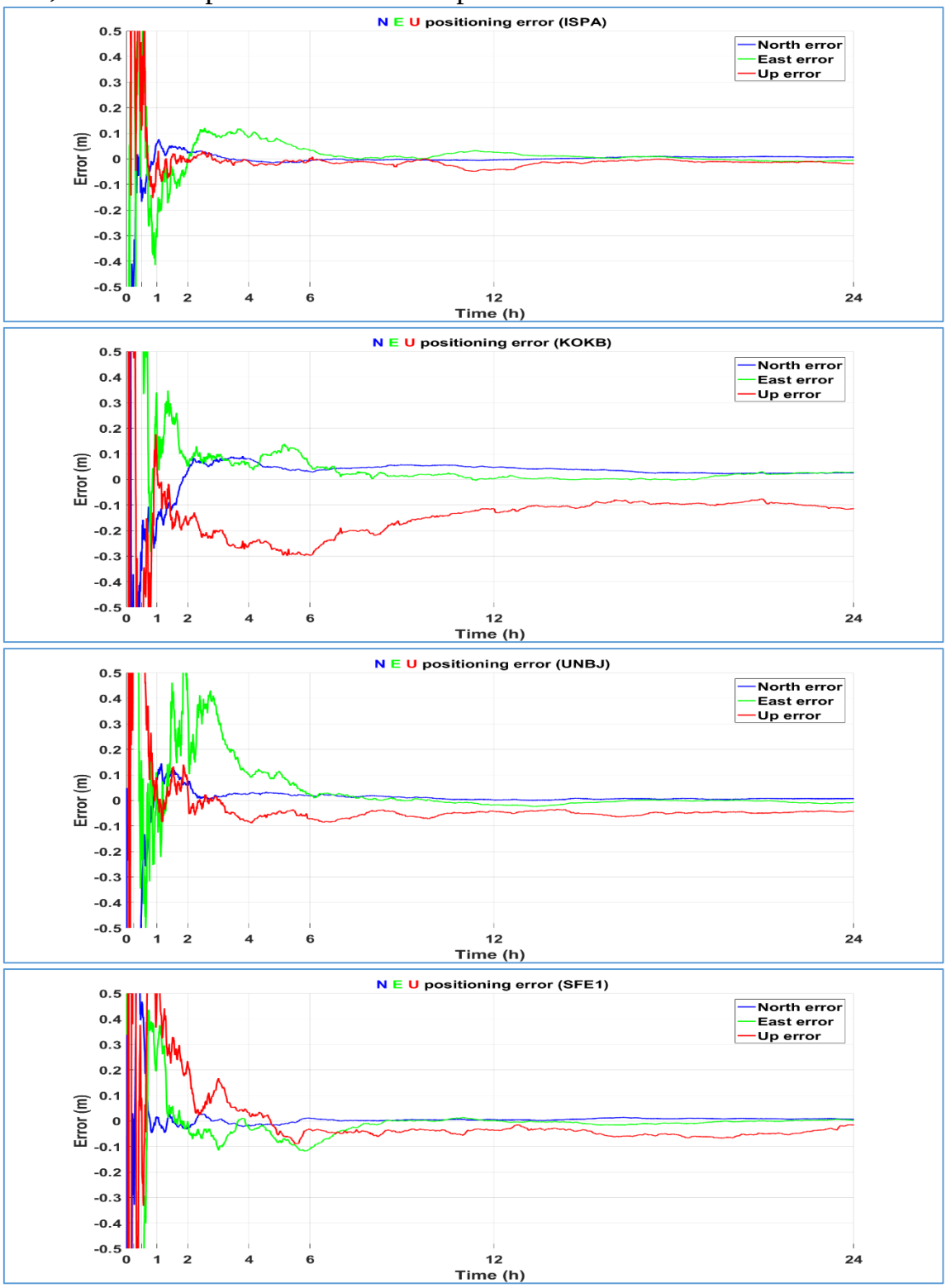

Figure (4.24) Processing results from static PPP using single frequency observations and ultra-rapid precise ephemeris over the day (DOY 70, 2015) for stations ISPA, KOKB, UNBJ and SFE1.

With respect to convergence time of PPP solution in this case, Table (A.11), in Appendix A, illustrates the processing results for all twelve IGS sites at different time sessions all the day in north, east and up directions. While Table (A.12) shows the processing results for station SFE1 from all seven days of observation. The statistical analysis results, maximum, minimum, mean and RMS (cm) errors, for the absolute positioning errors of static PPP from the twelve IGS sites at 95% confidence level are shown in Table (4.23). Also, Figure (4.25) display the mean errors at each time span.

Table (4.23) The statistical analysis for the absolute positioning errors of static PPP from the twelve IGS sites over the day (DOY 70, 2015) using single frequency observations and ultra-rapid precise ephemeris at 95% confidence level.

	Time (hr.)	Max (cm)	Min (cm)	Mean (cm)	RMS (cm)
North	0.25	108.69	3.21	47.30	56.89
	0.5	39.58	0.01	21.70	25.82
	1	15.29	0.47	7.18	8.52
	2	16.56	1.32	5.65	7.15
	4	5.11	0.14	1.89	2.49
	6	3.06	0.12	1.10	1.43
	12	2.37	0.22	1.03	1.27
	24	2.58	0.36	1.30	1.49
East	0.25	446.54	27.90	178.06	228.63
	0.5	98.53	3.36	35.94	44.03
	1	30.74	1.48	15.80	18.82
	2	41.91	0.02	13.48	20.00
	4	16.54	0.61	7.14	8.63
	6	11.86	0.05	3.61	4.74
	12	3.23	0.02	1.31	1.74
	24	2.74	0.25	1.23	1.47
Up	0.25	189.84	20.58	96.22	111.19
	0.5	82.29	9.38	42.81	49.26
	1	49.35	3.14	22.89	28.58
	2	17.86	0.30	8.02	10.13
	4	26.20	0.62	9.50	12.57
	6	15.79	0.27	5.56	7.07
	12	11.41	0.25	4.94	5.90
	24	8.40	0.88	3.95	4.44

In this case it is observed that, from Table (4.23), the static PPP solution from the twelve IGS sites at 95% confidence level did not improve to level of 1 cm in horizontal and 4 cm in vertical component even after 24 hours. The solution reaches less than 2 cm in north direction after 4 hours. In the east direction the solution reaches less than 4 and 2 cm after 6 and 12 hours respectively. The vertical component needs more time to reach 5 cm. It reaches less than 5 cm after 12 hours.

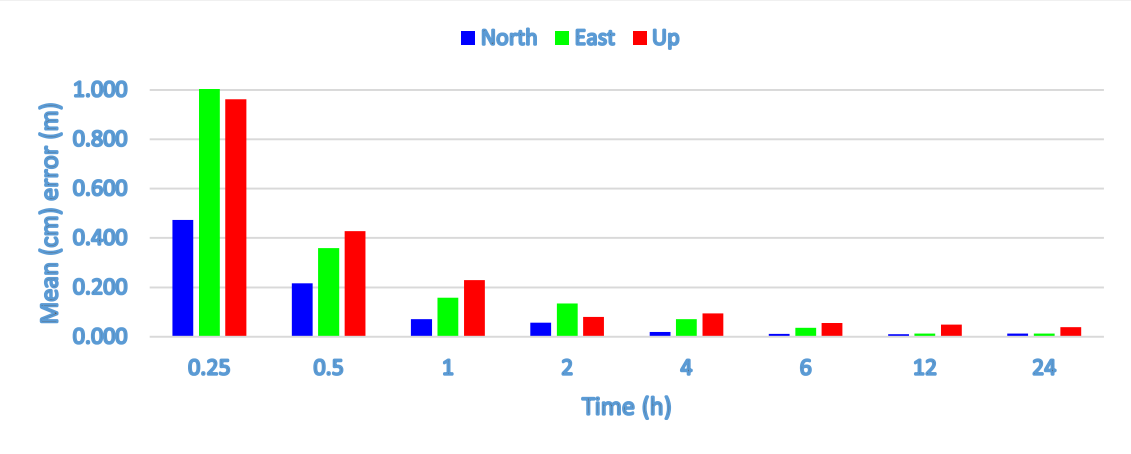

Figure (4.25) Absolute mean error of static PPP from the twelve IGS sites using single frequency observations and ultra-rapid precise ephemeris over the day (DOY 70, 2015) at 95% confidence level.

Besides, the statistical analysis results for the absolute positioning errors of static PPP from station SFE1 is shown in Table (4.24). Also, Figure (4.26) illustrates the mean errors at each time span at 95% confidence level. From Table (4.24) it is cleared observed that the static PPP solution at station SFE1 is similar to the results from IGS sites.

Table (4.24) The statistical analysis for the absolute positioning errors of static PPP from station SFE1 over the seven days using single frequency observations and ultra-rapid precise ephemeris at 95% confidence level.

	Time (hr.)	Max (cm)	Min (cm)	Mean (cm)	RMS (cm)
North	0.25	135.35	3.59	51.33	67.74
	0.5	44.52	4.55	21.43	24.63
	1	13.83	0.79	4.79	6.87
	2	5.53	2.05	4.16	4.38
	4	2.76	0.12	1.28	1.58
	6	2.13	0.06	0.84	1.08
	12	2.40	0.47	1.33	1.48
	24	2.10	0.59	1.21	1.30

East	0.25	197.71	42.66	131.18	145.48
	0.5	94.36	13.56	45.37	52.22
	1	82.10	19.55	53.04	58.20
	2	22.54	0.09	9.92	12.37
	4	13.60	0.12	6.31	7.70
	6	4.59	0.56	2.58	2.91
	12	3.19	0.15	1.78	2.06
	24	3.29	0.24	1.42	1.73
Up	0.25	160.25	10.52	87.52	105.77
	0.5	155.21	7.41	63.36	77.61
	1	105.27	49.54	72.09	74.68
	2	28.10	0.28	17.04	19.50
	4	7.61	2.80	4.80	5.12
	6	5.84	3.22	4.17	4.27
	12	8.00	0.15	3.68	4.45
	24	2.63	0.10	1.14	1.49

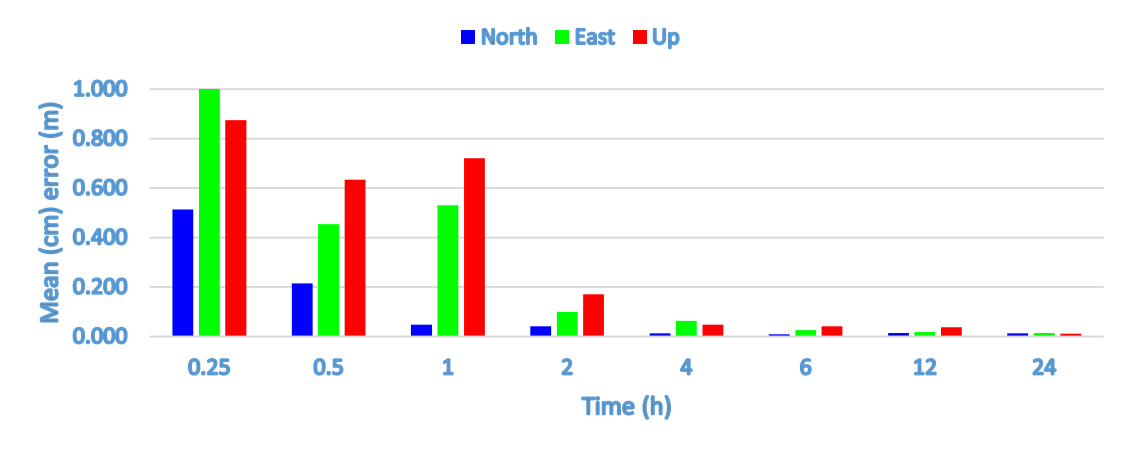

Figure (4.26) Absolute mean error of static PPP from station SFE1 over the seven days using single frequency observations and ultra-rapid precise ephemeris at 95% confidence level.

4.3.3 Assessment of Kinematic PPP In gLAB

In this assessment the performance of kinematic PPP will be evaluated using single and dual frequency observations with final, rapid and ultrarapid precise ephemeris across. Shown in Figure (4.27) the number of GPS satellites used in the data processing for the kinematic dataset. An average of 9 satellites was observed during PPK session. Besides, the number of

satellites in view, the satellite geometry (DOPs) shown in Figure (4.28) affects greatly the estimated position.

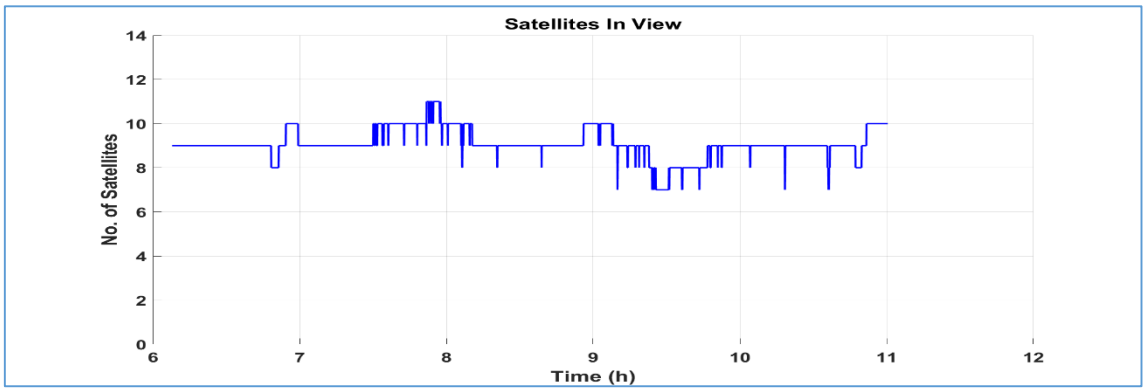

Figure (4.27) Satellite in view for the kinematic dataset.

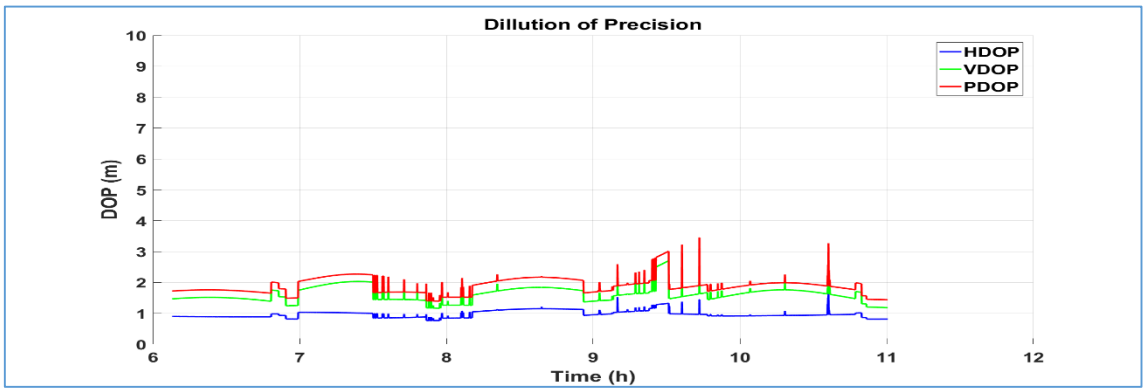

Figure (4.28) Satellite geometry (DOP) for the kinematic dataset.

Assessment of kinematic test was based on observations started with 1 hour static initialization followed by about 4 hours of continuous kinematic trajectory. Table (4.25) and Figure (4.29) shows the processing results of dual frequency observations and final precise orbits and clock products at 95% confidence level, including the positioning errors in east, north and up directions with respect to the true coordinates of stations obtained from relative solution. These graphs represent the accuracy of PPP solution which reflect how different the position estimate is from its true coordinates

Table (4.25) Absolute positioning errors in cm of kinematic PPP solution using dual frequency observations and final precise ephemeris at 95% confidence level.

	Max (cm)	*Min (cm)*	*Mean (cm)*	*RMS (cm)*
North	***2.91***	***0.00***	***1.07***	***1.34***
East	***4.00***	***0.00***	***1.96***	***2.20***
Up	***16.24***	***0.00***	***6.26***	***7.75***

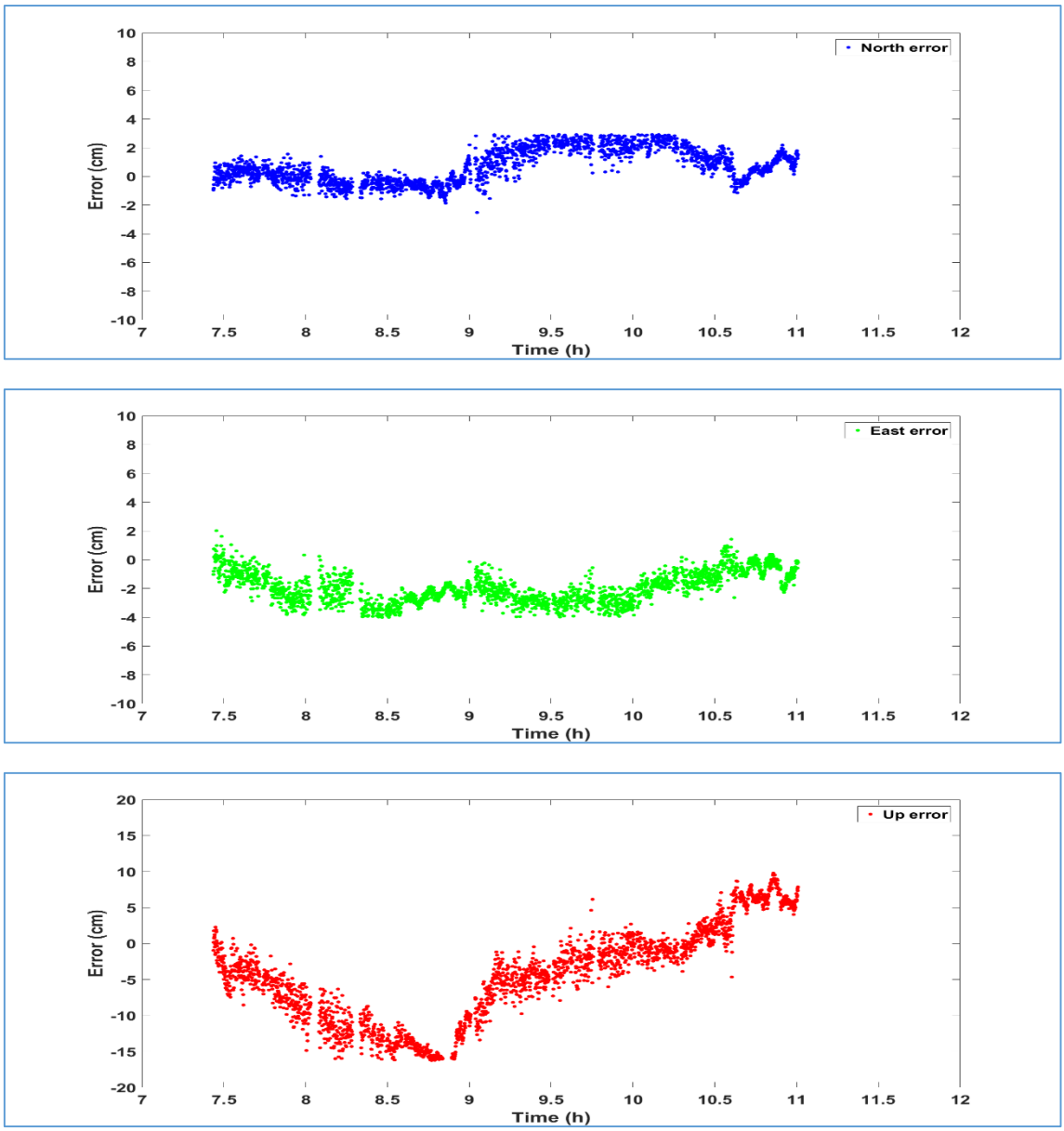

Figure (4.29) Positioning errors in cm of kinematic PPP solution for North (blue), East (green) and Up (red) components respectively using dual observations and final precise ephemeris at 95% confidence level.

From Table (4.25), it can be deduced that kinematic PPP solution reaches a high accuracy from dual frequency observations and final precise ephemeris. The absolute mean errors of results were about 1.07 cm, 1.96 cm and 6.26 cm in north, east and up directions respectively at 95% confidence level. The RMS (cm) also depicts this high accuracy with values 1.34 cm, 2.20 cm and 7.75 cm in north, east and up directions respectively. These high results are possible be interpreted due to the good DOP values at the observation time. With the aim of take advantage of latency of rapid precise ephemeris, kinematic PPP solution was done using dual frequency observations and

rapid precise ephemeris. Table (4.26) and Figure (4.30) show the processing results of dual frequency observations and rapid precise orbits and clock products at 95% confidence level.

Table (4.26) Absolute positioning errors in cm of kinematic PPP solution using dual frequency observations and rapid precise ephemeris at 95% confidence level.

	Max (cm)	*Min (cm)*	*Mean (cm)*	*RMS (cm)*
North	***3.68***	***0.00***	***1.26***	***1.54***
East	***4.93***	***0.00***	***1.63***	***2.02***
Up	***19.36***	***0.00***	***5.68***	***7.13***

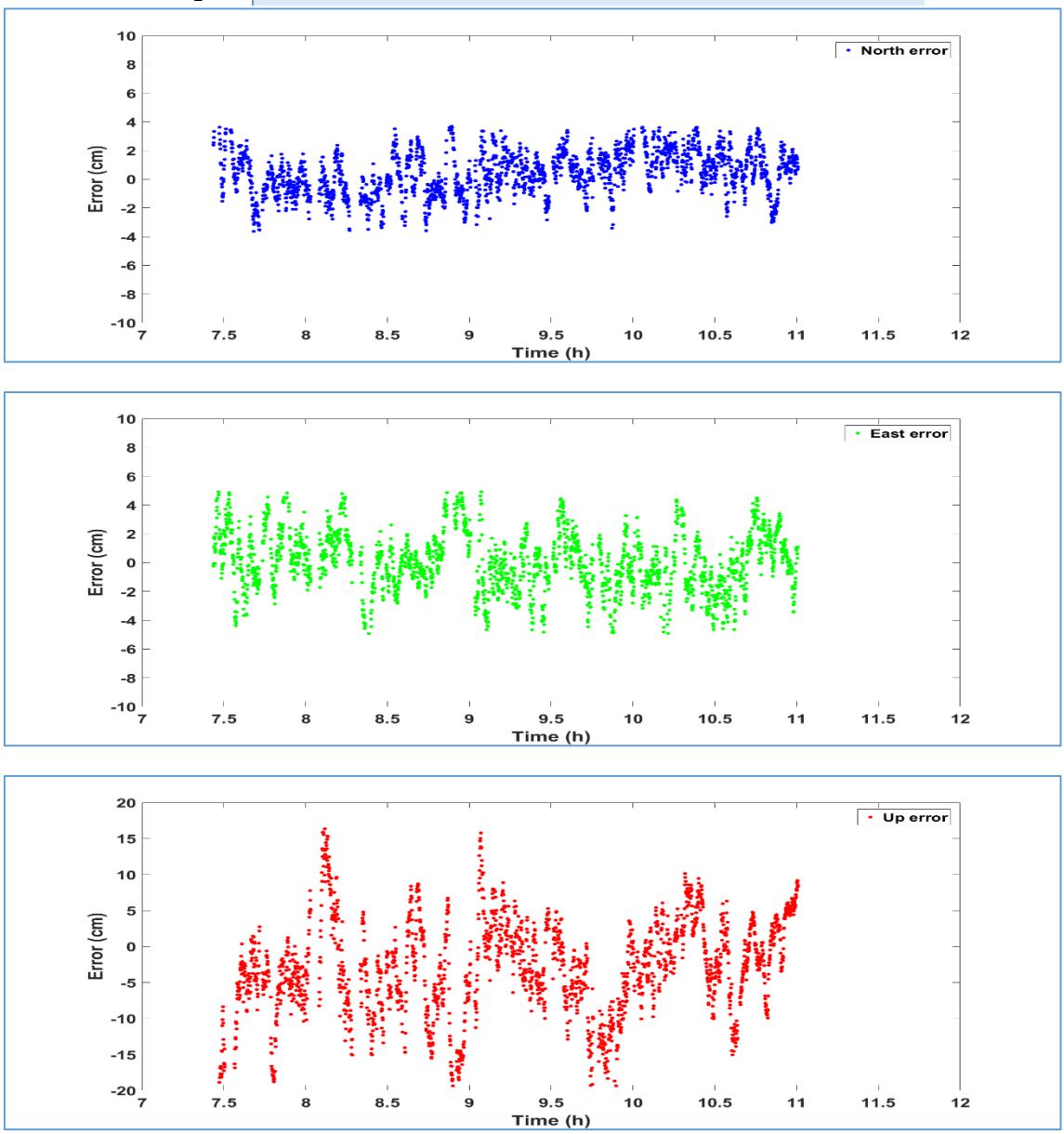

Figure (4.30) Positioning errors in cm of kinematic PPP solution for North (blue), East (green) and Up (red) components respectively using dual frequency observations and rapid precise ephemeris at 95% confidence level.

From Table (4.26), it can be concluded that kinematic PPP solution from dual frequency observations and rapid precise ephemeris almost close to that solution from final precise ephemeris. The absolute mean errors of results from rapid precise ephemeris were 1.26 cm, 1.63 cm and 5.68 cm in north, east and up directions respectively at 95% confidence level. Moreover, the RMS (cm) values was 1.54 cm, 2.02 cm and 7.13 cm in north, east and up directions respectively. It is observed that, from Tables (4.25) and (4.26), the results from final and rapid ephemeris using dual frequency observations were almost the same with a slight improvement using rapid ephemeris. Therefore, there is no need to wait 14-18 days to download and use final precise ephemeris. This can be interpreted due to good DOP values at the observation time and the long initialization time of one hour.

Additionally, the processing results from dual frequency observations and ultrarapid ephemeris are shown in Table (4.27) and Figure (4.31). It is noticed that the mean error of kinematic PPP solution using ultrarapid ephemeris increased to reach about 3 cm in north and east components and about 13 cm in vertical component. The increase of mean error may be due to low accuracy of ultrarapid precise ephemeris compared to final or rapid ephemeris as it is published after only three hours of observation process.

Table (4.27) Absolute positioning errors in cm of kinematic PPP solution using dual frequency observations and ultrarapid precise ephemeris at 95% confidence level.

	Max (cm)	*Min (cm)*	*Mean (cm)*	*RMS (cm)*
North	***7.24***	***0.00***	***2.66***	***3.18***
East	***6.44***	***0.00***	***2.41***	***2.90***
Up	***34.10***	***0.01***	***12.21***	***14.66***

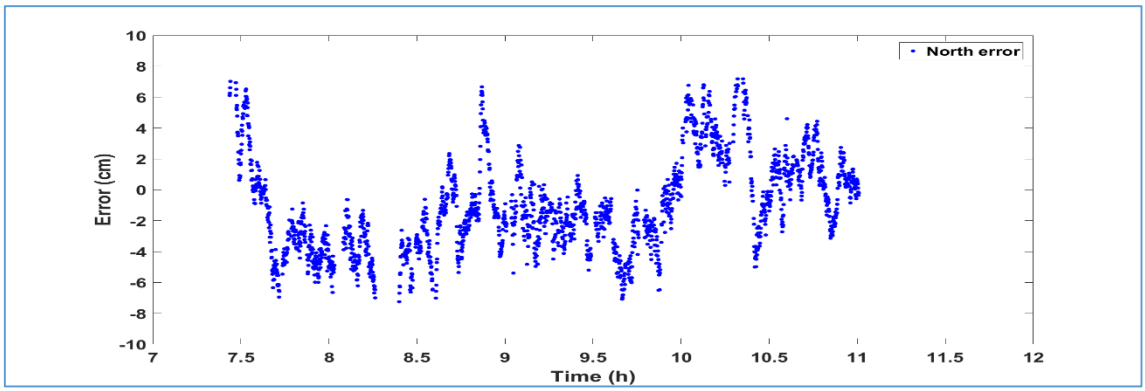

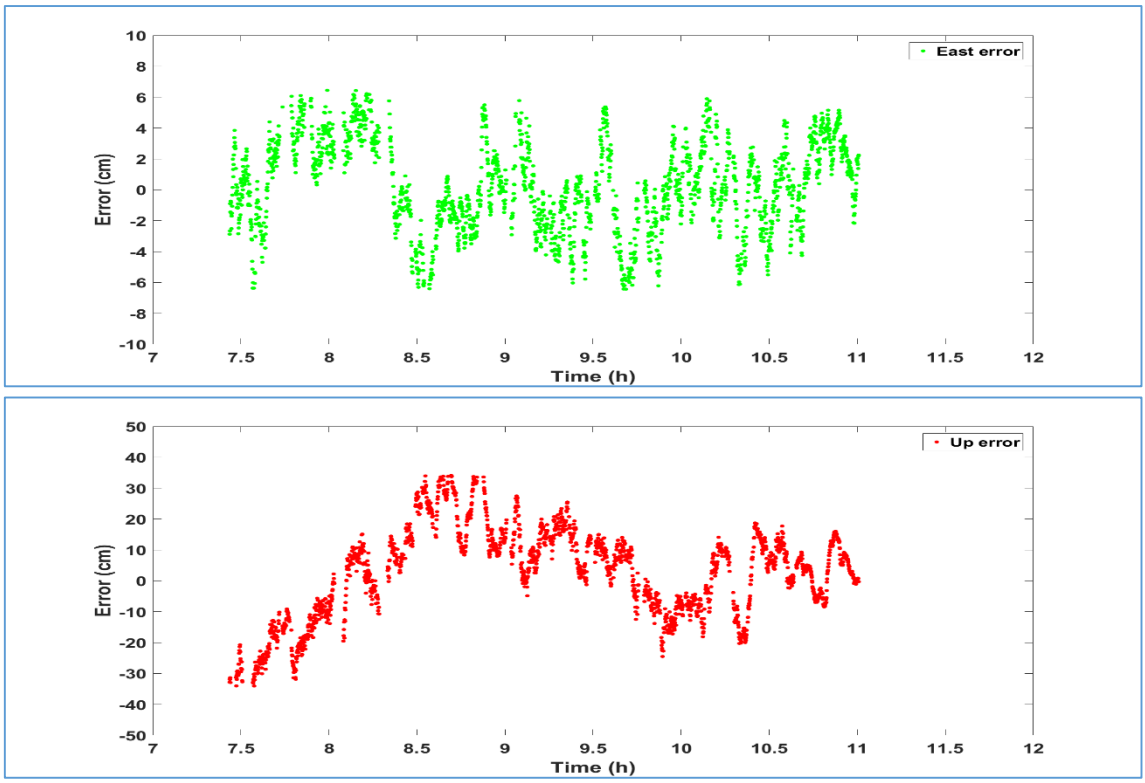

Figure (4.31) Positioning errors in cm of kinematic PPP solution for North (blue), East (green) and Up (red) components respectively using dual frequency observations and ultrarapid precise ephemeris at 95% confidence level.

To assess the accuracy of kinematic PPP using single frequency observations, Table (4.28) and Figure (4.32) show the processing results of single frequency observations and final precise orbits and clock products at 95% confidence level, including the positioning errors in east, north and up directions respectively.

Table (4.28) Absolute positioning errors in cm of kinematic PPP solution using single observations and final precise ephemeris at 95% confidence level.

	Max (cm)	*Min (cm)*	*Mean (cm)*	*RMS (cm)*
North	***18.49***	***0.01***	***6.71***	***8.14***
East	***23.44***	***0.01***	***8.38***	***10.19***
Up	***62.66***	***0.02***	***22.85***	***27.68***

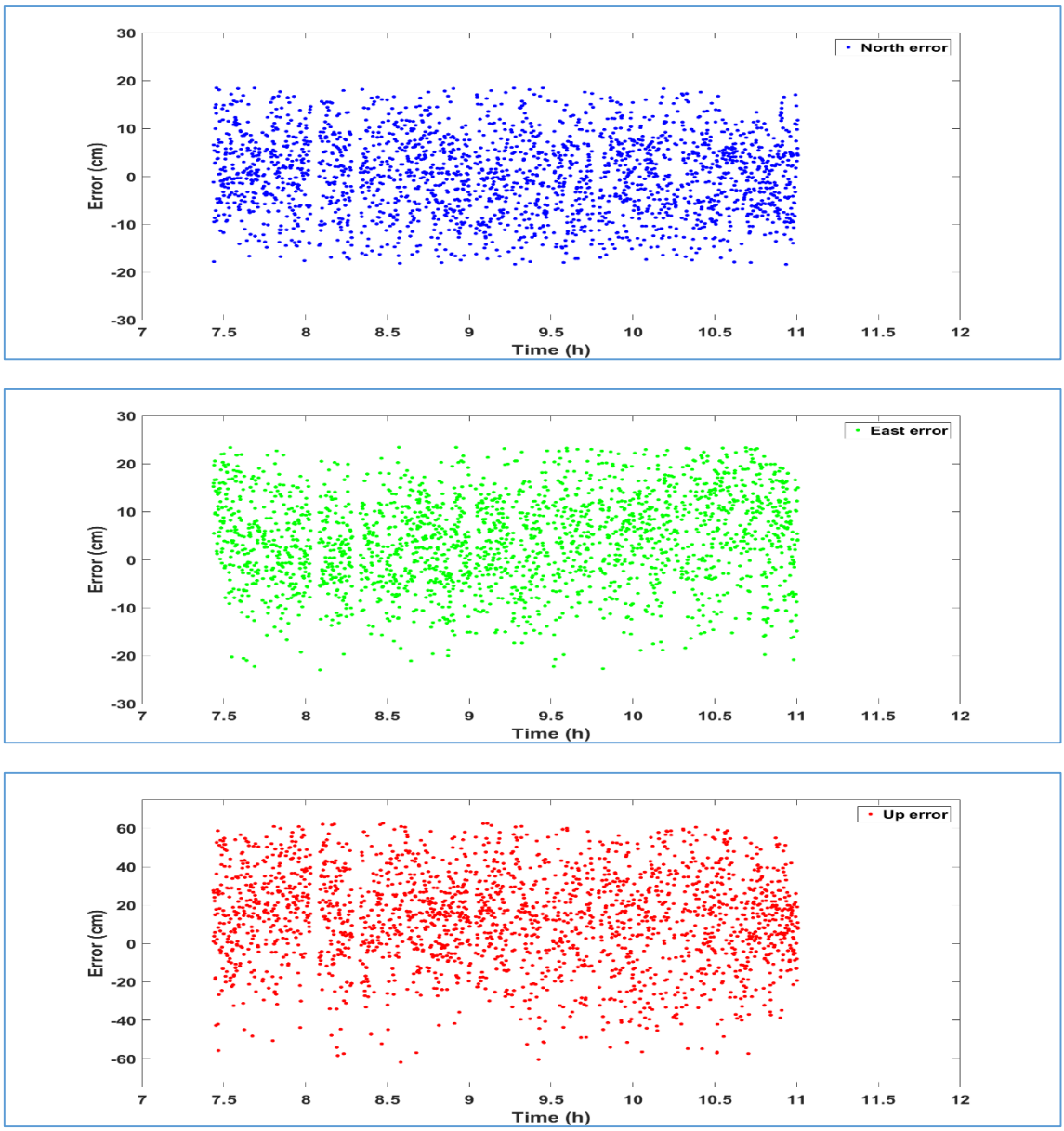

Figure (4.32) Positioning errors in cm of kinematic PPP solution for North (blue), East (green) and Up (red) components respectively using single observations and final precise ephemeris at 95% confidence level.

Also, Table (4.29) and Figure (4.33) show the processing results of kinematic PPP solution from single frequency observations and rapid precise orbits and clock products at 95% confidence level, including the positioning errors in east, north and up directions respectively.

Table (4.29) Absolute positioning errors in cm of kinematic PPP solution using single observations and rapid precise ephemeris at 95% confidence level.

	Max (cm)	*Min (cm)*	*Mean (cm)*	*RMS (cm)*
North	***19.08***	***0.00***	***6.85***	***8.33***
East	***25.90***	***0.01***	***9.47***	***11.48***
Up	***64.31***	***0.03***	***23.61***	***28.51***

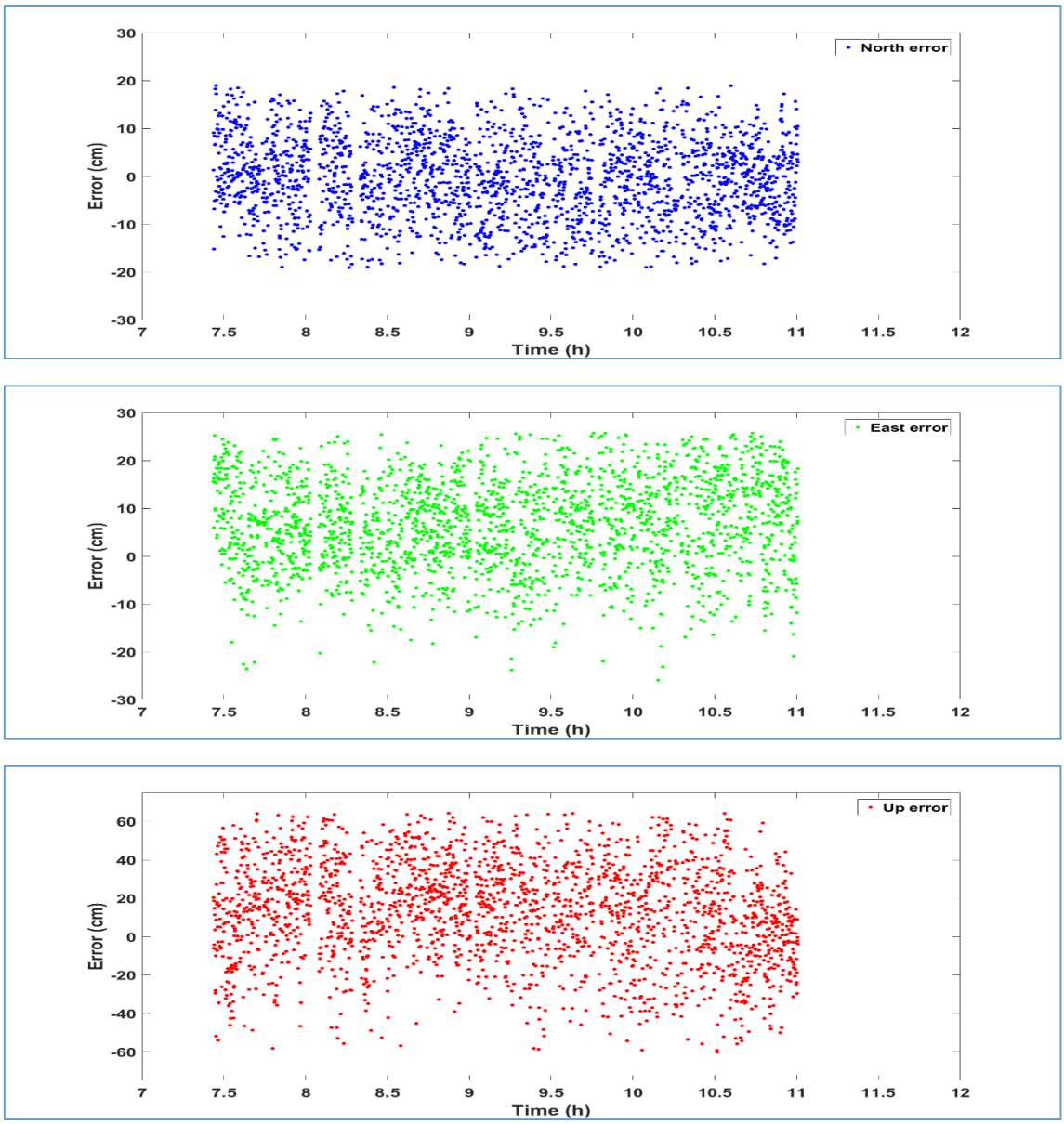

Figure (4.33) Positioning errors in cm of kinematic PPP solution for North (blue), East (green) and Up (red) components respectively using single observations and rapid precise ephemeris at 95% confidence level.

From Tables (4.28) and (4.29), the kinematic PPP solution from single frequency observations and final or rapid precise ephemeris reaches about 7 and 9 cm in horizontal and vertical directions and about 23 cm in vertical direction. Although, using final precise ephemeris, there was a disparity of PPP results from single and dual frequency observations. This disparity is duo to using precise ionospheric models to eliminate the ionospheric delay in PPP solution which can eliminate only 50-60 of the error. On the contrary, ionosphere free linear combinations were used in dual frequency observations to mitigate 99.9 of the ionosphere error.

Furthermore, Table (4.30) and Figure (4.34) indicates to results from single frequency observations and ultrarapid precise ephemeris. The results from ultrarapid ephemeris almost close to ones from final or rapid ephemeris.

Table (4.30) Absolute positioning errors in cm of kinematic PPP solution using single frequency observations and ultrarapid precise ephemeris at 95% confidence level.

	Max (cm)	*Min (cm)*	*Mean (cm)*	*RMS (cm)*
North	20.49	0.00	7.33	8.92
East	25.94	0.01	9.62	11.66
Up	66.64	0.03	24.92	30.03

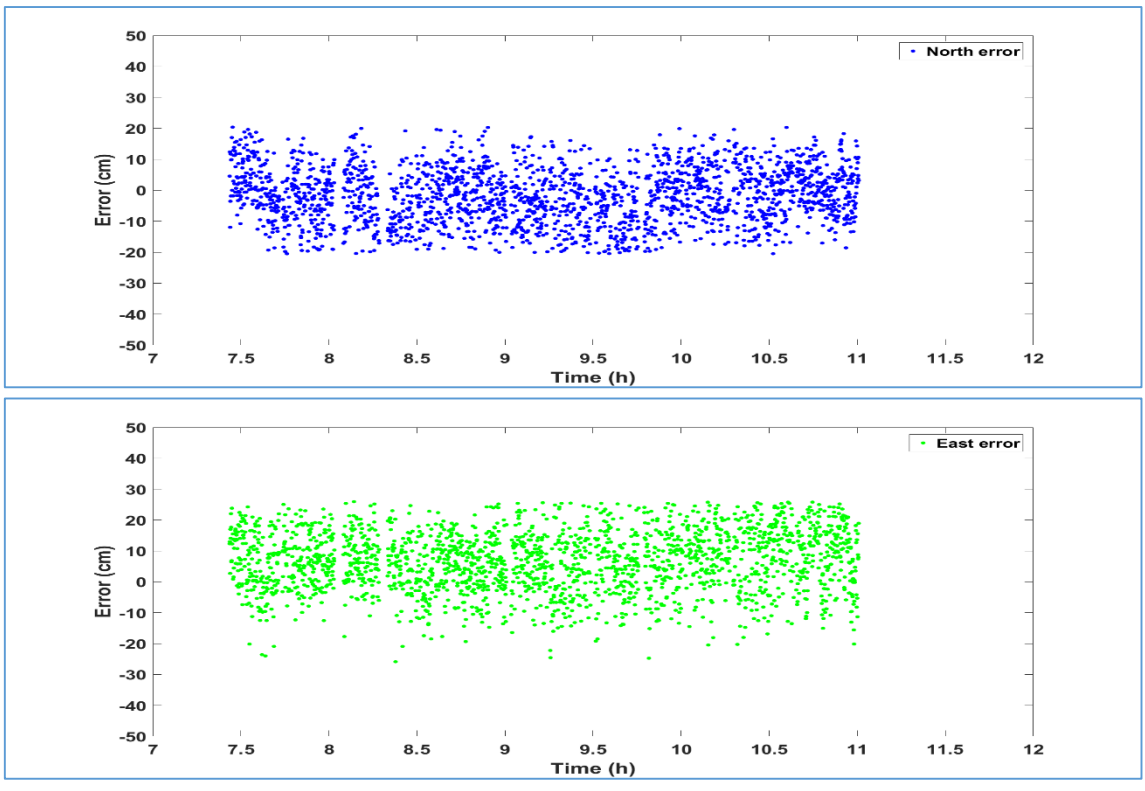

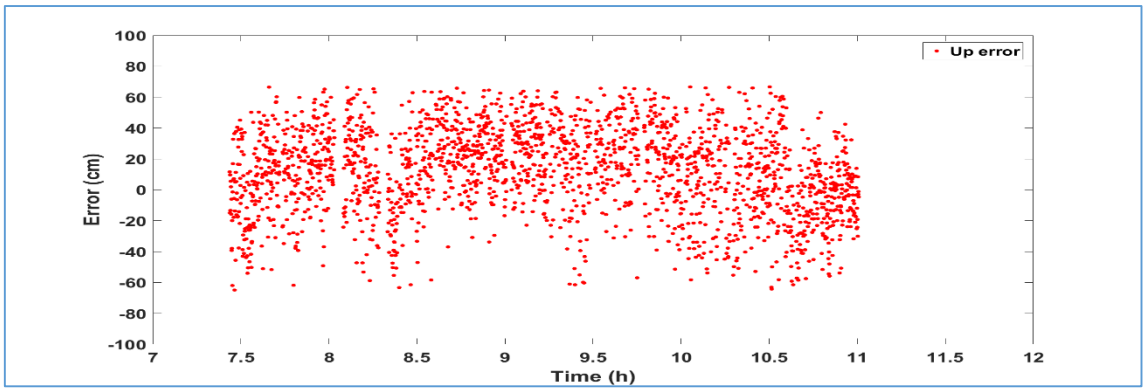

Figure (4.34) Positioning errors in cm of kinematic PPP solution for North (blue), East (green) and Up (red) components respectively using single frequency observations and ultrarapid precise ephemeris at 95% confidence level.

4.4 Results from CSRS-PPP Online Service

Recently, several web-based on-line processing services are used to estimate PPP-derived coordinates. The use of these processing services has become widely popular because of their ease of use, being free of charge and no requirement of a license and knowledge of a GPS processing software (R.M. Alkan et al., 2013). The only thing for users is to upload RINEX observation files in the web-based workspace or send them via e-mail which will be processed automatically and estimated coordinates will send back to the user. Figure (4.35) shows the website for CSRS-PPP service. CSRS-PPP service uses NRCan-PPP software operated by the Geodetic Survey Division of Natural Resources, Canada. The CSRS-PPP service was used to assess the PPP solution in static and kinematic mode using dual frequency observations from GPS-Only and GPS+GLONASS satellites.

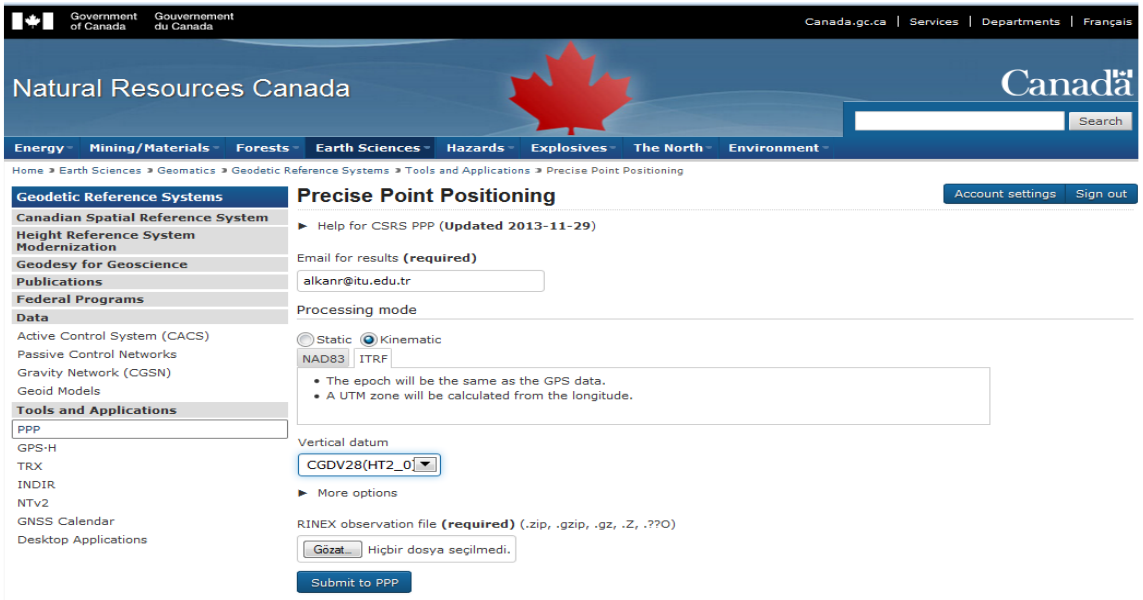

Figure (4.35) CSRS-PPP Online Service (http://www.nrcan.gc.ca/).

4.4.1 Assessment of Static PPP from CSRS-PPP Online Service

In this section, the results obtained from CSRS-PPP online service in static mode will be demonstrated. Dual frequency observations were considered from GPS-Only and GPS+GLONASS satellites and final precise ephemeris. In order to assess the accuracy performance of PPP technique by using CSRS-PPP on-line service in static mode, twelve IGS sites were used in addition to observations from station SFE1 located at the roof of Faculty of Engineering at Shoubra. The site coordinates from International GNSS Service and fixed coordinates of station SFE1 were used as true coordinates to assess the accuracy of PPP solution. The estimated three-dimension coordinate from PPP solution has been converted to position discrepancies in north, east, and up components with respect to the true coordinates.

At first, Figures (4.36) and (4.37) show the change in number of satellites in view and Geometric Dillution Of Precision (GDOP) due to using GPS-Only and GPS+GLONASS satellites.

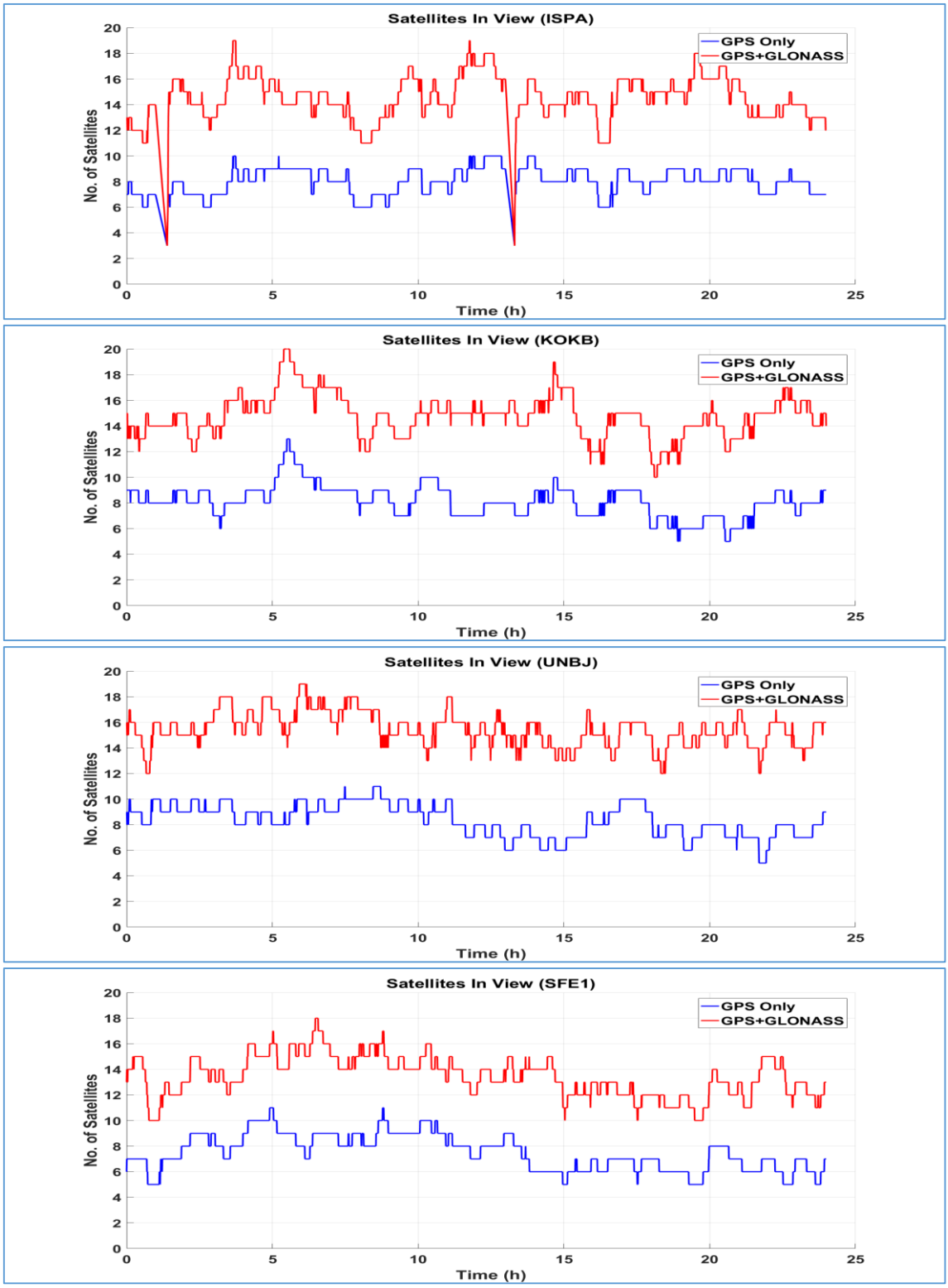

Figure (4.36) Number of satellites in view for stations ISPA, KOKB, UNBJ and SFE1 using GPS-Only and GPS+GLONASS satellites.

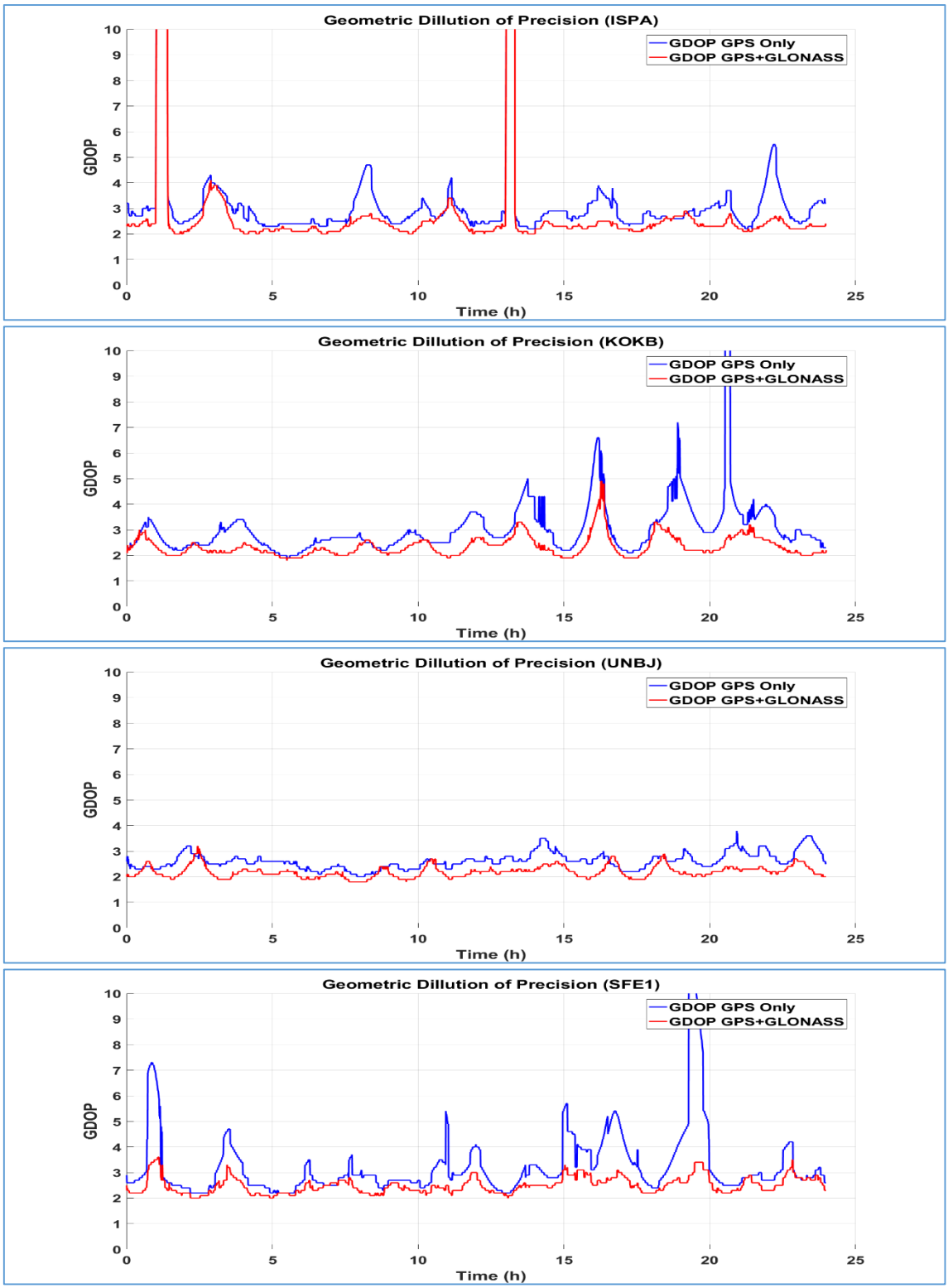

Figure (4.37) Satellite geometry (DOP) for stations ISPA, KOKB, UNBJ and SFE1 using GPS-Only and GPS+GLONASS satellites.

Figure (4.38) shows the processing results of four stations ISPA, KOKB, UNBJ and SFE1 using dual frequency GPS-Only observations and final precise ephemeris, including the positioning errors in east, north and up

directions with respect to the true coordinates. These figures illustrate the accuracy of CSRS-PPP solutions over the day.

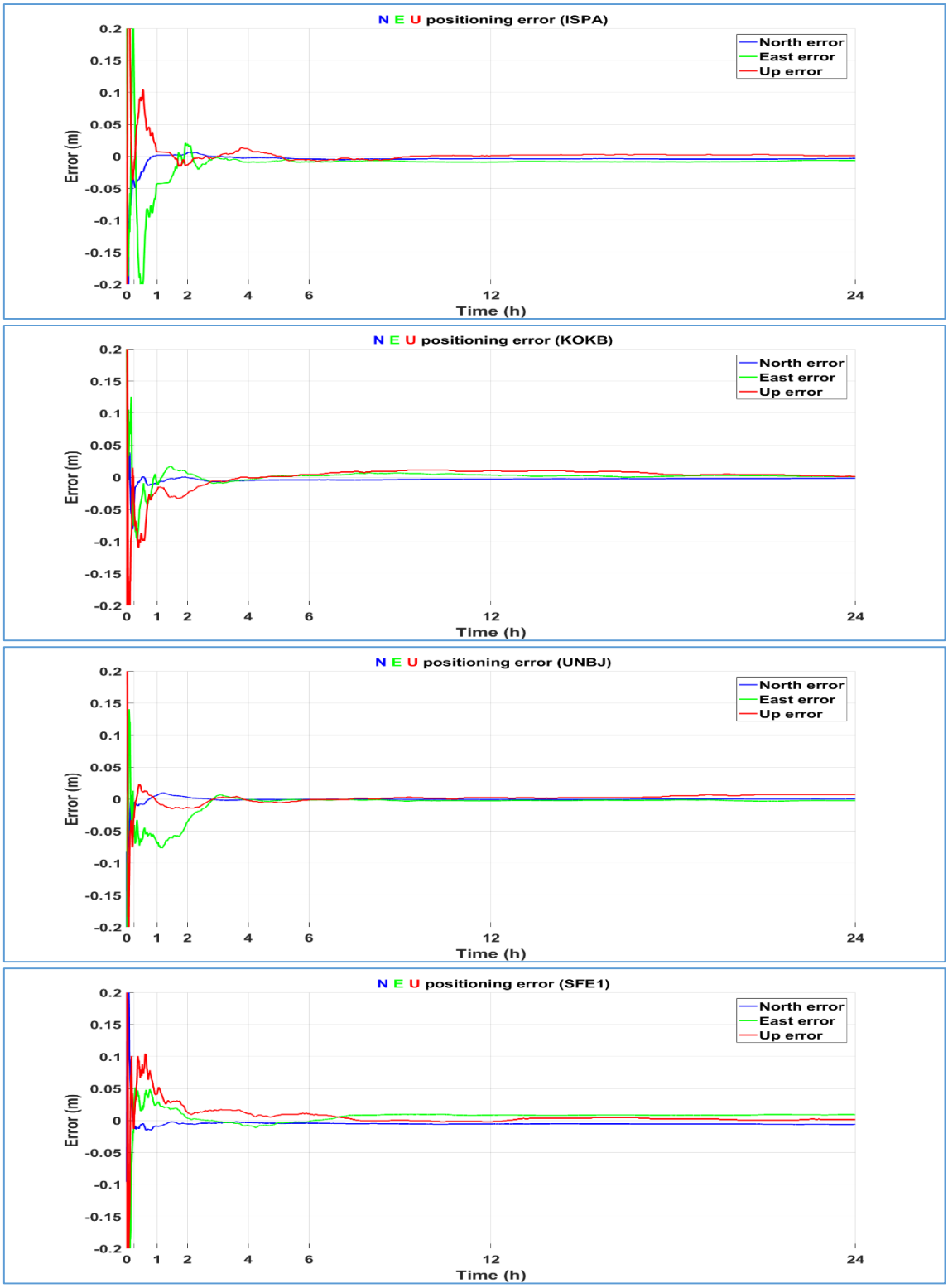

Figure (4.38) CSRS-PPP results from static PPP using dual frequency GPS-Only observations and final precise ephemeris over the day (DOY 70, 2015) for stations ISPA, KOKB, UNBJ and SFE1.

To clarify the accuracy performance of CSRS-PPP solution at different intervals all the day, a statistical analysis, including maximum, minimum, mean and RMS (cm) errors, for the absolute positioning errors from the twelve IGS sites using dual frequency GPS-Only observations at 95% confidence level is illustrated in Table (4.31). Also, Figures (4.39) displays the mean errors at each time span at 95% confidence level.

Table (4.31) CSRS-PPP statistical results for the absolute positioning errors of static PPP from the twelve IGS sites using dual frequency GPS-Only observations and final precise ephemeris over the day (DOY 70, 2015) at 95% confidence level.

	Time (hr.)	Max (cm)	Min (cm)	Mean (cm)	RMS (cm)
North	0.25	4.36	0.42	1.87	2.22
	0.5	1.85	0.10	0.81	0.94
	1	1.06	0.00	0.45	0.57
	2	0.83	0.00	0.32	0.42
	4	0.78	0.01	0.29	0.38
	6	0.75	0.00	0.27	0.39
	12	0.35	0.04	0.15	0.18
	24	0.40	0.03	0.17	0.21
East	0.25	17.13	1.10	7.67	9.34
	0.5	11.64	0.32	4.00	5.23
	1	6.64	0.65	2.12	2.68
	2	3.16	0.19	1.32	1.54
	4	1.30	0.09	0.50	0.65
	6	0.86	0.01	0.38	0.47
	12	0.55	0.02	0.27	0.33
	24	0.38	0.04	0.18	0.21
Up	0.25	11.98	0.37	3.26	4.67
	0.5	9.28	0.15	3.36	4.80
	1	5.38	0.37	2.11	2.53
	2	2.60	0.32	1.57	1.73
	4	1.95	0.08	0.69	0.87
	6	1.47	0.02	0.63	0.75
	12	1.28	0.05	0.55	0.66
	24	0.90	0.01	0.42	0.51

From Table (4.31), it is seen that the static CSRS-PPP solution of dual GPS-Only observations and final precise ephemeris from IGS sites reaches less than 1 cm in north and less than 2.5 cm in east and up components after one hour. The solution converges to less than 0.5 cm in north and less than 1.5 cm in east and up directions after two hours. After four hours, it is cleared that the CSRS-PPP solution stabilizes under 0.5 cm in horizontal direction and 1 cm in vertical direction.

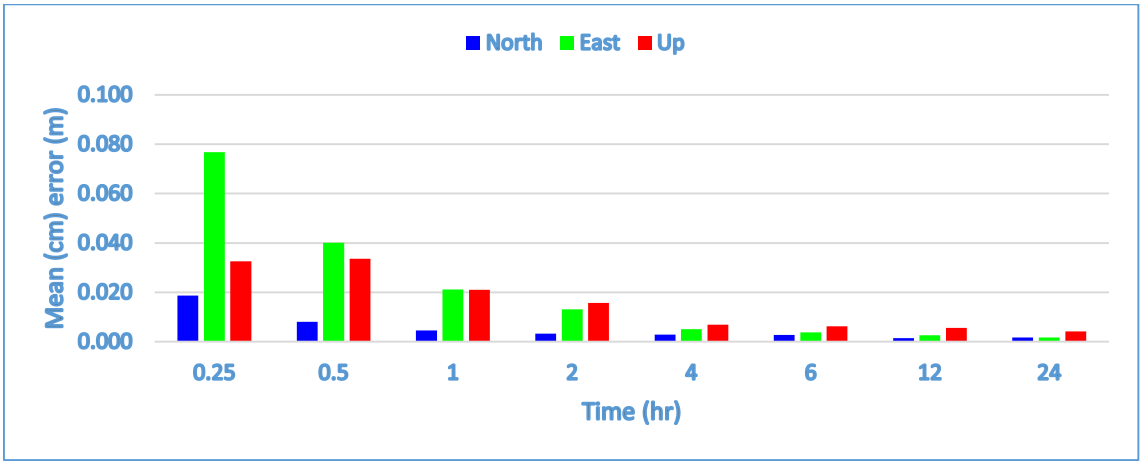

Figure (4.39) Absolute mean error of static CSRS-PPP from the twelve IGS sites using dual frequency GPS-Only observations and final precise ephemeris over the day (DOY 70, 2015) at 95% confidence level.

Moreover, the maximum, minimum, mean and RMS (cm) errors, for the absolute positioning errors from station SFE1 using dual GPS-Only observations at 95% confidence level are shown in Table (4.32). Besides, Figure (4.40) illustrates the mean errors at each time span at 95% confidence level.

Table (4.32) CSRS-PPP statistical results for the absolute positioning errors of static PPP from station SFE1 over the seven days using dual frequency GPS-Only observations and final precise ephemeris at 95% confidence level.

	Time (hr.)	Max (cm)	Min (cm)	Mean (cm)	RMS (cm)
North	0.25	2.45	0.36	1.01	1.21
	0.5	1.73	0.26	0.96	1.10
	1	1.62	0.66	0.96	1.01
	2	0.95	0.12	0.52	0.61
	4	0.63	0.01	0.26	0.34
	6	0.63	0.07	0.32	0.38
	12	0.55	0.18	0.42	0.45

	24	0.66	0.34	0.52	0.53
East	0.25	13.13	2.27	6.06	6.96
	0.5	7.56	1.62	4.92	5.44
	1	3.95	1.28	2.46	2.63
	2	2.21	0.37	1.01	1.19
	4	1.20	0.09	0.51	0.62
	6	1.12	0.13	0.53	0.62
	12	1.14	0.85	0.99	1.00
	24	1.25	0.90	1.07	1.07
Up	0.25	13.37	0.13	6.05	7.91
	0.5	11.97	0.13	6.68	7.81
	1	4.27	1.77	3.38	3.49
	2	2.17	0.37	1.15	1.30
	4	1.27	0.07	0.68	0.78
	6	1.07	0.27	0.67	0.72
	12	0.43	0.03	0.19	0.22
	24	0.57	0.07	0.29	0.34

Table (4.32) shows that the CSRS-PPP solution from SFE1 reaches 0.5 cm in north, 1 cm in east and 1.2 cm in up directions after two hours. The solution reaches less than 0.5 cm in horizontal and less than 1 cm in vertical after four hours. But, in east direction there is an increase in the error after 12 and 24 hours. This increase can be interpreted due to using cut off angle 15^{o} at station SFE1.

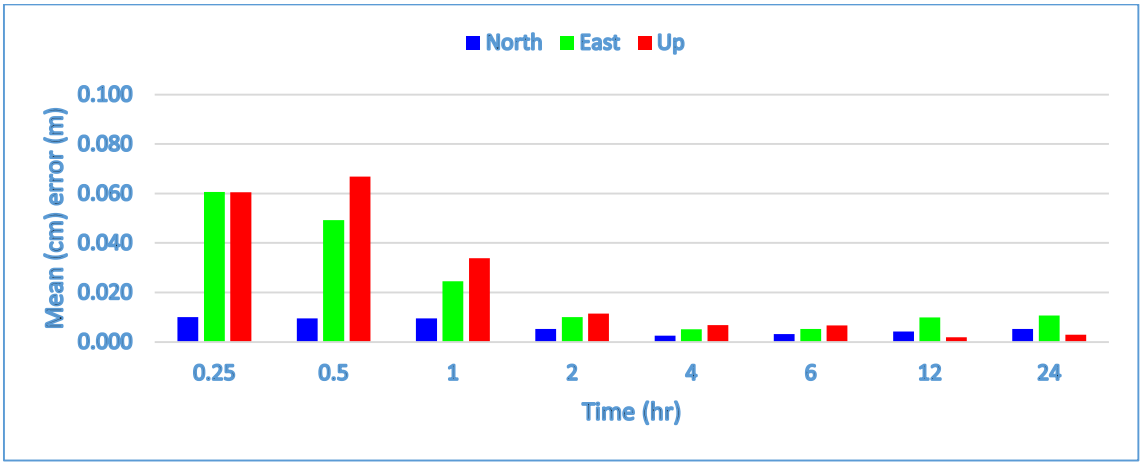

Figure (4.40) Absolute mean error of static CSRS-PPP from station SFE1 over the seven days using dual frequency GPS-Only observations and final precise ephemeris at 95% confidence level.

On the other hand, one of the advantages of CSRS-PPP online service over others is its capability to process GPS plus GLONASS observations. So here, we will explain the results from merging GPS and GLONASS observations in PPP solution. Figure (4.41) illustrates the processing results of four stations ISPA, KOKB, UNBJ and SFE1 using dual frequency GPS+GLONASS observations and final precise ephemeris, including the positioning errors in east, north and up directions with respect to the true coordinates.

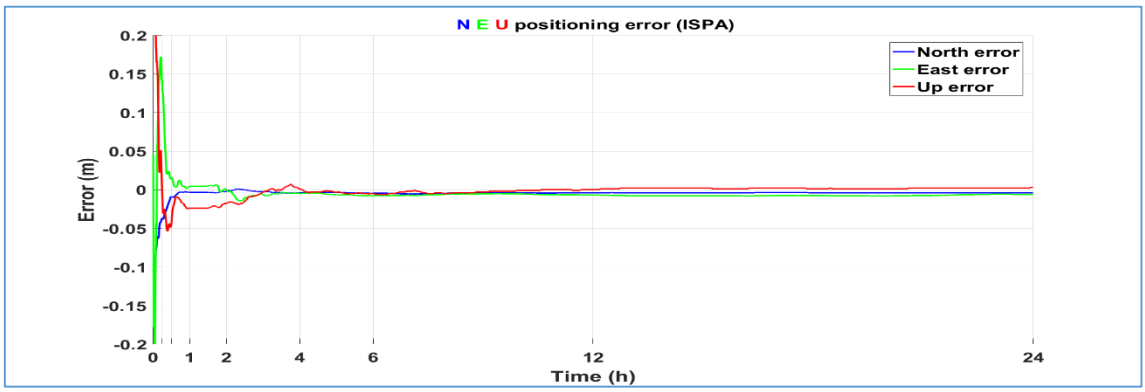

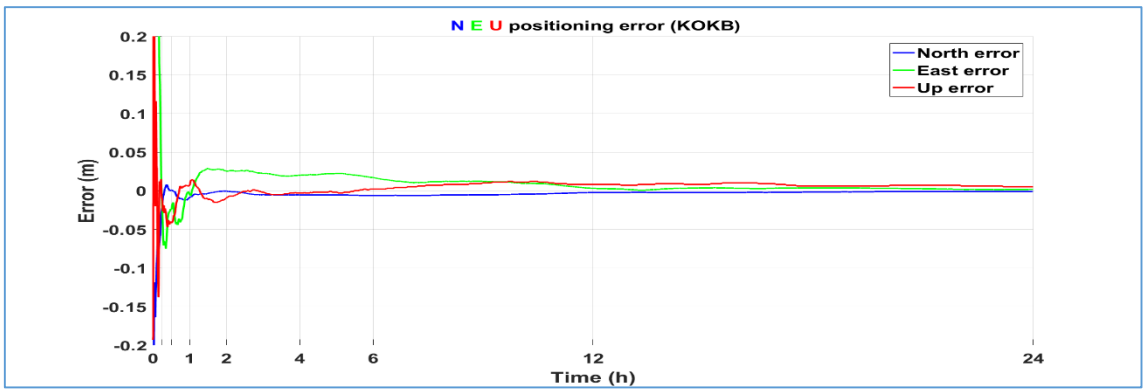

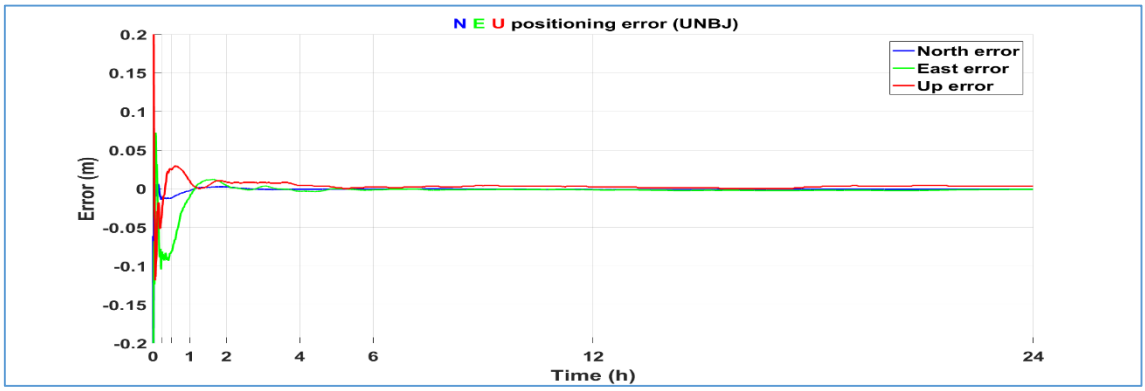

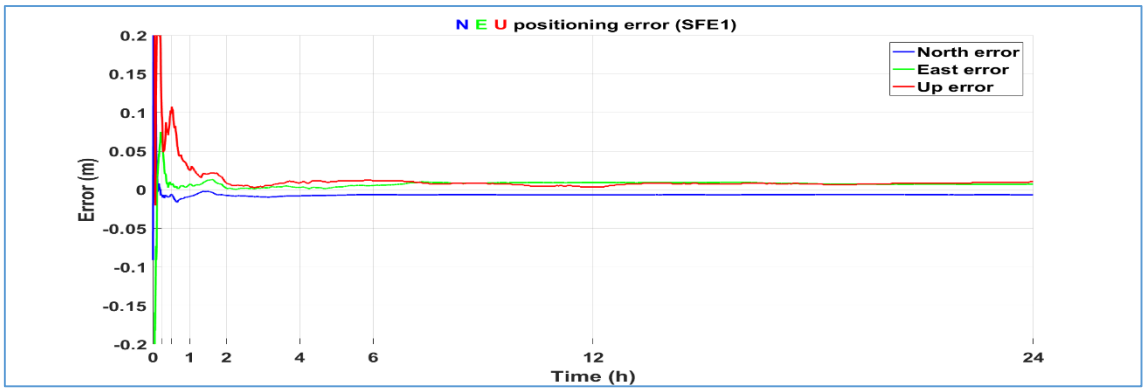

Figure (4.41) CSRS-PPP results from static PPP using dual frequency GPS+GLONASS observations and final precise ephemeris over the day (DOY 70, 2015) for stations ISPA, KOKB, UNBJ and SFE1.

Additionally, Table (4.33) shows CSRS-PPP solution from IGS sites using dual GPS+GLONASS observations and final precise ephemeris at different time sessions at 95% confidence level. It displays minimum, maximum, mean and RMS (cm) errors occurred all the day. For more clarification Figure (4.42) illustrates the mean errors at each time interval.

Table (4.33) CSRS-PPP statistical results for the absolute positioning errors of static PPP from the twelve IGS sites using dual frequency GPS+GLONASS observations and final precise ephemeris over the day (DOY 70, 2015) at 95% confidence level.

	Time (hr.)	Max (cm)	Min (cm)	Mean (cm)	RMS (cm)
North	0.25	3.66	0.12	1.48	1.86
	0.5	1.17	0.02	0.61	0.75
	1	0.84	0.08	0.42	0.49
	2	0.73	0.02	0.30	0.40
	4	0.78	0.01	0.34	0.42
	6	0.75	0.01	0.34	0.44
	12	0.38	0.04	0.17	0.19
	24	0.40	0.04	0.19	0.23
East	0.25	17.13	2.03	7.68	9.38
	0.5	8.07	1.10	3.41	4.14
	1	3.11	0.03	1.17	1.56
	2	2.55	0.00	1.00	1.29
	4	1.30	0.13	0.49	0.61
	6	0.78	0.01	0.35	0.47
	12	0.67	0.02	0.30	0.37
	24	0.40	0.04	0.19	0.22

Up	0.25	5.70	0.37	2.24	2.85
	0.5	4.48	0.28	1.88	2.32
	1	2.88	0.35	1.34	1.57
	2	2.98	0.32	1.38	1.56
	4	0.97	0.12	0.46	0.54
	6	2.18	0.02	0.75	1.03
	12	1.98	0.02	0.71	0.95
	24	0.80	0.15	0.40	0.44

From Table (4.33), an improvement for PPP solution was noticed after processing observations from GPS and GLONASS satellites only in the early hours of the day. The CSRS-PPP solution from IGS sites using GPS+GLONASS observations and final precise ephemeris reaches less than 0.5 cm in north component and less than 1.5 cm in east and up components after one hour. The solution reaches less than 0.5 cm in horizontal direction and less than 1 cm in vertical direction after 4 hours of observations.

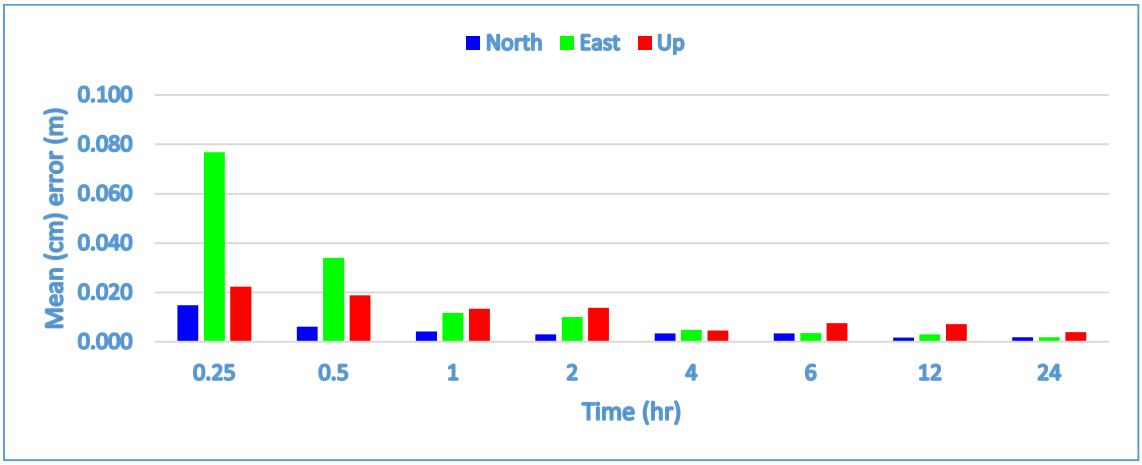

Figure (4.42) Absolute mean error of static CSRS-PPP from the twelve IGS sites using dual frequency GPS+GLONASS observations and final precise ephemeris over the day (DOY 70, 2015) at 95% confidence level.

Regarding station SFE1, Table (4.34) represents the maximum, minimum, mean and RMS (cm) errors, for the absolute positioning errors using dual GPS+GLONASS observations at 95% confidence level. Also, Figure (4.43) illustrates the mean errors at each time span at 95% confidence level.

Table (4.34) CSRS-PPP statistical results for the absolute positioning errors of static PPP from station SFE1 over the seven days using dual frequency GPS+GLONASS observations and final precise ephemeris at 95% confidence level.

	Time (hr.)	Max (cm)	Min (cm)	Mean (cm)	RMS (cm)
North	0.25	2.55	0.01	1.22	1.54
	0.5	1.57	0.01	0.80	0.94
	1	1.27	0.82	0.93	0.95
	2	1.03	0.42	0.82	0.84
	4	0.82	0.28	0.60	0.63
	6	0.79	0.20	0.52	0.56
	12	0.68	0.18	0.50	0.54
	24	0.74	0.31	0.55	0.57
East	0.25	6.41	1.36	4.03	4.49
	0.5	6.49	0.63	2.51	3.21
	1	3.01	0.41	1.43	1.64
	2	2.29	0.21	1.20	1.37
	4	1.68	0.12	0.86	1.00
	6	1.25	0.55	0.84	0.87
	12	1.17	0.50	0.86	0.89
	24	1.17	0.61	0.90	0.92
Up	0.25	14.23	0.97	6.98	8.11
	0.5	4.93	0.07	2.23	2.70
	1	2.87	0.67	1.96	2.12
	2	2.87	0.87	1.61	1.74
	4	1.07	0.07	0.68	0.76
	6	1.17	0.37	0.76	0.80
	12	0.77	0.07	0.31	0.38
	24	1.07	0.47	0.73	0.76

From Table (4.34) it is observed that the CSRS-PPP solution of station SFE1 from dual GPS and GLONASS observations and final precise ephemeris reaches less than 1 cm in north direction after one hour but reaches less than 1 cm also in east and up directions after 4 hours. Additionally, an improvement in CSRS-PPP solution was noticed at the early 0.5 and 1 hours after adding GLONASS observations.

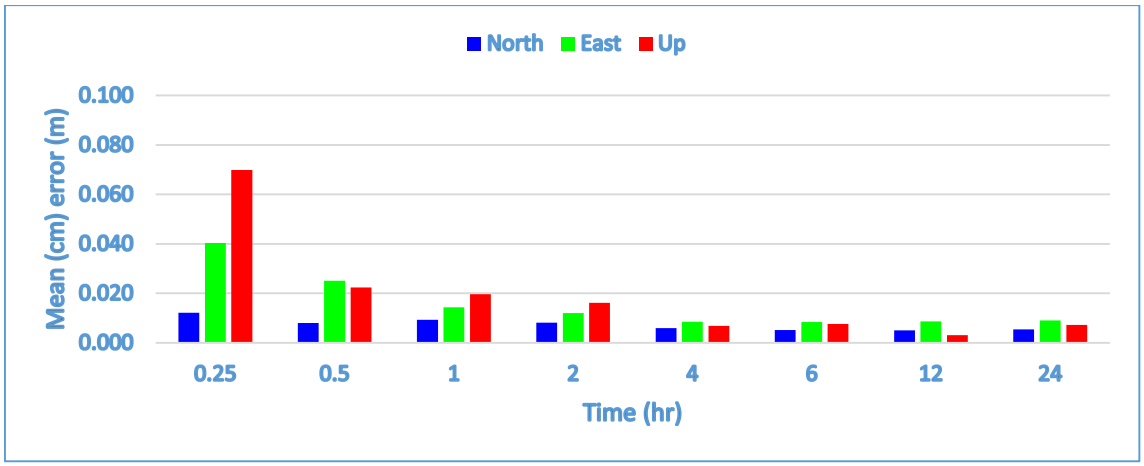

Figure (4.43) Absolute mean error of static CSRS-PPP from station SFE1 over the seven days using dual frequency GPS+GLONASS observations and final precise ephemeris at 95% confidence level.

4.4.2 Assessment of Kinematic PPP from CSRS-PPP Online Service

In this part, the results from CSRS-PPP online service in kinematic mode will be explained. In this assessment, only dual frequency observations were considered. Also, the CSRS-PPP solution will be evaluated along with GPS-Only and GPS+GLONASS observations. Fixed coordinates of PPK test were obtained from differential solution of base and rover receiver observations using Trimble Business Center software. These coordinates were used as true coordinates to assess the accuracy of PPP solution. The three-dimension station coordinate estimates from PPP solution have been converted to position discrepancies in north, east, and up components with respect to the true coordinates.

Firstly, Figures (4.44) and (4.45) display number of satellites in view and Geometric Dillution Of Precision (GDOP) using GPS-Only and GPS+GLONASS satellites during time of observation.

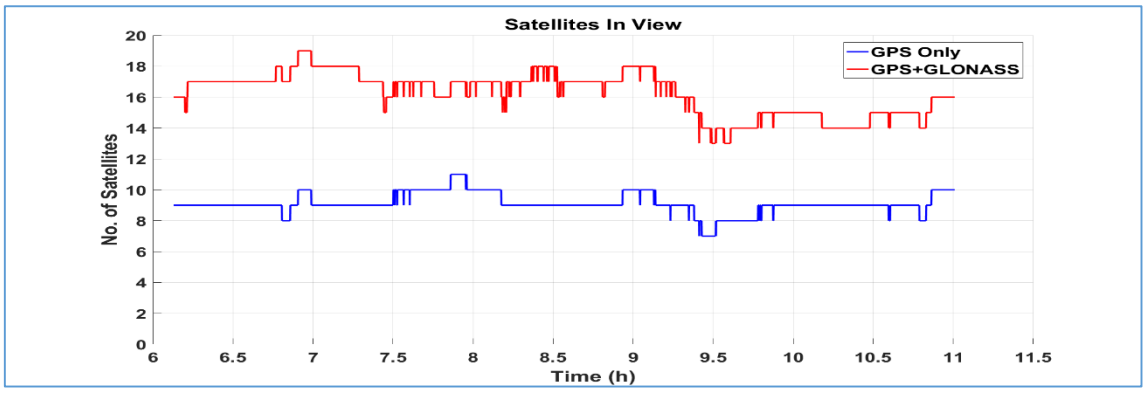

Figure (4.44) Satellite in view using GPS-Only and GPS+GLONASS satellites.

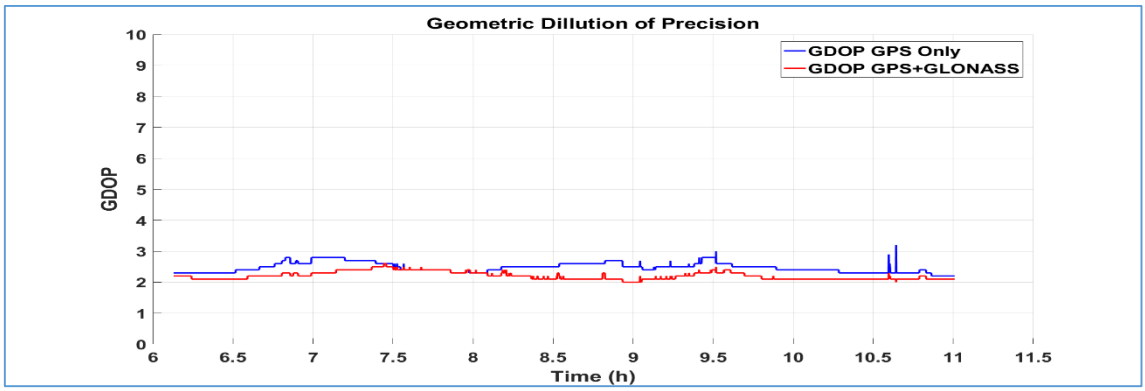

Figure (4.45) Satellite geometry (GDOP) using GPS-Only and GPS+GLONASS satellites.

Figure (4.46) and Table (4.35) show the processing results of CSRS-PPP kinematic solution from dual GPS-Only observations and final precise ephemeris at 95% confidence level, including the positioning errors in east, north and up directions with respect to the true coordinates of stations obtained from relative solution. From Table (4.35), it can be noticed that kinematic CSRS-PPP solution from dual GPS-Only observations and final precise ephemeris can reach mean error less than 2 cm in north direction and less than 3 cm in east and up directions. These high results is applicable to a lot of applications as topographic survey.

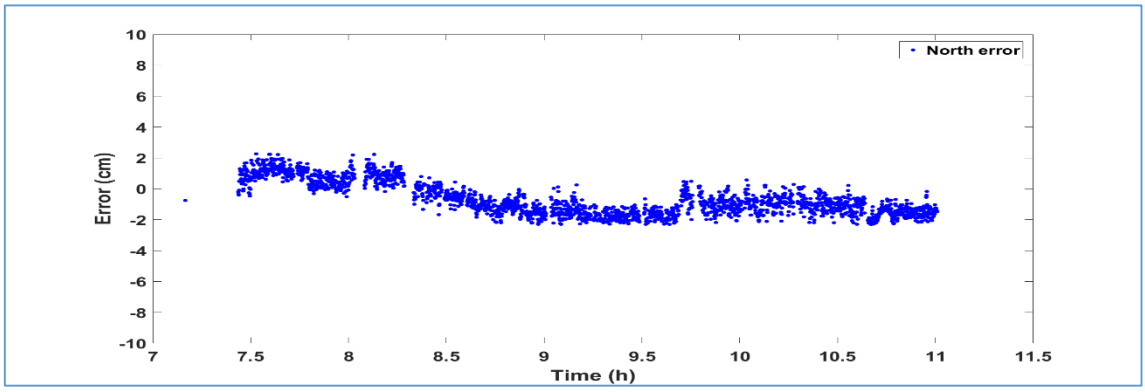

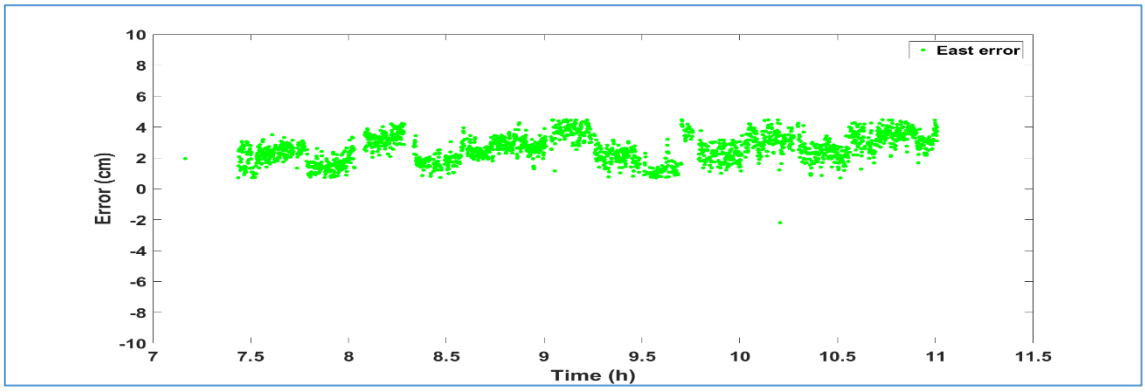

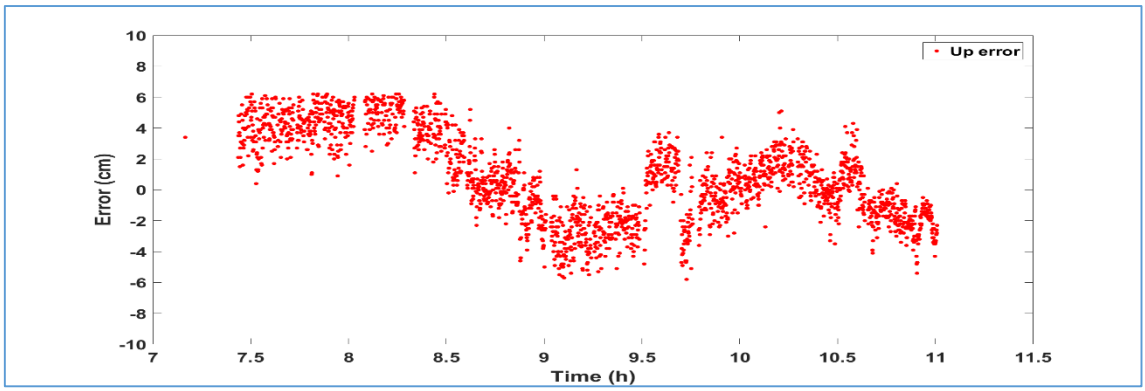

Figure (4.46) Positioning errors of CSRS-PPP kinematic solution for North (blue), East (green) and Up (red) components respectively using dual frequency GPS-Only observations and final precise ephemeris at 95% confidence level.

Table (4.35) Absolute positioning errors in cm of CSRS-PPP kinematic solution using dual frequency GPS-Only observations and final precise ephemeris at 95% confidence level.

	Max (cm)	*Min (cm)*	*Mean (cm)*	*RMS (cm)*
North	***2.30***	***0.00***	***1.12***	***1.25***
East	***4.47***	***0.70***	***2.59***	***2.72***
Up	***6.20***	***0.00***	***2.36***	***2.87***

On the other hand, Figure (4.47) and Table (4.36) illustrate the positioning errors of kinematic CSRS-PPP solution from dual GPS and GLONASS observations and final precise ephemeris at 95% confidence level. It is cleared observed that adding GLONASS observations did not improve the kinematic CSRS-PPP solution in our test. The reason may be that adding GLONASS to GPS does not cause a significant improvement to the DOP values as shown in Figure (4.45). Also, initialization time of one hour can be one of the reasons.

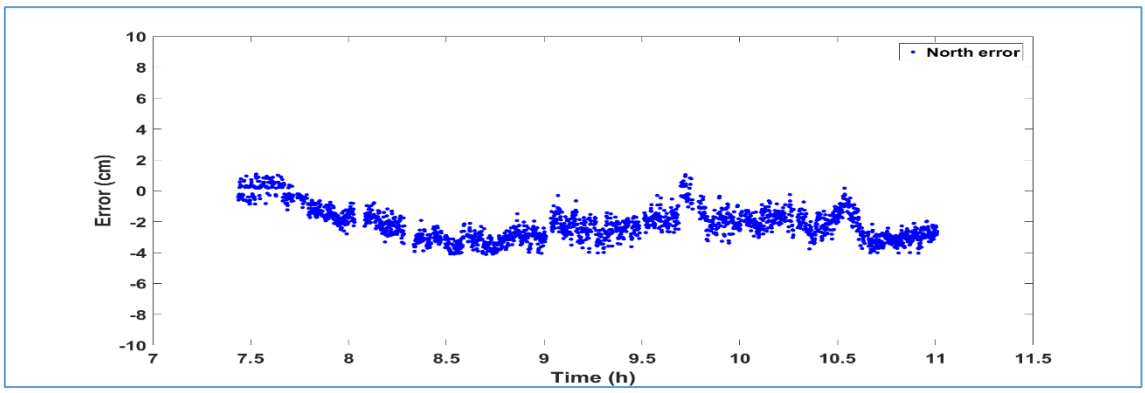

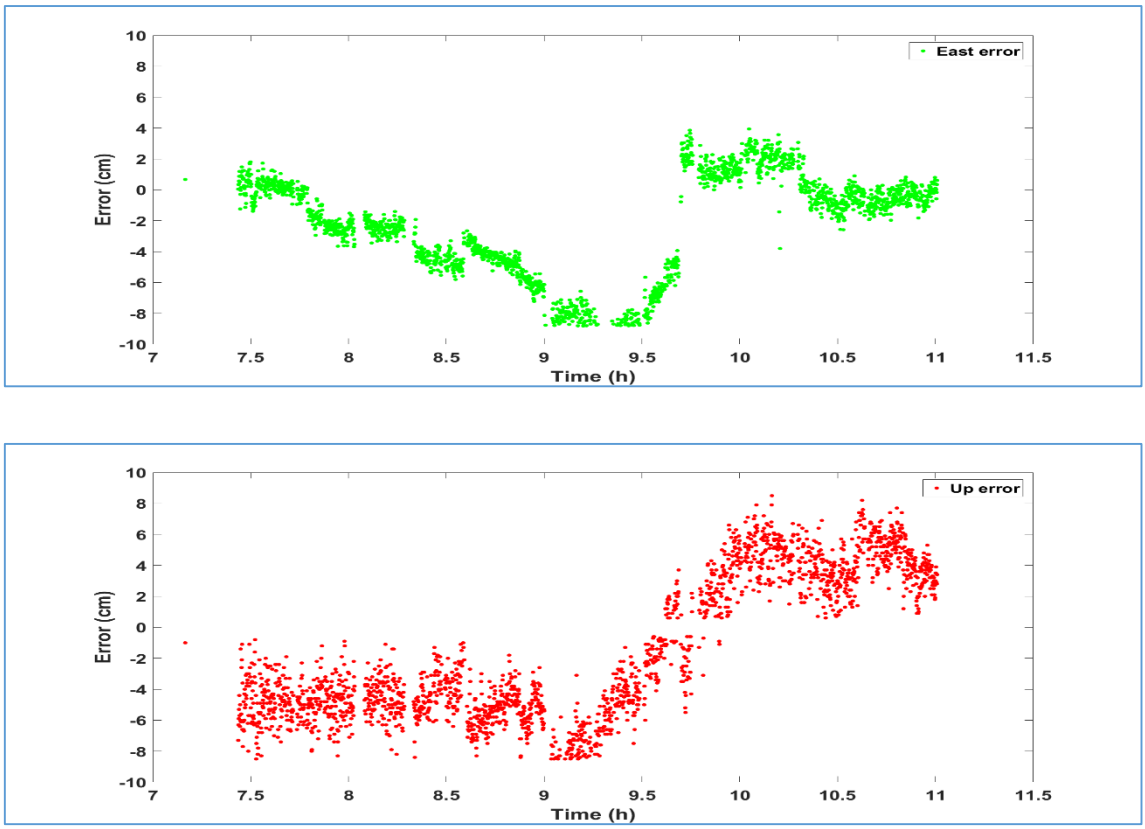

Figure (4.47) Positioning errors of CSRS-PPP kinematic solution for North (blue), East (green) and Up (red) components respectively using dual frequency GPS+GLONASS observations and final precise ephemeris at 95% confidence level.

Table (4.36) Absolute positioning errors in cm of CSRS-PPP kinematic solution using dual frequency GPS+GLONASS observations and final precise ephemeris at 95% confidence level.

	Max (cm)	*Min (cm)*	*Mean (cm)*	*RMS (cm)*
North	***4.11***	***0.16***	***2.19***	***2.39***
East	***8.81***	***0.00***	***2.82***	***3.73***
Up	***8.50***	***0.60***	***4.48***	***4.78***

4.5 Results from BKG Ntrip Client (BNC)

The International GNSS Service (IGS) launched, on April 1, 2014, the Real-Time Service (RTS) which provides access to real-time precise orbits and clock products for real-time applications. RTS is established on a global network of IGS stations, data centers and analysis centers (http://www.igs.org/rts). In this section we will demonstrate a brief of how Real-Time Precise Point Positioning (RT-PPP) is done with an experiment using an IGS station (NICO) and station SFE1 located at the roof of Faculty of Engineering at Shoubra. Table (4.37) lists available data streams of the IGS-RTS.

Table (4.37) Different IGS-RTS streams (http://www.igs.org/).

Stream name	Combination type	Ref. point	Transmitted RTCM Messages (sample interval in seconds)	Supported systems
IGS01	Single-Epoch	APC	1059 (5), 1060 (5)	GPS
IGC01	Single-Epoch	CoM	1059 (5), 1060 (5)	GPS
IGS02	Kalman Filter	APC	1057 (60), 1058 (10), 1059 (10)	GPS
IGS03	Kalman Filter	APC	1057 (60), 1058 (10), 1059 (10), 1063 (60), 1064 (10), 1065 (10)	GPS, GLONASS

To achieve our test in RT-PPP, we used the BKG Ntrip Client (BNC) program to do precise point positioning in real-time mode. Figure (4.48) shows a flow chart of BNC connected to a GNSS receiver providing observations via serial or TCP communication link for the purpose of Precise Point Positioning.

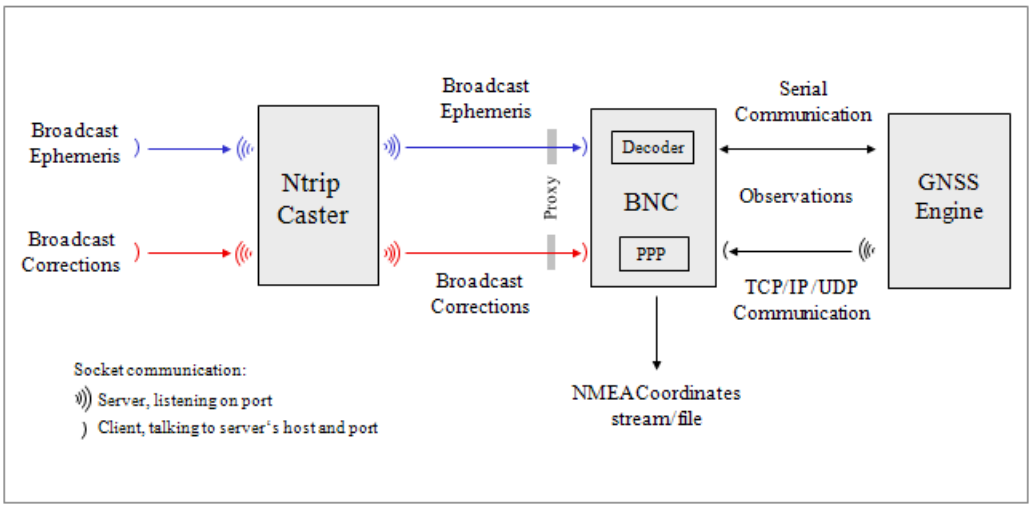

Figure (4.48) Flowchart of BNC connected to a GNSS rover for Precise Point Positioning.

In RT-PPP test, we used IGS03 stream which provides precise products for GPS and GLONASS observations. Table (4.38) and Figure (4.49) show the results of RT-PPP from the IGS station NICO in north, east and up directions respectively. The test continued about two hours. It is noticed that the RT-PPP solution from NICO reached less than 6 cm in horizontal direction and 11 cm in vertical all the time of the test. These results can be suitable for many applications. Moreover, Table (4.39) and Figure (4.50) display the results of RT-PPP solution for stations SFE1.

Table (4.38) Statistical analysis of RT-PPP solution for station NICO.

	Max (cm)	Min (cm)	Mean (cm)	RMS (cm)
North	6.40	0.00	1.60	2.20
East	5.60	0.00	2.10	2.50
Up	10.20	0.00	3.10	3.80

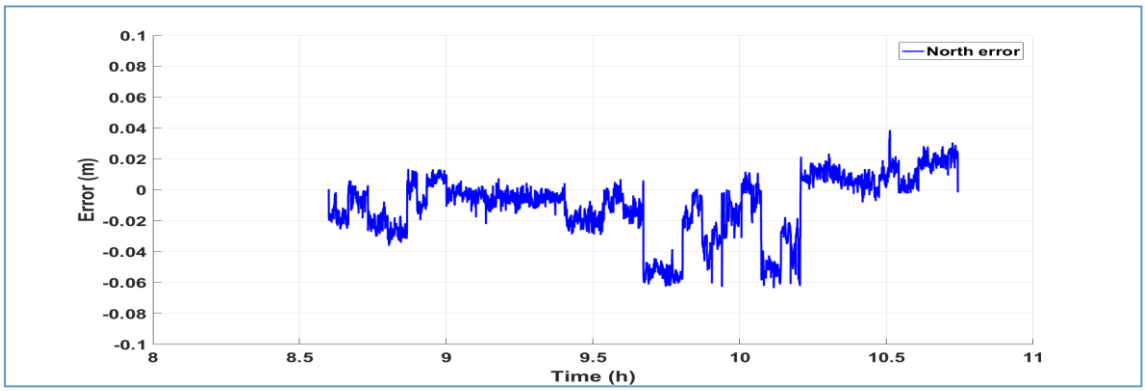

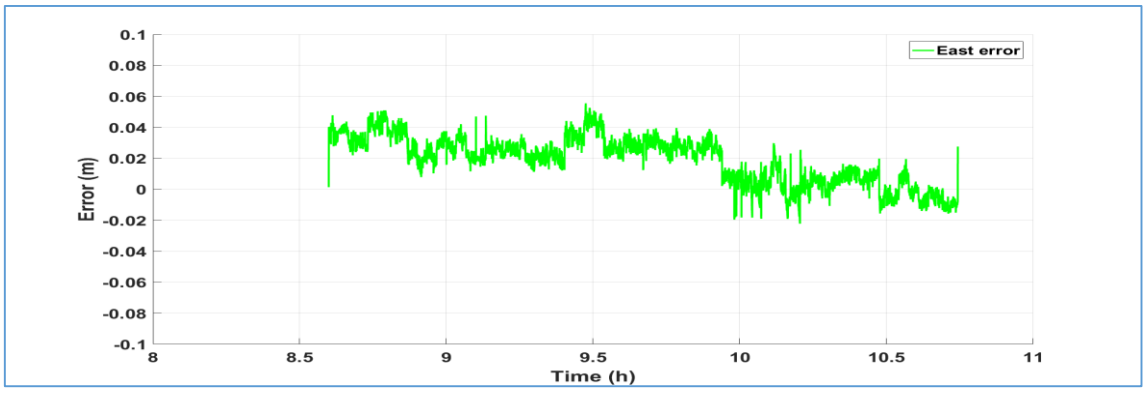

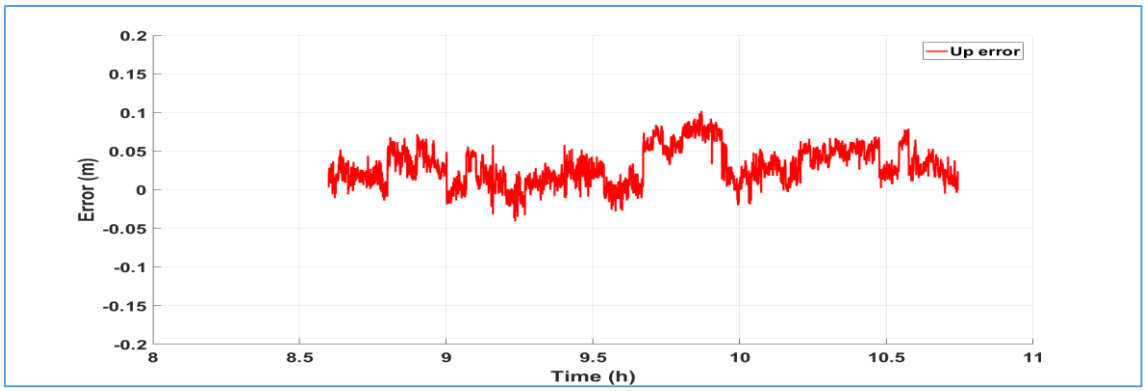

Figure (4.49) RT-PPP results from IGS station NICO in north, east and up directions using dual GPS and GLONASS observations.

Table (4.39) Statistical analysis of RT-PPP solution for station SFE1.

	Max (cm)	Min (cm)	Mean (cm)	RMS (cm)
North	4.60	0.00	1.40	1.60
East	9.60	3.50	6.90	7.00
Up	16.60	0.00	4.70	5.90

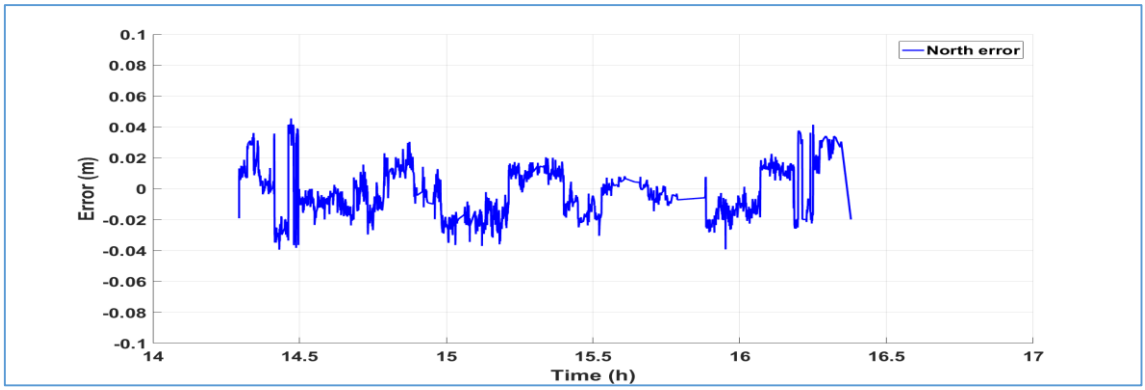

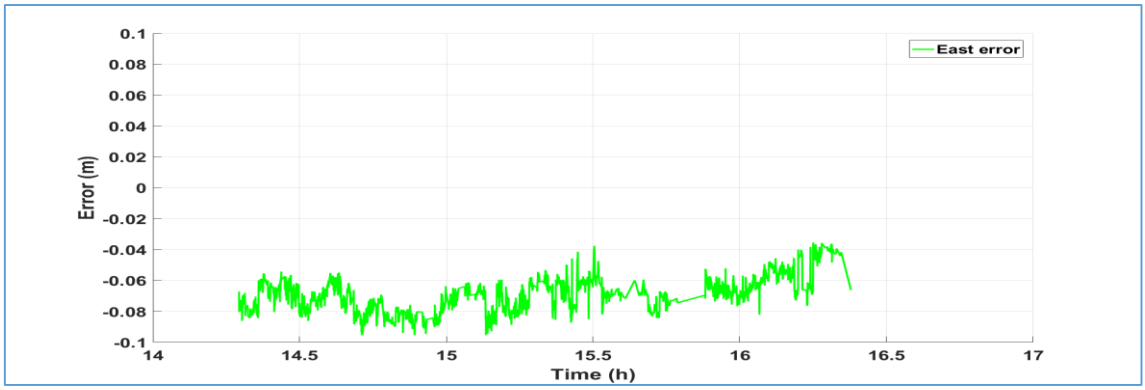

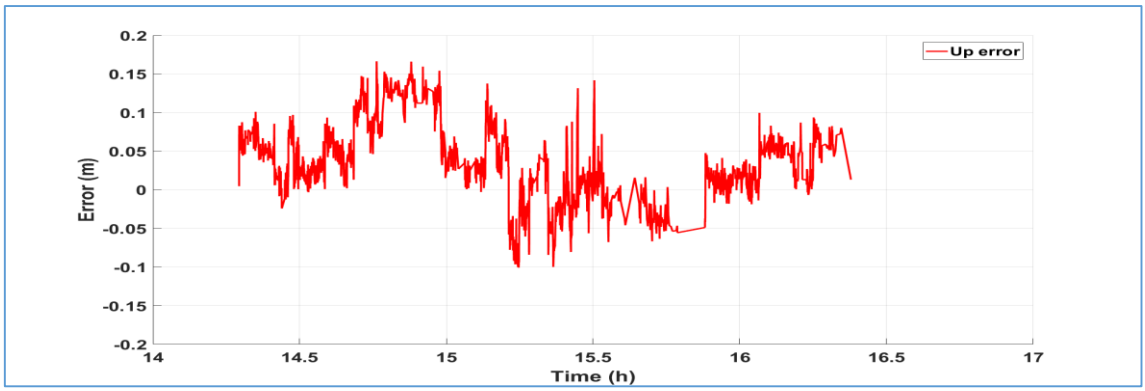

Figure (4.50) RT-PPP results from station SFE1 in north, east and up directions using dual GPS and GLONASS observations.

From Table (4.39), the RT-PPP solution from station SFE1 was less accurate than one from NICO station. It reached less than 5 and 10 cm in north and east directions respectively along the two hours of the test. Also, the solution reached less than 20 cm in the vertical direction. The reason for these less accurate results may be due to surroundings of station SFE1.

CHAPTER FIVE

SUMMARY, CONCLUSIONS AND RECOMMENDATIONS

5.1 Summary

The main objective of this research was to study, investigate and evaluate the novel Precise Point Positioning (PPP) technique in static and kinematic modes using undifferenced single and dual frequency observations. In addition to using single and dual code and carrier phase observations, different types of precise orbits and clock products such as final, rapid and ultra-rapid ephemeris are also used in processing. The evaluation procedure of the PPP performance in static mode was in terms of positioning accuracy from a reference solution and convergence time which means how long it takes a position filter to reach a stable condition. As to kinematic PPP, the assessment was rely on the positioning accuracy of PPP results from a differential solution. To meet our goal, static data was collected from a few IGS permanent sites and station SFE1 located at the roof of Faculty of Engineering at Shoubra, Cairo, Egypt. Kinematic data was observed by ourselves using dual frequency receiver.

Three different PPP software packages were applied to complete all practical work. The first one is gLAB tool which process only GPS observations. From results, gLAB is a powerful tool for PPP solution especially in static mode. The static PPP solution from gLAB in horizontal direction can reach less millimeters after 4 hours in horizontal direction using final and rapid ephemeris with dual frequency observations. While the PPP solution is about 3 cm or less after 4 hours of observation using final and rapid ephemeris and reaches less than 2 cm after 6 hours in vertical direction. Using gLAB tool with single frequency observations needs long time to reach less than 5 cm due in both horizontal and vertical direction due to ionospheric delay error. Kinematic PPP solution from gLAB achieves 3 and 7 cm in horizontal and vertical directions respectively from dual frequency observations using final or rapid precise ephemeris but the solution reaches decimeters from single frequency observations.

The second tool used in doing practical work is NRCan-PPP software through CSRS-PPP online service. It is a worldwide web-based and free of charge online processing service used to estimate PPP-derived coordinates. It was used to assess the PPP solution in static and kinematic mode using dual frequency observations from GPS-Only and GPS+GLONASS satellites. It is clearly observed that the PPP results from CSRS-PPP online service had an improvement than ones from gLAB software especially in the early times of observations. Also, the results from CSRS-PPP indicate that adding GLONASS observations decrease the convergence time for PPP technique to reach a better solution.

The BKG Ntrip Client (BNC) is the third software used in our research. It is an Open Source multi-stream client program designed for a variety of real-time GNSS applications. Test for Real-Time PPP (RT-PPP) was done using one of the IGS permanent site (NICO) and station SFE1. The results indicate that the RT-PPP solution reaches less than 10 and 20 cm in horizontal and vertical directions respectively.

Conclusions from this research and recommendations for future research have been made and are provided in the following.

5.2 Conclusions

1. The PPP approach offers a significant cost saving since base stations do not need to be deployed.

2. PPP solutions have the ability to be used as independent solutions for static positioning and as an alternative to DGPS solutions.

3. PPP as an absolute method for positioning can be of much benefits in its applications in surveying. Table (5.1) displays the accuracy of PPP in horizontal and vertical directions, the means used to be achieved and possible applications.

Table (5.1) Accuracy of PPP and recommended applications.

Accuracy		How To Achieve	Applications
Horizontal	Vertical		
< 1 cm		Daily static PPP using dual frequency observations and final precise ephemeris.	- Establishment of CORS networks. - Crustal deformation monitoring - Plate tectonic motions
1 cm	2 cm	Hourly (6 hours) static PPP using dual frequency observations and final or rapid precise ephemeris.	- Densification of CORS networks - Control points for RTK applications - Aerial triangulation
< 5 cm	< 10 cm	Kinematic PPP from dual frequency observations and final or precise ephemeris.	- Topographic survey - Hydrographic applications
< 10 cm	< 20 cm	Real-Time PPP using dual frequency observations from GPS+GLONASS satellites.	- Surveying applications demands this accuracy

4. Satellites are the direct homogenous and consistent reference system for PPP with the quality of the solution depending on the satellite geometry (in addition to station specific environment).

5. The overall results indicate that additional GNSS constellation allows for more reliable and precise surveying, especially in urban areas and short observation periods, in general when the satellite signals are blocked by various obstacles.

6. The results show that both the length of the session and observing conditions significantly affect the position determination accuracy.

7. For the assessment of performance of PPP in static mode from dual frequency measurements using gLAB tool, which uses observations from GPS-Only satellites, it is clearly observed that the static PPP solution in horizontal direction can reach less than 2 cm of mean error after two hours of observation and millimeters after 4 hours using final and rapid ephemeris. While, the PPP solution from ultrarapid ephemeris reaches less than 10 and 5 cm after 2 and 4 hours respectively and needs 12 hours for providing millimeter accuracy. In vertical direction the static PPP solution is about 3 cm or less after 4 hours of observation using final and rapid ephemeris and reaches less than 2 cm after 6 hours. Nevertheless, using ultrarapid ephemeris the PPP solution reaches less than 3 cm after 6 hours.

8. One of the goals of the research is to evaluate PPP technique using single frequency observations. Regarding results from single frequency observations, it is concluded that 4 hours is needed to reach horizontal accuracy less than 10 cm and 6 hours to reach accuracy less than 5 cm. But the solution takes 12 hours to converge with value less than 3 cm. In vertical direction, the PPP solution reaches less than 10 and 5 cm after 6 and 12 hours respectively. The main limitation with single frequency PPP solution is due to the ionospheric delay error. The ionospheric delay correction estimated from global agencies such as IGS can overcome only 50-60 % of the ionospheric error. So, the PPP solution cannot reach millimeters even though after 24 hours of observations.

9. A kinematic experiment was carried out to evaluate the performance of kinematic PPP using gLAB tool. The results indicate that the PPP solution can reach a high accuracy from dual frequency observations and final or rapid precise ephemeris. It is cleared that the mean error was less than 3 and 7 cm in horizontal and vertical directions

respectively at 95% confidence level. However, kinematic PPP with single frequency observations can reach decimeters due to the ionospheric delay error.

10. Currently PPP solution can be obtained from a worldwide online services. So, CSRS-PPP online service was used as an example to assess the performance of PPP technique in static and kinematic modes using only dual frequency observations from GPS-Only and GPS+GLONASS satellites among with final precise ephemeris. It is concluded that the CSRS-PPP solution reaches less than 2 and 1 cm in horizontal direction after 2 and 4 hours respectively in both GPS-Only and GPS+GLONASS solution. It also achieved the same results in the vertical direction. Adding GLONASS observations to GPS ones creates a little improvement to the PPP solution especially in the first 2 hours of observations. The PPP solution from GPS-Only observations needs 2 hours to be less than 2 cm in horizontal and vertical components but it needs only 1 hour to attain the same accuracy from GPS and GLONASS observations. These results indicate that adding GLONASS observations decrease the convergence time for PPP technique.

11. Regarding kinematic CSRS-PPP test, it is noticed that the kinematic PPP solution from GPS-Only observations has a little improvement than GPS+GLONASS observations. This can be interpreted from that adding GLONASS observations did not improve the DOP values as illustrated in Figure (4.68) in chapter 4.

12. Another test for Real-Time PPP (RT-PPP) was done using one of the IGS permanent site (NICO) and station SFE1. The results indicates that we can reach accuracy less than 10 cm in horizontal direction and less than 20 cm in vertical direction. These results can be suitable for applications that do not require high accuracy.

5.3 Recommendations

For future, the following recommendations can be taken into consideration.

1. The convergence time for PPP technique must be further researched to reduce the time for better solution to be comparable with differential methods.

2. Single frequency PPP till now does not provide more accurate results because of ionospheric delay error and so there is a need for more accurate global ionospheric models.

3. Nowadays, the growth of Global Navigation Satellite System (GNSS) must be exploited and move us to multi constellation PPP.

4. Investigation of ionosphere free linear combinations from triple or more frequencies.

5. The next step will be a performance assessment of PPP from a multi constellation systems including Galileo and Beidou.

6. Assessment of available online PPP services and make a comparison between the results to determine the accuracy for all of them.

References

Abdallah, A., Schwieger, V. (2014): Accuracy Assessment Study of GNSS Precise Point Positioning for Kinematic Positioning. In: Schattenberg, J., Minßen, T.-F.: Proceedings on 4th International Conference on Machine Control and Guidance. TU Braunschweig, Braunschweig, 2014

Abdel-salam, M.A. (2005). Precise Point Positioning Using Un-Differenced Code and Carrier Phase Observations. Calgary: University of Calgary, PhD Thesis, 2005.

Abhijit Dey, Dr.V.Malleswara Rao. Study and analysis of Differential GNSS and Precise Point Positioning. Journal of Electrical and Electronics Engineering, Volume 9, Issue 2 Ver. I (Mar – Apr. 2014), PP 53-59.

Angel Martín, Ana B. Anquela, José L. Berné and Miriam Sanmartin. Kinematic GNSS-PPP results from various software packages and raw data configurations. Scientific Research and Essays Vol. 7(3), pp. 419-431, 23 January, 2012.

Beran, Tomas (2008). Single-Frequency, Single-Receiver Terrestrial and Spaceborne Point Positioning. Ph.D. dissertation, Department of Geodesy and Geomatics Engineering, Technical Report No. 257, University of New Brunswick, Fredericton, New Brunswick, Canada, 185 pp.

Bernhard Hofmann-Wellenhof, Herbert Lichtenegger and Elmar Wasle. GNSS – Global Navigation Satellite Systems, 2008. doi:10.1007/978-3-211-73017-1.

Black, H.D., Eisner, A., 1984. Correcting satellite doppler datat for tropospheric effects. J. Geophys. Res. 89 (D2), 2616–2626.

Changsheng Cai, (2009) .Precise Point Positioning Using Dual-Frequency GPS and GLONASS Measurements. Calgary: University of Calgary, Master Thesis, 2009.

Chang-sheng CAI, Xiao-min LUO, Jian-jun ZHU. Modified algorithm of combined GPS/GLONASS precise point positioning for applications in open-pit mines. Trans. Nonferrous Met. Soc. China 24(2014) 1547−1553.

Chris RIZOS, Volker JANSSEN, Craig ROBERTS and Thomas GRINTER, Australia. Precise Point Positioning: Is the Era of Differential GNSS Positioning Drawing to an End? , FIG Working Week 2012.

Collins P., F. Lahaye, P. Heroux and S. Bisnath (2008) "Precise Point Positioning with Ambiguity Resolution using the Decoupled Clock Model," Proceedings of the 21st International Technical Meeting of the Satellite Division of The Institute of Navigation (ION GNSS 2008), Savannah, GA, September 2008, pp. 1315-1322.

Dawod G., Ismail S. and Mohamed H. (2007): ``Assessment of A Cost-Effective GPS Data Processing Alternative In Egypt Utilizing International On-line Processing Services". Civil Engineering Research Magazine (CREM), Al-Azhar College of Engineering V.29, No. (2), April 2007.

De Bakker, P.F. (2015). On User Algorithms for GNSS Precise Point Positioning. Delft University of Technology (TU Delft), PhD Thesis. doi:10.4233/uuid:98b1de71-6d51-446a-b161-c8fb58fbcafd.

Dow, J.M., Neilan, R. E., and Rizos, C., The International GNSS Service in a changing landscape of Global Navigation Satellite Systems, Journal of Geodesy (2009) 83:191–198, DOI: 10.1007/s00190-008-0300-3.

Grinter T. and Roberts C. (2011). Precise Point Positioning: Where are we now?. International Global Navigation Satellite Systems Society, IGNSS Symposium 2011.

Grinter T. and Roberts C. (2013). Real time Precise Point Positioning: Are we there yet?. International Global Navigation Satellite Systems Society, IGNSS Symposium 2013.

G. Seepersad, S. Bisnath. ASSESSING THE ACCURACY OF PPP.

Hofmann-Wellenhof, B., H. Lichtenegger, and E. Wasle (2008). GNSS – Global Navigation Satellite Systems. 2008 Springer-Verlag Wien.

Huisman, Lennard and Teunissen, Peter J. and Hu, Congwei. 2012. GNSS precise point positioning in regional reference frames using real-time broadcast corrections. Journal of Applied Geodesy. 6 (1): pp. 15-23.

J. Sanz Subirana, J.M. Juan Zornoza and M. Hernández-Pajares, GNSS Data Processing, Vol. I: Fundamentals and Algorithms (ESA TM-23/1, May 2013)

J. Sanz Subirana, J.M. Juan Zornoza and M. Hernández-Pajares, GNSS Data Processing, Vol. II: Laboratory Exercises (ESA TM-23/2, May 2013)

Jakub Kalita, Zofia Rzepecka, Izabela Szuman-Kalita. The application of Precise Point Positioning in Geosciences. The 9th Conference

Environmental Engineering. Selected Papers, Article number: enviro.2014.215.

Juan, J. M., J. Sanz, M. Hernández-Pajares, J. Samson, M. Tossaint, A. Aragón-Àngel, and D. Salazar (2012), Wide Area RTK: A satellite navigation system based on precise real-time ionospheric modelling, Radio Sci., 47, RS2016, doi:10.1029/2011RS004880.

Junbo Shi (2012). Precise Point Positioning Integer Ambiguity Resolution with Decoupled Clocks. Calgary: University of Calgary, PhD Thesis, 2012.

Kouba, J. and P. Héroux, 2001, Precise Point Positioning Using IGS Orbit and Clock Products, GPS Solutions, Vol. 5, No.2, pp.12-28.

Kouba, J. (2009a). A Guide to Using International GNSS Service (IGS) Products.Technical report, IGS.

Landau, H., X. Chen, S. Klose, R. Leandro, and U. Vollath (2008). Trimbles Rtk And Dgps Solutions In Comparison With Precise Point Positioning. In International Association of Geodesy Symposia.

Leandro, R. F. (2009). Precise Point Positioning with GPS: A New Approach for Positioning, Atmospheric Studies, and Signal Analysis. Ph.D. dissertation, Department of Geodesy and Geomatics Engineering, Technical Report No. 267, University of New Brunswick, Fredericton, New Brunswick, Canada, 232 pp.

L. H. Estey and C. M. Meertens, TEQC: The Multi-Purpose Toolkit for GPS/GLONASS Data, GPS Solutions, Vol. 3, No. 1, pp. 42-49, doi:10.1007/PL00012778, 1999.

Lin Pan, Changsheng Cai, Rock Santerre and Jianjun Zhu. Combined GPS/GLONASS Precise Point Positioning with Fixed GPS Ambiguities. Sensors 2014, 14, 17530-17547; doi:10.3390/s140917530.

Min Li, Lizhong Qu, Qile Zhao, Jing Guo, Xing Su and Xiaotao Li. Precise Point Positioning with the BeiDou Navigation Satellite System. Sensors 2014, 14, 927-943; doi:10.3390/s140100927.

Ramadan H. Abdel-Maguid. Evaluation of GPS Precise Point Positioning for Geoinformatics Community. Journal of Engineering and Computer Sciences Qassim University, Vol. 6, No. 1, pp. 1-10 (January 2013/Safar 1434H).

R.M. Alkan and T. Öcalan. Usability of the GPS Precise Point Positioning Technique in Marine Applications. THE JOURNAL OF NAVIGATION (2013), 66, 579–588. doi:10.1017/S0373463313000210.

Sanz, J.; Rovira-Garcia, Adria.; Hernandez, M.; Juan, J.; Ventura-Traveset, J.; Lopez, C.; Hein, G. The ESA/UPC GNSS-Lab Tool (gLAB): An advanced educational and professional package for GNSS data processing and analysis. 6th ESA Workshop on Satellite Navigation Technologies Multi-GNSS Navigation Technologies. Proceedings ISBN: 978-1-4673-2010-8, DOI: 10.1109/NAVITEC.2012.6423100. Noordwijk, the Netherlands. December 2012.

Suelynn Choy , Shaocheng Zhang , François Lahaye & Pierre Héroux (2013) A comparison between GPS-only and combined GPS+GLONASS Precise Point Positioning, Journal of Spatial Science, 58:2, 169-190, DOI: 10.1080/14498596.2013.808164.

Thomas Grinter and Craig Roberts. Real Time Precise Point Positioning: Are We There Yet?. International Global Navigation Satellite Systems Society, IGNSS Symposium, 2013. Outrigger Gold Coast, Qld, Australia.

Thomas Grinter and Volker Janssen. Post-Processed Precise Point Positioning: A Viable Alternative?. Proceedings of the 17th Association of Public Authority Surveyors Conference (APAS2012) Wollongong, New South Wales, Australia, 19-21 March 2012.

Witchayangkoon, B. (2000). Elements of GPS Precise Point Positioning. PhD Thesis, University of Maine, 2000.

Zhang, X. (2006). Precise Point Positioning: Evaluation and Airborne Lidar Calibration. Danish National Space Center.

Zumberge, J. F., M. B. Heflin, D.C. Jefferson, M. M.Watkins, M.M. and F. H. Webb, 1997, Precise point positioning for the efficient and robust analysis of GPS data from large networks. J. Geophys. Res., 102, 5005-5017.

Table (A.1) Processing results (in meters) for all twelve IGS stations from static PPP at different time spans over the day (DOY 70, 2015) in north, east and up directions using dual frequency observations and final precise ephemeris.

	Time (h)	ALIC	GLPS	ISPA	IRKJ	KOKB	KIRU	LHAZ	NICO	PDEL	STHL	UNBJ	YSSK
North	**0.25**	0.119	-0.047	0.143	-0.039	0.098	0.121	-0.009	0.059	-0.160	-0.065	-0.009	0.072
	0.5	0.049	-0.038	0.047	-0.012	0.040	0.001	0.005	0.019	0.030	-0.022	-0.031	0.057
	1	0.002	-0.012	0.014	0.001	0.004	-0.003	0.032	0.014	-0.001	-0.031	0.014	-0.010
	2	0.002	-0.007	0.017	0.002	0.016	-0.008	0.042	-0.010	-0.004	-0.020	0.006	-0.002
	4	0.004	-0.006	0.012	0.004	0.023	0.004	-0.002	-0.004	0.008	-0.005	0.001	-0.012
	6	0.006	-0.006	0.016	0.000	0.014	0.001	-0.005	-0.001	-0.001	-0.014	0.002	-0.009
	12	0.005	0.001	0.012	-0.001	0.010	0.003	0.000	0.002	-0.007	-0.004	0.000	0.000
	24	0.002	-0.001	0.010	-0.001	0.009	0.001	-0.001	0.001	-0.003	-0.001	0.003	0.001
East	**0.25**	-0.249	0.105	0.150	-0.309	-0.496	-0.187	-0.087	0.362	-0.716	0.089	-0.133	0.262
	0.5	-0.121	0.015	-0.038	-0.078	-0.147	-0.103	-0.277	0.173	-0.355	0.024	-0.057	0.247
	1	-0.051	-0.016	-0.007	-0.011	0.000	0.004	-0.165	0.004	-0.019	0.026	-0.060	0.080
	2	-0.021	-0.012	0.014	0.002	-0.008	0.013	0.000	0.012	-0.011	0.016	-0.005	-0.029
	4	0.022	-0.013	0.008	-0.009	-0.009	0.000	0.001	-0.004	0.004	-0.002	-0.008	0.007
	6	0.014	-0.015	0.018	-0.011	-0.012	-0.004	-0.005	-0.005	0.005	0.007	-0.009	0.001
	12	0.005	0.006	0.003	-0.007	-0.004	0.001	-0.007	0.000	0.010	0.003	-0.003	-0.001
	24	0.000	0.001	-0.002	-0.004	-0.005	0.001	-0.003	-0.003	0.006	-0.001	-0.001	-0.002
Up	**0.25**	0.238	-0.067	-0.003	-0.031	-0.167	-0.047	0.042	0.501	-0.200	-0.059	0.020	-0.223
	0.5	0.025	0.002	-0.056	-0.047	0.008	0.035	0.070	0.269	-0.221	-0.110	-0.007	-0.214
	1	0.044	-0.044	-0.016	-0.034	0.039	-0.038	0.017	0.033	-0.026	0.027	-0.016	-0.067
	2	0.021	-0.038	0.023	-0.034	0.015	-0.015	-0.014	0.036	-0.016	0.020	-0.023	-0.021
	4	-0.001	-0.040	0.009	-0.021	0.002	0.003	-0.004	0.014	-0.031	0.014	-0.024	-0.012
	6	-0.004	-0.036	-0.002	-0.025	-0.017	0.002	-0.032	0.011	-0.009	0.006	-0.023	-0.003
	12	0.000	-0.021	-0.001	-0.026	-0.013	-0.006	-0.026	0.004	0.017	0.000	-0.014	-0.024
	24	-0.006	-0.006	-0.009	-0.029	-0.022	-0.007	-0.027	-0.003	-0.002	-0.010	-0.010	-0.032

Table (A.2) Processing results (in meters) for station SFE1 from static PPP at different time spans over the seven days in north, east and up directions using dual frequency observations and final precise ephemeris.

	Time (h)	Day 1	Day 2	Day 3	Day 4	Day 5	Day 6	Day 7
North	**0.25**	0.062	0.140	0.083	0.034	-0.048	0.068	0.016
	0.5	0.009	0.031	0.032	0.015	-0.056	0.008	-0.008
	1	-0.020	-0.011	-0.004	-0.011	-0.023	-0.018	-0.020
	2	-0.021	-0.018	-0.015	-0.024	-0.016	-0.018	-0.017
	4	-0.008	-0.007	-0.003	-0.006	0.002	0.000	0.000
	6	-0.004	-0.003	0.000	-0.002	0.005	0.002	0.002
	12	-0.001	0.000	0.001	-0.001	0.003	0.002	0.004
	24	0.000	0.001	-0.001	-0.001	0.002	0.001	0.003
East	**0.25**	0.412	0.362	0.487	0.413	0.209	0.460	0.414
	0.5	0.253	0.170	0.202	0.136	0.282	0.168	0.106
	1	0.094	0.051	0.021	0.039	0.073	0.047	0.046
	2	0.026	0.022	0.021	0.024	0.032	0.040	0.043
	4	0.019	0.011	-0.001	-0.002	0.003	0.004	0.009
	6	0.007	0.000	-0.003	-0.008	-0.002	0.001	0.004
	12	0.006	0.005	0.005	0.003	0.006	0.007	0.004
	24	0.005	0.004	0.005	0.004	0.009	0.007	0.006
Up	**0.25**	0.354	0.303	0.223	0.347	-0.017	0.377	0.321
	0.5	0.278	0.172	0.207	0.202	0.128	0.104	-0.015
	1	0.083	0.032	-0.006	0.020	-0.016	0.001	-0.029
	2	-0.020	-0.022	-0.030	-0.044	-0.072	-0.046	-0.060
	4	-0.029	-0.030	-0.027	-0.022	-0.032	-0.027	-0.029
	6	-0.012	-0.012	-0.009	-0.006	-0.014	-0.009	-0.009
	12	-0.015	-0.015	-0.014	-0.018	-0.021	-0.015	-0.017
	24	-0.018	-0.016	-0.014	-0.019	-0.021	-0.018	-0.016

Table (A.3) Processing results (in meters) for all twelve IGS stations from static PPP at different time spans over the day (DOY 70, 2015) in north, east and up directions using dual frequency observations and rapid precise ephemeris.

	Time (h)	ALIC	GLPS	ISPA	IRKJ	KOKB	KIRU	LHAZ	NICO	PDEL	STHL	UNBJ	YSSK
North	0.25	0.122	-0.052	0.178	-0.119	-0.057	-0.086	-0.051	0.053	-0.176	-0.043	-0.052	-0.039
	0.5	0.049	-0.021	0.036	-0.056	-0.035	-0.028	0.003	0.021	-0.012	-0.010	-0.035	0.007
	1	0.000	-0.006	0.007	-0.004	-0.012	-0.001	0.027	0.015	-0.011	-0.026	0.012	-0.002
	2	0.000	-0.008	0.014	0.003	0.009	-0.004	0.041	-0.010	-0.008	-0.022	0.003	-0.002
	4	0.000	-0.007	0.009	0.004	0.018	0.006	-0.006	-0.004	0.007	-0.005	0.000	-0.012
	6	0.003	-0.007	0.014	0.001	0.010	0.003	-0.005	0.000	0.000	-0.014	0.000	-0.010
	12	0.002	0.000	0.011	-0.001	0.009	0.004	0.000	0.003	-0.006	-0.004	0.000	-0.001
	24	0.001	-0.002	0.008	-0.001	0.008	0.001	0.000	0.001	-0.002	-0.001	0.003	0.002
East	0.25	-0.141	0.142	0.506	-0.336	-0.261	-0.028	-0.101	0.267	-0.420	0.100	0.051	0.147
	0.5	-0.085	0.045	0.091	-0.141	0.087	-0.019	-0.098	0.165	-0.119	0.053	0.034	0.109
	1	-0.036	0.008	0.044	0.016	0.005	0.011	-0.083	0.012	0.003	0.019	0.017	0.035
	2	-0.037	-0.009	0.009	-0.003	0.000	0.009	0.049	0.015	-0.009	0.013	-0.014	-0.022
	4	0.017	-0.009	0.007	-0.008	-0.006	0.001	-0.011	-0.002	-0.002	-0.007	-0.008	0.012
	6	0.010	-0.015	0.016	-0.013	-0.014	-0.002	-0.006	-0.007	-0.001	0.001	-0.009	0.005
	12	0.002	0.004	0.000	-0.008	-0.005	-0.001	-0.007	-0.002	0.008	0.001	-0.002	0.000
	24	-0.001	0.000	-0.002	-0.004	-0.006	-0.001	-0.007	-0.003	0.006	-0.002	0.000	-0.001
Up	0.25	-0.070	-0.103	0.021	-0.479	-0.007	0.035	0.019	0.607	-0.027	-0.066	-0.012	-0.238
	0.5	-0.019	-0.026	-0.066	-0.215	0.102	0.036	0.024	0.303	-0.052	-0.106	-0.013	-0.155
	1	0.053	-0.079	-0.016	-0.047	0.041	-0.040	0.007	0.040	0.014	0.045	0.002	-0.064
	2	0.038	-0.046	0.018	-0.047	0.018	-0.023	-0.020	0.043	-0.011	0.027	-0.030	-0.028
	4	0.004	-0.047	0.005	-0.022	0.003	-0.006	0.010	0.016	-0.035	0.009	-0.023	-0.012
	6	-0.003	-0.043	-0.002	-0.025	-0.015	-0.002	-0.034	0.015	-0.026	0.003	-0.021	-0.003
	12	0.006	-0.023	-0.002	-0.025	-0.010	-0.009	-0.022	0.005	0.001	-0.001	-0.012	-0.021
	24	-0.003	-0.006	-0.007	-0.028	-0.022	-0.008	-0.016	-0.001	-0.013	-0.011	-0.011	-0.029

Table (A.4) Processing results (in meters) for station SFE1 from static PPP at different time spans over the seven days in north, east and up directions using dual frequency observations and rapid precise ephemeris.

	Time (h)	Day 1	Day 2	Day 3	Day 4	Day 5	Day 6	Day 7
North	0.25	0.021	-0.043	0.022	-0.038	-0.148	-0.009	-0.007
	0.5	0.005	-0.002	0.045	-0.016	-0.102	-0.005	-0.035
	1	-0.020	-0.018	-0.001	-0.023	-0.043	-0.021	-0.024
	2	-0.024	-0.021	-0.011	-0.023	-0.021	-0.021	-0.019
	4	-0.010	-0.007	-0.003	-0.004	-0.002	-0.002	-0.003
	6	-0.003	-0.002	0.001	-0.001	0.001	0.000	0.000
	12	0.000	0.002	0.002	0.000	0.003	0.002	0.003
	24	0.001	0.002	0.000	0.000	0.002	0.002	0.003
East	0.25	0.715	0.775	0.181	0.621	0.436	0.256	0.159
	0.5	0.289	0.222	0.150	0.169	0.408	0.108	0.109
	1	0.130	0.061	0.028	0.058	0.106	0.038	0.054
	2	0.038	0.031	0.025	0.021	0.045	0.036	0.040
	4	0.022	0.018	0.004	-0.002	0.004	0.003	0.010
	6	0.007	0.001	-0.001	-0.011	0.002	0.001	0.002
	12	0.007	0.003	0.005	0.001	0.005	0.006	0.002
	24	0.005	0.003	0.004	0.003	0.009	0.006	0.004
Up	0.25	0.468	0.818	-0.011	0.729	0.315	0.296	0.304
	0.5	0.296	0.236	0.237	0.201	0.450	0.071	0.133
	1	0.129	0.059	0.015	0.041	0.054	0.034	0.046
	2	-0.003	-0.003	-0.016	-0.018	-0.053	-0.033	-0.033
	4	-0.025	-0.015	-0.015	-0.005	-0.024	-0.022	-0.018
	6	-0.008	-0.009	-0.002	-0.001	-0.011	-0.004	-0.003
	12	-0.014	-0.013	-0.009	-0.017	-0.014	-0.010	-0.013
	24	-0.016	-0.016	-0.011	-0.018	-0.017	-0.015	-0.015

Table (A.5) Processing results (in meters) for all twelve IGS stations from static PPP at different time spans over the day (DOY 70, 2015) in north, east and up directions using dual frequency observations and ultra-rapid precise ephemeris.

	Time (h)	ALIC	GLPS	ISPA	IRKJ	KOKB	KIRU	LHAZ	NICO	PDEL	STHL	UNBJ	YSSK
North	**0.25**	-0.655	-0.011	-0.127	0.424	-0.133	-0.501	-0.086	-0.072	-0.331	-0.219	-0.263	0.069
	0.5	-0.405	-0.160	-0.193	0.009	-0.033	-0.155	-0.094	0.128	0.038	-0.113	-0.231	-0.087
	1	-0.123	0.054	-0.007	-0.019	-0.068	-0.101	0.009	-0.077	-0.133	-0.009	-0.015	-0.088
	2	-0.040	0.021	0.023	0.011	-0.019	-0.054	0.015	-0.019	-0.036	-0.035	0.007	-0.005
	4	-0.009	0.019	0.003	0.012	0.016	-0.016	-0.053	-0.012	-0.004	0.004	-0.001	-0.014
	6	-0.005	0.018	0.000	0.010	0.015	-0.002	-0.021	-0.002	-0.007	-0.013	0.002	-0.008
	12	-0.004	-0.010	-0.008	-0.005	0.011	0.000	-0.008	-0.002	-0.013	-0.003	-0.003	-0.006
	24	-0.005	-0.011	-0.001	-0.005	0.005	0.000	-0.002	-0.003	-0.008	-0.003	0.001	-0.005
East	**0.25**	-0.424	0.356	-0.434	0.074	-0.528	-0.571	-0.042	-0.228	-0.435	0.128	0.264	0.747
	0.5	-0.105	0.283	-0.428	0.444	-0.109	-0.255	-0.202	0.057	-0.779	0.487	0.110	-0.042
	1	0.151	0.052	-0.406	0.018	0.091	-0.052	-0.319	-0.159	0.118	0.033	-0.079	-0.052
	2	0.056	0.036	-0.085	0.001	-0.058	-0.036	-0.085	-0.054	0.069	0.027	0.117	-0.132
	4	-0.025	0.042	0.009	-0.020	-0.097	-0.016	-0.082	-0.055	0.018	0.006	0.041	-0.025
	6	-0.012	0.035	-0.030	-0.008	-0.005	-0.010	-0.018	-0.026	0.002	-0.018	0.008	-0.009
	12	-0.009	0.037	0.010	-0.007	-0.007	-0.003	-0.018	-0.001	0.004	0.007	-0.004	-0.003
	24	-0.004	0.007	0.001	-0.001	-0.010	0.001	-0.007	-0.001	0.007	0.001	0.001	-0.002
Up	**0.25**	0.827	-0.234	-0.576	-1.748	0.440	1.034	-1.364	1.855	1.125	-0.485	0.269	-0.463
	0.5	0.148	0.202	-0.294	-0.384	0.132	0.354	0.243	0.701	-0.192	-0.018	0.073	-0.033
	1	-0.044	0.046	-0.276	-0.243	0.182	-0.149	0.086	0.023	0.225	0.014	-0.035	0.003
	2	-0.124	0.019	-0.032	0.009	0.044	0.046	-0.033	0.068	0.027	-0.029	-0.015	-0.020
	4	-0.014	0.036	0.032	0.005	-0.072	0.043	0.049	-0.014	-0.032	0.021	-0.020	0.021
	6	-0.006	0.037	0.036	-0.015	-0.071	0.034	-0.039	-0.016	-0.020	0.009	-0.034	-0.009
	12	-0.018	-0.034	-0.008	-0.004	-0.040	0.003	-0.033	-0.015	0.010	0.010	-0.010	-0.032
	24	-0.016	0.014	-0.006	-0.004	-0.037	-0.004	-0.018	-0.011	-0.009	-0.012	-0.015	-0.023

Table (A.6) Processing results (in meters) of station SFE1 from static PPP at different time spans over the seven days in north, east and up directions using dual frequency observations and ultra-rapid precise ephemeris.

	Time (h)	Day 1	Day 2	Day 3	Day 4	Day 5	Day 6	Day 7
North	**0.25**	-0.231	-0.252	-0.172	-0.151	0.184	0.182	0.005
	0.5	-0.070	0.087	-0.111	0.079	-0.017	-0.244	0.005
	1	0.037	0.069	0.007	-0.115	-0.074	-0.089	0.022
	2	-0.008	-0.039	-0.001	-0.027	0.016	-0.003	-0.051
	4	0.006	-0.026	-0.001	-0.011	0.007	0.005	-0.017
	6	-0.007	-0.015	0.011	-0.004	0.003	-0.003	-0.006
	12	-0.004	0.002	0.007	-0.005	0.009	0.001	0.003
	24	0.002	-0.001	0.004	-0.005	0.003	0.000	0.004
East	**0.25**	1.284	-0.136	0.040	-0.256	-0.039	0.119	0.269
	0.5	0.620	0.278	0.066	-0.190	0.569	0.505	-0.100
	1	0.394	0.134	0.158	-0.026	0.347	0.259	0.157
	2	0.100	0.093	-0.109	-0.065	-0.003	0.101	-0.086
	4	0.056	0.010	-0.065	-0.068	-0.023	0.034	0.042
	6	0.002	-0.001	-0.042	-0.021	0.004	0.016	0.032
	12	0.004	-0.008	-0.006	0.003	-0.005	-0.003	0.019
	24	0.010	-0.001	-0.008	0.008	0.011	0.008	0.005
Up	**0.25**	0.271	0.510	1.827	1.243	0.236	1.067	-0.599
	0.5	-0.283	0.147	0.356	0.110	0.631	0.868	-0.135
	1	0.281	-0.107	0.408	0.189	0.670	0.353	-0.184
	2	0.094	-0.215	-0.025	0.020	-0.093	0.038	-0.043
	4	0.042	-0.136	-0.022	-0.020	-0.039	-0.063	-0.027
	6	0.002	-0.082	0.006	-0.031	0.018	-0.061	0.007
	12	0.002	-0.047	-0.022	-0.046	0.005	-0.043	-0.014
	24	-0.021	-0.046	-0.044	-0.037	-0.033	-0.037	-0.011

Table (A.7) Processing results (in meters) for all twelve IGS stations from static PPP at different time spans over the day (DOY 70, 2015) in north, east and up directions using single frequency observations and final precise ephemeris.

	Time (h)	ALIC	GLPS	ISPA	IRKJ	KOKB	KIRU	LHAZ	NICO	PDEL	STHL	UNBJ	YSSK
North	0.25	0.196	-0.342	-0.082	1.207	0.022	-0.857	0.615	-0.280	0.214	0.264	-1.415	0.155
	0.5	-0.637	-0.098	0.091	0.092	-0.212	-0.221	0.219	0.104	0.068	0.082	-0.143	-0.288
	1	-0.262	-0.067	0.097	-0.017	-0.092	-0.038	0.001	0.021	0.111	0.028	0.149	0.076
	2	-0.041	0.006	0.017	0.049	0.087	-0.020	0.148	-0.034	0.025	0.001	0.059	0.146
	4	-0.033	-0.013	0.009	0.021	0.093	0.019	-0.015	-0.004	0.040	-0.007	0.027	0.005
	6	-0.030	-0.008	0.008	-0.003	0.037	0.010	-0.020	-0.002	0.006	-0.014	0.018	0.002
	12	-0.015	-0.014	0.012	0.017	0.049	0.015	0.003	0.004	-0.011	-0.007	0.004	-0.001
	24	-0.011	-0.012	0.018	0.020	0.031	0.019	0.002	0.002	-0.012	-0.003	0.008	-0.007
East	0.25	0.412	2.784	0.038	0.130	1.936	0.003	2.618	1.460	0.271	0.513	3.256	0.321
	0.5	-0.164	0.718	0.169	0.138	0.912	0.115	-0.366	0.013	-0.265	0.184	-0.650	0.238
	1	-0.126	0.231	-0.048	-0.101	0.134	-0.019	-2.429	-0.059	-0.132	0.188	-0.060	-0.329
	2	-0.476	0.031	0.092	-0.095	0.079	-0.002	-0.371	-0.023	-0.015	0.098	0.292	-0.229
	4	-0.093	-0.051	0.075	-0.053	0.087	0.002	0.079	0.022	0.008	0.045	0.064	-0.138
	6	0.015	-0.019	0.059	-0.034	0.017	-0.006	0.083	0.006	0.021	-0.011	0.009	-0.150
	12	0.015	0.019	0.018	0.014	0.003	0.001	0.024	0.005	0.034	-0.013	-0.017	-0.113
	24	0.008	0.008	-0.010	0.028	0.029	-0.005	0.004	-0.012	0.015	-0.022	-0.009	-0.047
Up	0.25	-0.399	-2.084	0.618	0.908	-0.929	0.152	-3.815	1.319	0.212	0.155	1.588	2.066
	0.5	-2.332	-0.570	0.275	-0.002	-0.964	-0.630	-0.183	0.451	-0.077	-0.071	0.727	0.233
	1	-0.719	-0.642	0.123	-0.044	-0.125	-0.362	0.780	0.235	-0.014	-0.189	0.040	-0.292
	2	-0.023	-0.226	0.061	-0.160	-0.044	-0.099	0.092	0.063	-0.104	-0.009	0.013	-0.165
	4	0.018	-0.095	-0.034	-0.084	-0.111	-0.101	-0.122	0.065	-0.150	0.017	-0.094	-0.315
	6	-0.001	-0.070	-0.044	-0.105	-0.168	-0.078	0.012	0.037	-0.068	-0.022	-0.068	-0.205
	12	0.009	-0.044	-0.034	-0.074	-0.057	-0.062	-0.040	0.037	0.004	-0.020	-0.054	-0.051
	24	0.012	-0.055	-0.017	-0.068	-0.075	-0.055	0.023	0.031	-0.034	-0.016	-0.041	-0.079

Table (A.8) Processing results (in meters) for station SFE1 from static PPP at different time spans over the seven days in north, east and up directions using single frequency observations and final precise ephemeris.

	Time (h)	Day 1	Day 2	Day 3	Day 4	Day 5	Day 6	Day 7
North	**0.25**	0.204	-0.779	0.145	0.133	-0.700	0.840	0.489
	0.5	-0.125	-0.080	0.400	0.428	0.085	0.095	0.277
	1	-0.034	0.087	0.087	0.129	0.006	-0.183	-0.028
	2	-0.049	-0.036	-0.040	-0.023	-0.045	-0.062	-0.014
	4	-0.016	0.006	-0.008	-0.013	-0.006	-0.029	-0.006
	6	0.006	0.011	0.008	0.010	0.021	0.003	0.015
	12	0.015	0.016	0.018	0.010	0.012	0.008	0.016
	24	0.012	0.015	0.014	0.011	0.012	0.009	0.011
East	**0.25**	0.937	2.692	0.255	-0.913	1.584	1.021	1.177
	0.5	-0.334	0.121	0.060	-0.339	0.344	0.485	1.163
	1	0.394	0.127	0.236	0.354	0.524	0.595	0.733
	2	0.074	0.089	0.102	0.102	0.118	0.171	0.160
	4	0.049	0.041	0.035	0.034	0.057	0.093	0.073
	6	-0.022	-0.042	-0.009	-0.084	0.029	0.002	-0.027
	12	0.014	0.020	0.037	0.006	0.036	0.034	0.002
	24	0.005	0.011	0.012	0.000	0.025	0.023	0.006
Up	**0.25**	0.028	1.468	0.362	0.865	0.672	0.489	0.334
	0.5	-0.713	0.142	0.180	0.094	0.330	0.688	1.626
	1	0.694	0.611	0.293	0.387	0.495	0.548	0.757
	2	0.162	0.148	0.144	0.190	0.074	0.173	0.143
	4	0.059	0.068	0.082	0.050	0.064	0.050	0.051
	6	0.026	0.031	0.037	-0.005	0.116	-0.016	0.010
	12	0.008	0.012	0.075	0.005	0.051	-0.022	-0.008
	24	0.007	-0.002	0.020	-0.001	0.010	-0.016	-0.006

Table (A.9) Processing results (in meters) for all twelve IGS stations from static PPP at different time spans over the day (DOY 70, 2015) in north, east and up directions using single frequency observations and rapid precise ephemeris.

	Time (h)	ALIC	GLPS	ISPA	IRKJ	KOKB	KIRU	LHAZ	NICO	PDEL	STHL	UNBJ	YSSK
North	0.25	1.747	-1.207	0.633	1.971	-1.828	-1.222	0.373	0.531	1.992	0.785	-2.879	-0.055
	0.5	-0.121	-0.059	-0.448	-0.048	-0.348	-0.434	0.822	0.314	0.345	0.253	-0.879	-0.439
	1	-0.173	-0.114	0.127	-0.026	-0.011	-0.163	-0.143	0.031	0.141	0.124	-0.306	0.123
	2	-0.112	0.018	-0.015	0.078	0.027	-0.091	-0.030	-0.029	0.038	0.040	-0.114	0.149
	4	-0.056	0.006	0.025	0.031	0.041	0.035	0.244	0.017	0.044	0.012	-0.013	0.023
	6	-0.037	-0.007	0.029	-0.010	0.034	0.031	0.096	0.012	0.010	-0.004	-0.010	0.011
	12	-0.024	-0.010	0.010	0.049	0.051	0.020	-0.005	0.012	-0.011	-0.011	-0.006	-0.005
	24	-0.018	-0.011	0.030	0.040	0.018	0.021	0.005	0.007	-0.013	-0.002	-0.010	-0.005
East	0.25	0.011	0.610	-1.110	-2.823	3.590	-0.459	0.957	-0.166	2.927	0.280	4.819	-0.095
	0.5	-0.420	-0.031	0.859	1.546	1.093	-0.291	1.234	0.038	0.258	-0.876	-1.816	-0.126
	1	-0.155	0.054	0.353	1.367	-0.359	-0.224	-2.400	-0.069	-0.018	-0.070	1.419	-0.256
	2	-0.458	0.002	0.575	0.634	0.165	-0.096	-1.604	-0.036	-0.002	0.161	0.886	-0.220
	4	-0.064	-0.003	-0.018	0.107	0.065	-0.069	0.565	-0.007	0.015	-0.058	0.378	-0.139
	6	0.010	-0.005	0.009	0.016	-0.013	-0.065	0.261	-0.013	0.024	-0.058	-0.038	-0.131
	12	0.012	0.019	-0.054	0.033	-0.060	-0.022	0.024	0.008	0.033	-0.010	-0.031	-0.099
	24	0.024	0.014	0.001	0.041	-0.046	-0.010	-0.007	-0.006	0.019	-0.010	0.005	-0.045
Up	0.25	1.395	1.601	0.372	2.446	-0.147	0.909	-2.616	-1.965	2.642	2.073	-0.471	1.688
	0.5	-2.022	-0.687	0.883	-0.215	-0.828	-1.166	-2.510	0.063	0.249	0.649	0.330	-0.017
	1	-0.661	-0.379	0.442	-0.175	-0.359	-0.457	-0.387	0.408	-0.032	-0.170	-0.256	-0.168
	2	0.032	-0.271	0.296	-0.327	-0.228	-0.312	-0.403	0.048	-0.140	-0.090	-0.015	-0.175
	4	0.021	-0.056	-0.038	-0.099	-0.178	-0.210	-0.522	0.062	-0.153	-0.069	0.044	-0.330
	6	-0.045	0.022	0.005	-0.202	-0.224	-0.146	-0.303	0.047	-0.072	-0.082	-0.039	-0.190
	12	-0.046	0.078	-0.028	-0.154	0.004	-0.055	-0.106	0.027	-0.005	-0.066	0.015	-0.043
	24	-0.010	0.019	-0.042	-0.088	-0.028	-0.089	0.024	0.022	-0.039	-0.026	0.033	-0.067

Table (A.10) Processing results (in meters) for station SFE1 from static PPP at different time spans over the seven days in north, east and up directions using single frequency observations and rapid precise ephemeris.

	Time (h)	Day 1	Day 2	Day 3	Day 4	Day 5	Day 6	Day 7
North	0.25	-0.319	-1.781	-0.065	1.240	0.536	-0.181	-0.061
	0.5	-0.814	-0.647	0.441	0.829	0.176	-0.326	0.505
	1	-0.258	0.035	0.048	0.187	-0.132	-0.364	0.204
	2	-0.079	-0.015	-0.083	-0.036	-0.096	-0.096	0.004
	4	-0.050	0.007	-0.057	-0.021	-0.010	-0.008	-0.008
	6	-0.006	0.011	0.002	-0.002	0.016	0.009	0.023
	12	0.005	0.023	0.021	0.002	-0.005	-0.009	0.027
	24	0.015	0.022	0.005	0.005	0.001	0.001	0.017
East	0.25	5.046	-1.138	-1.630	1.564	1.221	2.948	-0.009
	0.5	1.762	0.197	-0.918	2.030	-0.846	1.779	2.324
	1	0.714	-0.484	-0.032	0.274	0.370	0.273	1.312
	2	0.250	0.006	0.284	0.071	0.049	-0.219	0.438
	4	0.114	0.036	0.045	-0.002	0.002	0.057	0.197
	6	0.021	-0.051	0.016	-0.088	-0.053	0.014	-0.026
	12	0.063	0.029	0.094	0.013	-0.024	0.093	-0.007
	24	0.041	0.037	0.036	0.016	-0.014	0.055	0.010
Up	0.25	1.274	0.472	-3.547	6.745	-0.594	2.598	-2.665
	0.5	0.970	2.287	-1.670	0.632	-0.082	0.681	-0.074
	1	1.119	0.531	0.077	0.154	0.315	0.162	0.295
	2	0.433	0.418	-0.064	0.038	0.402	0.119	0.210
	4	0.038	0.069	-0.114	-0.018	0.068	-0.058	-0.040
	6	-0.022	-0.020	-0.004	-0.030	0.150	-0.052	-0.088
	12	0.010	-0.047	0.012	0.014	0.038	-0.059	-0.139
	24	0.055	-0.091	-0.046	-0.020	0.004	-0.087	-0.078

Table (A.11) Processing results (in meters) for all twelve IGS stations from static PPP at different time spans over the day (DOY 70, 2015) in north, east and up directions using single frequency observations and ultra-rapid precise ephemeris.

	Time (h)	ALIC	GLPS	ISPA	IRKJ	KOKB	KIRU	LHAZ	NICO	PDEL	STHL	UNBJ	YSSK
North	**0.25**	-0.155	-0.625	-0.410	0.434	-0.687	-1.087	0.844	-0.586	-0.032	-0.069	-1.779	0.276
	0.5	-1.033	-0.276	-0.167	0.000	-0.348	-0.369	0.356	0.139	-0.020	-0.060	-0.396	-0.257
	1	-0.387	-0.051	0.062	-0.028	-0.153	-0.126	0.123	-0.082	0.005	0.032	0.096	0.033
	2	-0.078	0.013	0.024	0.105	0.035	-0.060	0.180	-0.045	0.014	-0.024	0.058	0.166
	4	-0.046	-0.011	-0.006	0.012	0.080	0.001	-0.051	-0.010	0.030	-0.006	0.025	0.009
	6	-0.039	-0.012	-0.008	-0.003	0.031	0.007	-0.022	-0.004	0.001	-0.016	0.018	0.002
	12	-0.024	-0.022	-0.004	0.010	0.046	0.014	-0.006	-0.002	-0.017	-0.008	0.002	-0.004
	24	-0.019	-0.020	0.007	0.011	0.026	0.021	-0.004	-0.004	-0.017	-0.007	0.007	-0.014
East	**0.25**	0.279	3.614	1.124	0.678	3.365	-0.648	3.311	0.361	0.957	0.617	4.465	1.949
	0.5	-0.064	1.186	0.205	0.293	0.985	-0.034	0.536	-0.293	-0.369	0.512	-0.194	0.470
	1	0.015	0.299	-0.307	-0.071	0.204	-0.054	-1.097	-0.254	-0.096	0.196	-0.035	-0.207
	2	-0.386	0.027	0.000	-0.271	0.059	0.004	-0.003	-0.107	0.000	0.110	0.419	-0.232
	4	-0.150	-0.036	0.086	-0.092	0.058	0.006	0.025	-0.041	0.019	0.078	0.102	-0.165
	6	-0.019	-0.035	0.033	-0.059	0.054	-0.017	0.119	-0.022	0.021	0.001	0.018	-0.151
	12	-0.002	0.020	0.026	0.015	0.002	-0.002	0.026	0.000	0.032	-0.002	-0.017	-0.122
	24	0.003	0.015	-0.006	0.026	0.027	-0.004	0.009	-0.013	0.017	-0.008	-0.008	-0.048
Up	**0.25**	-0.206	-1.841	0.732	0.820	0.480	0.549	-5.604	1.898	1.241	0.322	1.434	1.060
	0.5	-2.612	-0.286	0.199	0.293	-0.823	-0.404	-0.703	0.647	0.114	0.094	0.695	-0.452
	1	-0.801	-0.459	-0.042	-0.158	0.070	-0.494	0.383	0.175	0.145	-0.114	0.031	-0.448
	2	-0.152	-0.168	-0.011	0.012	-0.179	0.003	-0.062	0.103	-0.103	0.037	0.053	-0.303
	4	0.025	-0.070	-0.013	-0.006	-0.255	-0.054	-0.125	0.050	-0.136	0.059	-0.083	-0.262
	6	0.010	-0.070	0.003	-0.034	-0.295	-0.047	-0.107	0.031	-0.063	0.019	-0.071	-0.158
	12	0.003	-0.058	-0.043	-0.049	-0.114	-0.061	-0.109	0.020	0.013	0.036	-0.043	-0.044
	24	0.009	-0.046	-0.019	-0.041	-0.114	-0.055	-0.084	0.029	-0.032	0.020	-0.043	-0.057

Table (A.12) Processing results (in meters) for station SFE1 from static PPP at different time spans over the seven days in north, east and up directions using single frequency observations and ultra-rapid precise ephemeris.

	Time (h)	Day 1	Day 2	Day 3	Day 4	Day 5	Day 6	Day 7
North	0.25	-0.036	-1.354	-0.118	-0.151	-0.523	0.896	0.516
	0.5	-0.200	-0.131	0.247	0.445	0.135	-0.046	0.297
	1	0.008	0.138	0.091	0.017	-0.021	-0.285	0.011
	2	-0.031	-0.054	-0.048	-0.027	-0.021	-0.055	-0.055
	4	0.001	-0.012	-0.009	-0.016	-0.002	-0.028	-0.023
	6	0.005	-0.001	0.014	0.011	0.021	-0.002	0.006
	12	0.012	0.015	0.024	0.006	0.018	0.005	0.013
	24	0.013	0.013	0.021	0.006	0.014	0.006	0.012
East	0.25	1.887	1.977	0.427	-1.970	1.234	0.435	1.253
	0.5	0.342	0.287	0.136	-0.707	0.457	0.305	0.944
	1	0.575	0.196	0.368	0.256	0.692	0.805	0.821
	2	0.146	0.146	0.022	-0.001	0.102	0.225	0.051
	4	0.080	0.049	0.001	-0.029	0.038	0.136	0.109
	6	-0.021	-0.046	-0.027	-0.109	0.039	0.017	-0.006
	12	0.012	0.014	0.032	0.002	0.023	0.031	0.011
	24	0.010	0.013	0.010	0.002	0.024	0.033	0.007
Up	0.25	-0.105	1.541	1.603	1.446	0.516	0.682	0.234
	0.5	-0.927	0.268	0.565	0.074	0.496	0.554	1.552
	1	0.677	0.519	0.700	0.495	0.958	1.053	0.645
	2	0.281	-0.003	0.128	0.235	0.097	0.277	0.172
	4	0.141	-0.037	0.076	0.032	0.066	0.028	0.050
	6	0.047	-0.034	0.044	-0.032	0.142	-0.058	0.034
	12	0.024	-0.014	0.059	-0.036	0.080	-0.044	-0.002
	24	0.005	-0.026	0.001	-0.016	0.003	-0.024	0.005

جامعة بنـها
كلية الهندسة بشبرا
قسم هندسة المساحة

عنوان الرسالة

استخدام مستقبل واحد لتحديد موضع نقطة بدقة عالية

رسالة مقدمة كجزء من متطلبات الحصول علي درجة الماجستير في هندسة المساحة

مقدمة من

المهندس/ محمد نصر على البيه
بكالوريوس هندسةالمساحة (2010)

إشراف

أ.د/ سعد زكى بلبل
أستاذ المساحة والجيوديسيا
كلية الهندسة بشبرا-جامعة بنـها

أ.د/ عمرو حنفى على
أستاذ المساحة والجيوديسيا
كلية الهندسة بشبرا-جامعة بنـها

أ.م.د/ منى سعدالسيد
أستاذ المساحة والجيوديسيا المساعد
كلية الهندسة بشبرا- جامعة بنـها

جامـــعة بنـــها
كلية الهندسة بشبرا
قسم هندسة المساحة

القبول النهائى للرسالة

استخدام مستقبل واحد لتحديد موضع نقطة بدقة عالية

رســـــالة مقدمة من

المهندس/ محمد نصر على البيه
بكالوريوس هندسة المساحة (2010)

كجزء من متطلبات الحصول علي درجة الماجستير في هندسة المساحة تخصص المساحة والجيوديسيا

وقد تمت مناقشة الرسالة والتوصية بالموافقة علي منح درجة الماجستير في هندسة المساحة تخصص المساحة والجيوديسيا من لجنة الممتحنين

أعضاء لجنة الحكم والمناقشة

أ.د / محمود النقراشى على — التوقيع: .....

أستاذ المساحة والجيوديسيا بكلية الهندسة - جامعة الازهر

أ.د / سعد زكى بلبل — التوقيع: .....

أستاذ المساحة والجيوديسيا بكلية الهندسة بشبرا - جامعة بنها

أ.د / عبدالله احمد سعد — التوقيع: .....

أستاذ المساحة والجيوديسيا بكلية الهندسة بشبرا - جامعة بنها

أ.د / عمرو حنفى على — التوقيع: .....

أستاذ المساحة والجيوديسيا بكلية الهندسة بشبرا - جامعة بنها

استخدام مستقبل واحد لتحديد موضع نقطة بدقة عالية

مقدمة :

حديثاً تم تطوير أنظمة الملاحة العالمية لتحديد المواقع باستخدام الأقمار الصناعية (GNSS) مثل النظام الأمريكى (GPS) أو النظام الروسى (GLONASS) أو النظام الأوروبى (GALILEO) سواء كان هذا التطوير بشكل جزئى أو كلى ، وقد أدى هذا التطوير الى زيادة الدقة المرغوب فيها عند تحديد موقع ما وبالتالى كانت هناك الفرصة لظهور تقنية جديدة تسمى بـ (Precise Point Positioning) وتعنى التحديد الدقيق لاحداثيات نقطة باستخدام جهاز استقبال واحد . وتعتبر هذه التقنية بداية لأسلوب جديد فى تحديد المواقع وقد جذبت الانتباه اليها من قبل المختصين بهذا المجال نظرا لأنها وسيلة مفيدة فى كثير من التطبيقات لبساطتها ، قلة تكاليفها ، دقتها التى تتحسن باستمرار وكذلك لأنها لا تتطلب وجود نقطة مرجعية .

وتختلف هذه الطريقة عن الطرق التقليدية التفاضلية (DGNSS) – التى تتطلب وجود نقطة مرجعية أو أكثر أثناء عملية الرصد – فى أنها تحتاج فقط الى وجود جهاز استقبال واحد على النقطة المراد رصدها أى لا تحتاج الى حتمية وجود جهاز استقبال آخر على نقطة مرجعية وبالتالى نستطيع التغلب على مشكلة المسافة المحدودة والأرصاد الآنية بين كل من النقطة المرجعية والنقطة المراد رصدها فى الطرق التفاضلية . وفى الوقت الراهن نستطيع أن نحصل من هذه التقنية الجديدة على دقة قد تصل الى سنتيمتر فى حالة الرصد الثابت او ديسيمتر فى حالة الرصد المتحرك ، ولكى نصل لهذه الدقة لابد من عمل تصحيحات لكل الأخطاء التى قد نواجهها أثناء عملية الرصد .

موضوع البحث :

الموضوع الذى سوف نتعرض له من خلال هذة الدراسة هو كيفية تحديد موضع نقطة بدقة عالية باستخدام جهاز استقبال واحد عن طريق أرصاد الأكواد والموجات الحاملة مع استخدام عناصر دقيقة لمدارات الأقمار الصناعية . ولكى نصل لدقة عالية من خلال هذا الأسلوب لابد من التغلب على كل الأخطاء التى قد نواجهها سواء تلك المتعلقة بالأقمار الصناعية ، انتشار الاشارة ، البيئة المحيطة وكذلك أجهزة الاستقبال على عكس الأسلوب التفاضلى الذى يستطيع تحقيق دقة عالية أيضا من خلال الأرصاد الآنية بين نقطتين التى تلاشى كليا أو جزئيا معظم هذه الأخطاء ، ولا نستطيع عمل ذلك فى التقنية الجديدة حيث يتوفر لدينا فقط أرصاد من جهاز استقبال واحد فقط على النقطة المراد تحديد موقعها .

وهذه الأخطاء يمكن تصنيفها الى :

- أخطاء متعلقة بالأقمار الصناعية
- أخطاء متعلقة بجهاز الاستقبال
- أخطاء متعلقة بالغلاف الجوى

حيث يعتمد هذا الاسلوب على معالجة هذه الاخطاء للحصول على دقة تقارب الطرق التفاضلية. ويتميز هذا الاسلوب بأنه ذات تكلفة أقل ويناسب كثير من التطبيقات.

أهداف البحث :

الهدف الرئيسى من البحث هو دراسة وتقييم تقنية الـ (PPP) ، ولتحقيق هذا الهدف سوف نقوم ببعض المهام مثل :

1- التعرف على التطورات الحديثة المتعلقة بنظم الملاحة العالمية المختلفة .
2- دراسة الأخطاء المتعلقة بهذة الأنظمة وكذلك الطرق المختلفة لمعالجتها .
3- تقييم دقة تقنية الـ (PPP) فى حالة الرصد الثابت أو المتحرك وكذلك فى حالة المعالجة بعد عملية الرصد أو أثناء عملية الرصد .

أبواب الرسالة :

تشتمل الرسالة على خمسة فصول كالآتى :

1- الفصل الأول .
ويشتمل على الخطوط العريضة للبحث ، التعرف على الوضع الحالى لتقنية (PPP) مع تحديد أهداف البحث ومحتوياته.

2- الفصل الثانى .
ويوضح نبذة مختصرة عن تقنية الـ (PPP) ودقتها فى الوقت الحالى وكذلك معوقات التقنية مع شرح مصادر الاخطاء المختلفة وطرق معالجتها .

3- الفصل الثالث .
وفى هذا الفصل يتم التعرف على النموذج الرياضي لتقنية الـ (PPP) والخطوات المتبعة لتفيذه. أيضا سوف يتم توضيح مسار تنفيذ تقنية الـ (PPP) بدءا من البيانات المختلفة المطلوبة , العمليات التى تجرى على هذه البيانات قبل المعالجة , معالجة مصادر الاخطاء المختلفة وصولا الى النواتج النهائية.

4- الفصل الرابع .
ويحتوى على مجموعات البيانات المختلفة التى تم استخدامها فى البحث وطرق الحصول عليها مع عرض طرق التقييم المختلفة لكل أسلوب رصد وكذلك النتائج التى تم التوصل اليها .

5- الفصل الخامس .
ويوضح النتائج المختلفة والخلاصة الناتجة من البحث والتوصيات المستقبلية .

- المراجع المستخدمة فى البحث
- الملحقات

نتائج البحث :

1- تقنية الـ (PPP) اتاحت الفرصة لكثير من المستخدمين فى الحصول على نتائج جيدة مع تكلفة اقل خصوصا انه يتم فيها استخدام جهاز استقبال واحد فقط.

2- اصبحت تقنية الـ (PPP) بديلا استراتيجيا لتقنية الـ (DGPS) الشائعة خصوصا فى اعمال الرصد الثابت وايضا كثير من التطبيقات المساحية الاخرى.

3- تتميز تقنية الـ (PPP) بعدم الاحتياج الى احداثيات نقاط موجودة مسبقا – والتى قد تكون بها بعض المشاكل – وبالتالى فان الاحداثيات الناتجة تكون مطابقة لوقت الرصد كما هو الحال فى نظام احداثيات الـ (ITRF).

4- دقة تقنية الـ (PPP) فى الرصد الثابت قد تصل الى اقل من 1 سم فى الاتجاه الافقى و 2 سم فى الاتجاه الراسى باستخدام ارصاد ثنائية التردد مع التصحيحات النهائية او السريعة لمدارات الاقمار الصناعية.

5- استخدام تقنية الـ (PPP) فى الرصد الثابت عن طريق الارصاد احادية التردد يمكن ان تعطى دقة اقل من 5 سم ولكن بعد فترة زمنية تتراوح بين 4 الى 6 ساعات من الرصد المستمر.

6- تقنية الـ (PPP) فى الرصد المتحرك يمكن ان تصل دقتها الى اقل من 5 سم فى الاتجاه الراسى و 10 سم فى الاتجاه الافقى.

7- توافر خدمة تقنية الـ (PPP) من خلال مواقع الانترنت المجانية يستفيد منها كثير من المستخدمين.

8- اضافة ارصاد منظومة الـ (GLONASS) الى ارصاد منظومة الـ (GPS) قد تحسن دقة تقنية الـ (PPP) خصوصا فى الفترات الاولى من عملية الرصد.

9- دقة تقنية الـ (PPP) فى الرصد المتحرك اللحظى تصل احيانا فى حدود 10 سم فى الاتجاه الافقى و 20 سم فى الاتجاه الراسى.

توصيات البحث :

1- يجب اجراء مزيد من الابحاث لتقليل الوقت الذى تستغرقة تقنية الـ (PPP) للوصول الى حل افضل لكى يمكن مقارنته بالطرق التقليدية.

2- لازالت الى الان تقنية الـ (PPP) باستخدام الارصاد احادية التردد تعطي نتائج اقل دقة بسبب اخطاء طبقة الايونوسفير ولذلك نحتاج الى تطوير نماذج مختلفة للتغلب على هذه الاخطاء.

3- لابد من استغلال التطورات الكبيرة فى الانظمة العالمية للرصد بالاقمار الصناعية وعمل تكامل بين هذه الانظمة داخل تقنية الـ (PPP).

4- يجب الاستفادة من اشارات الاقمار الصناعية الجديدة وعمل دمج بين هذه الاشارات للوصول الى اقصى استفادة ممكنة.